universität wien

DISSERTATION

Titel der Dissertation

Antiviral Drug Target Identification Using Yeast as a Model System

angestrebter akademischer Grad

Doktorin der Naturwissenschaften (Dr. rer.nat.)

Verfasserin:	Mag. Nathalie Landstetter
Matrikel-Nummer:	0101200
Dissertationsgebiet (lt. Studienblatt):	A 091 441 Dr.-Studium der Naturwissenschaften UniStG, Genetik – Mikrobiologie (Stzw)
Betreuerin / Betreuer:	A.o. Univ.-Prof. Dr. Karl Kuchler

Wien, am 11. August 2010

The most exciting phrase to hear in science, the one that heralds new discoveries, is not 'Eureka!' (I found it!), but 'That's funny ...'

Isaac Asimov (1920 - 1992)

Table of Contents

1. SUMMARY

Pyrrolidine dithiocarbamate (PDTC), a known inhibitor of NF-κB-activation, has anti-oxidative as well as antiviral activities. PDTC is effective against several virus families, indicating that its antiviral mechanism targets host rather than viral functions. To investigate its mode of action, we use baker's yeast as a simple eukaryotic model system and two types of genome-wide analysis. First, expression profiling using whole-genome DNA microarrays identifies more than 200 genes differentially regulated upon PDTC exposure. Interestingly, the Aft1-dependent iron regulon is a main target of PDTC, indicating a lack of iron availability. Additionally, the PDTC-caused zinc influx triggers a strong regulation of zinc transporters due to cytoplasmic zinc excess. Second, phenotypic screening the EUROSCARF collection of non-essential deletion mutants for PDTC hypersensitivity identifies numerous mutants implicated in vacuolar maintenance, acidification, as well as in transport, trafficking, mitochondrial organization and translation. Notably, the screening data indicate significant overlaps of genes whose deletions cause PDTC-sensitivity and those mediating zinc, as well as alkaline pH tolerance. Strikingly, PDTC inhibits the proteolytic activation of the alkaline pH-responsive transcription factor Rim101 in a zinc-dependent manner. Hence, our data show that PDTC-induced cytoplasmic zinc excess triggers vacuolar detoxification, which in turn disturbs iron homeostasis and activates the iron-dependent regulator Aft1. Consequently, PDTC links intracellular disturbance of iron and zinc homeostasis to other cellular processes, including vacuolar and vesicular transport, as well as pH regulation. Our work reveals for the first time a complex cross-talk between yeast ion homeostasis and the underlying genetic regulatory networks.

SUMMARY

2. ZUSAMMENFASSUNG

Pyrrolidine dithiocarbamate (PDTC), ein bekannter Inhibitor der NF-κB-Aktivierung, zeigt sowohl anti-oxidative als auch antivirale Aktivität. Da PDTC gegen verschiedene Virusfamilien wirksam ist, sind vermutlich eher Wirtsfunktionen Ziele des antiviralen Mechanismus. Um seine Wirkungsweise zu analysieren verwenden wir Bäckerhefe als einfaches eukaryontisches Modellsystem und zweierlei Strategien genomweiter Analyse. Genomweite Microarray Expressionsprofile identifizieren mehr als 200 Gene, die aufgrund von PDTC Zugabe differentiell reguliert werden. Interessanterweise ist das Aft1-abhängige Eisenregulon ein Hauptangriffspunkt von PDTC, was auf Eisenmangel deutet. Überdies verursachen der PDTC-induzierte Zinkeinstrom und der damit einhergehende cytoplasmatische Zinküberschuss eine starke Regulierung der zellulären Zinktransporter. Das phänotypische Screening der EUROSCARF Deletionssammlung zeigt, dass vor allem Mutanten in vakuolären Funktionen wie der Ansäuerung der Vakuole, aber auch jene mit Funktionen in Transportprozessen, mitochondrialer Organisation und Translation, sensitiv auf PDTC reagieren. Insbesondere gibt es erhebliche Überschneidungen von Genfunktionen, deren Deletion PDTC-Sensitivität hervorruft, mit jenen, die Resistenz bei Zinküberschuss oder alkalischem pH vermitteln. Bemerkenswerterweise inhibiert PDTC die proteolytische Aktivierung des Transkriptionsfaktors Rim101, die normalerweise als Antwort auf alkalischen pH erfolgt, in zinkabhängiger Weise. Folglich zeigen unsere Daten, dass PDTC cytoplasmatischen Zinkeinstrom induziert, was zur Speicherung des überschüssigen Zinks in der Vakuole führt. Dadurch kommt es zu einer Störung der Eisen-Zink-Homöostase, die wiederum den eisenabhängigen Regulator Aft1 aktiviert. Daher stellt PDTC durch die intrazelluläre Störung des Eisen-Zink-Gleichgewichts eine Verbindung zu anderen zellulären Prozessen wie vakuolären und vesikulären Transportprozessen und pH-Regulierung her. Unsere Arbeit zeigt erstmals eine komplexe Co-Regulation von intrazellulärer Ionenhomöostase und den zugrunde liegenden regulatorischen genetischen Netzwerken in Hefe auf.

3. INTRODUCTION

From garlic to red wine – trials to fight the common cold

Runny or stuffy nose, scratchy throat, sneezing all day long, cough, and headache – everyone knows the symptoms of a common cold. Human Rhinoviruses (HRVs), belonging to the family of *Picornaviridae*, are the most frequent cause of mild upper respiratory illnesses. Although neither life-threatening and with symptoms usually lasting for less than a week, the common cold is one of the leading causes for people staying at home from school or work. Even though normally self-limited, rhinoviruses are implicated in induction of serious disease in elderly people and in people suffering from asthma and chronic lung disease. Millions of lost work days and physician visits build up to an enormous social and economic burden annually (for review see (Dreschers *et al.*, 2007)).

The common cold is caused by numerous virus types that are associated with heterogeneous pathogenic symptoms. HRVs make up about 50% of upper respiratory infections. Additionally, coronavirus, influenzavirus, respiratory syncytial virus, parainfluenza virus and adenovirus have been related to the common cold. These agents account for minor proportions of the common cold syndrome and even cause lower respiratory illnesses and symptoms more typical for these viruses (Heikkinen and Jarvinen, 2003).

Beside some household remedies and symptomatic treatment, there are no antiviral drugs or marketed therapies preventing or curing the common cold available yet. First of all, the multitude of viruses causing common cold symptoms, accounts for the lack of a universal treatment. Due to the central role of HRVs in causing the common cold, potential antiviral drugs targeting HRVs are expected to be the most successful treatment (De Palma *et al.*, 2008). However, rhinoviruses, with their high diversity, exhibit a tremendous immunological resistance and variability. A total of 99 serotypes, and the fact that the main virus-host interaction site is barely accessible for antibodies, make vaccine development impracticable (McKinlay, 2001; Dreschers *et al.*, 2007). In search for an anti-rhinoviral therapy, many substances exhibited promising activity in cell culture, but failed to reach the market. Moreover, dependent on the short duration and mildness of the common cold, the safety-profile of an anti-rhinoviral drug has to be superior to

gain a perfectly balanced risk-to-benefit ratio (McKinlay, 2001; Dreschers *et al.*, 2007). Thus, screening for new antiviral substances is a main aim to fight the common cold.

The viral life cycle

To specifically target virus multiplication, one has to study the viral life cycle (Lin *et al.*, 2009). In the case of HRVs, the virus particle is internalized upon receptor binding. Receptor-mediated endocytosis results in uncoating and delivery of the viral RNA genome into the cytosol where translation takes place. The coding region of the viral genome covers one functional open reading frame which directs the expression of a polyprotein precursor of all the viral proteins. The central coding part of the genome can be divided into three regions P1, P2, and P3. P1 encodes the capsid proteins VP1 to VP4, P2 and P3 encode the non-structural proteins involved in co-translational cleavage of the polyprotein (viral proteases 2A and 3C), inhibition of host cell functions (proteases 2A, 3C, and L), determination of host range (2B, 2C) and replication of the viral RNA (2C, 3AB, Vpg and RNA polymerase 3D) (Fig. 1). Importantly, a viral protease cleaves the eukaryotic translation initiation factor 4G (eIF4G) leading to a shut-off of cap-dependent translation only allowing IRES-dependent translation of viral RNA. Finally, new viral particles, consisting of a newly synthesized RNA genome, non-structural proteins and capsid proteins, are assembled and then released by cell lysis (for review see (Whitton *et al.*, 2005; Lin *et al.*, 2009)).

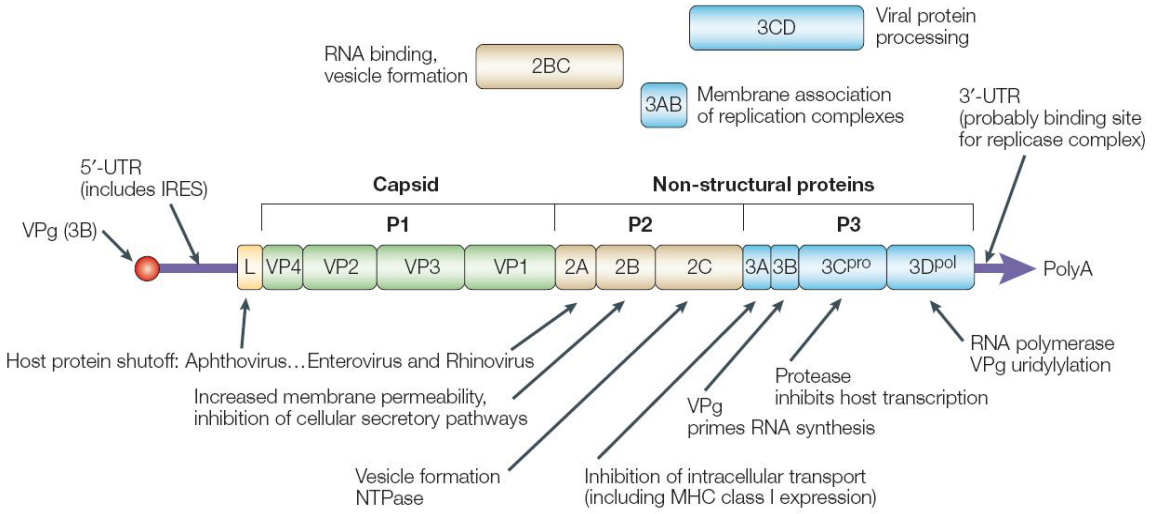

Figure 1: A diagrammatic representation of the Picornavirus genome, the polyprotein, its organization and the main function of the encoded proteins is shown. The three cleavage intermediates together with the 12 main resulting polypeptides are presented. Additionally, the key functions of the polypeptides are indicated. IRES, internal ribosome entry site; UTR, untranslated region; Vpg, viral protein genome-linked; (Whitton *et al.*, 2005).

Potential anti-rhinoviral approaches

Numerous studies of potential treatments and therapies against the common cold are available. They include red wine (Takkouche *et al.*, 2002), capsid blockers and protease inhibitors (De Palma *et al*., 2008), and even the effect of garlic (Lissiman *et al.*, 2009) on the infection course. Potential ways to prevent virus infections and inhibit virus multiplication are to block virus entry, to inhibit uncoating, replication or polyprotein processing, assembly and virus release (Lin *et al.*, 2009).

A historical old strategy of anti-rhinoviral therapy targets the viral capsid. So called WIN compounds bind to viruses and inhibit a conformational change in the capsid, thereby preventing RNA release (Otto *et al.*, 1985). In clinical trials, these substances failed due to pharmacokinetic problems, such as the applicable drug concentration range showed little efficacy. The most promising candidate of the capsid binding substances, Pleconaril, is considered as prove that capsidblockers can reduce severity and duration of common cold symptoms (Hayden *et al.*, 2003). However, in 2001, Pleconaril was not approved by the US Food and Drug Administration (FDA) for oral drug formulation for common colds because of its unconvincing safety profile. However, ViroPharma re-licensed Pleconaril to Schering-Plough, who completed a phase II trial in 2007 (http://www.clinicaltrials.gov/ct/gui/show/NCT00394914).

Beside capsid blockers, several compounds have been tested as protease 2A and 3C inhibitors (e.g. homophthalimides, rupintrivir, compound 1, keto-glutamine analogues). As viral replication inhibitor, guanidine hydrochloride was extensively studied. However, so far most of the substances failed to reduce and shorten the common cold symptoms in clinical trials (for review see (De Palma *et al*., 2008)). Notably, preventing transmission by smear infections using hand-disinfection provides an option to decrease the onset of the illness.

Zinc supplementation has often been suggested to reduce virus multiplication, thereby gaining more and more popularity as over-the-counter alternative therapy. Many studies on the effect of zinc supplied as lozenges, nasal sprays or oral therapy were performed. Some of them exert positive effects, whereas others found no inhibitory effect (for review see (Caruso *et al.*, 2007)). Overall controversial studies on the role of zinc in rhinovirus infections failed to convincingly prove clinical benefits.

As rhinovirus infections are often accompanied by oxidative stress in the host cell, several antioxidants were tested as potential antivirals. However, vitamin C, Trolox, 2-mercaptoethanol, and N-acetyl-L-cysteine failed to inhibit rhinovirus infection. Strikingly, pyrrolidine dithiocarbamate, a compound generally used as NF-κB inhibitor (Schreck *et al.*, 1992), was identified to inhibit virus replication (Gaudernak *et al.*, 2002).

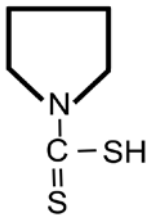

Figure 2: Structure of pyrrolidine dithiocarbamate (PDTC).

Pyrrolidine dithiocarbamate, a multifunctional compound

Pyrrolidine dithiocarbamate (PDTC), a low-molecular weight thiol compound, is a multifunctional drug exerting various effects in biological systems (Fig.2). For instance, it is a potent inhibitor of the nuclear factor kappa B (NF-κB) activation (Schreck *et al.*, 1992). It can exert pro-apoptotic and anti-apoptotic effects, dependent on the cellular system (Erl *et al.*, 2000; Morais *et al.*, 2006). Furthermore, PDTC shows inhibitory effects on protein degradation (Hayakawa *et al.*, 2003; Kim *et al.*, 2004), and induces transcription of the manganese superoxide dismutase and the heme oxygenase HO-1 (Borrello and Demple, 1997; Hartsfield *et al.*, 1998).

Interestingly, PDTC displays antiviral activity against picornaviruses, including human rhinovirus, poliovirus and coxsackievirus (Gaudernak *et al.*, 2002; Lanke *et al.*, 2007), as well as on influenza virus, the latter being orthomyxoviruses with a very different life cycle (Uchide *et al.*, 2002). PDTC prevents polyprotein processing and reduces virus titers mainly by causing zinc influx into host cells (Krenn *et al.*, 2005). This observation is consistent with the suggested modulation of metal ion availability as a prerequisite of NF-κB activation (Kim *et al.*, 2003). PDTC binds free or protein-bound metal ions, thereby forming lipophilic dithiocarbamate-metal complexes. These complexes transport zinc and copper from the extracellular medium into cells (Krenn *et al.*, 2005).

As PDTC inhibits multiplication of different virus families (Uchide *et al.*, 2002; Lanke *et al.*, 2007), and no resistant strains have been observed to date, it has been speculated that the antiviral mechanism of PDTC might target host cell gene functions rather than viral functions. To gain insight into the cellular mechanisms and control programs affected by PDTC, we decided to use the yeast *Saccharomyces cerevisiae* as a simple eukaryotic model organism.

Yeast as a model system

The budding yeast *Saccharomyces cerevisiae* is a versatile model organism invaluable for the unraveling of many fundamental biological processes including drug target identification by providing genome-wide chemogenomic approaches (Giaever, 2003; Parsons *et al.*, 2004). The availability of the whole-genome sequence and the ease, with which yeast can be genetically manipulated provide profound research strategies. Yeast is particularly suitable for large-scale screening techniques. Many experimental approaches have been developed in this model organism, from gene deletion collections, gene-tagging collections, whole-genome DNA or protein arrays, up to yeast-two-hybrid systems. Furthermore, high-throughput data have been generated by transcriptomics, metabolomics, and proteomics (Vizeacoumar *et al.*, 2009). All these data have been collected in databases building an immense information resource. Moreover, due to the high evolutionary conservation of essential cellular processes up to humans (Foury, 1997), phenotypic screening approaches in yeast have become advantageous for drug development and pharmacokinetic studies (Bharucha and Kumar, 2007).

Using chemical genetics for drug target identification

A key challenge is to identify interactions of small molecules with the genome and to understand the subsequent modulation of pathways and protein functions. This has become feasible with the availability of whole genome sequences. The field of chemical genetics and chemogenomics aims to identify drug targets by using cell-based or microorganism-based screening of bioactive compounds (Jacoby, 2006). Thus, chemical genetics entails to inhibit gene functions in an organism or cellular context by using small-molecule xenobiotics, thus exploring the mode of action of these bioactive compounds. The underlying idea is that a compound inhibiting a certain gene product phenocopies the

corresponding deletion of this gene. Thus, lack of a gene in combination with a sublethal dose of a drug can have a synthetic effect such as reduced fitness, thereby allowing the identification of genes or pathways that otherwise mediate tolerance to the drug. In contrast to classical "forward or reverse" genetics with gene mutations or deletions, the inhibitory effect of a drug on a certain gene function is conditional as drug supplementation, dose-dependency or removal of the drug can readily be adjusted (for review see (Stockwell, 2000)).

In principle, a drug can affect the growth, cell division and survival of a yeast cell in different ways. For instance, it can directly inhibit a protein that is crucial for a certain pathway or process (Stockwell, 2000). This direct inhibition should mimic the phenotype of the deletion of the corresponding gene. Furthermore, the transcription level of virtually every yeast gene can be altered and the changing drug sensitivities can easily be monitored. Consequently, the transcriptional changes of a drug-induced gene inhibition versus a gene deletion can be compared and allow for conclusions on drug action (Giaever *et al.*, 2004).

Genome-wide functional screening techniques

In the course of the Gene Deletion Project an as much as possible complete set of single gene deletion strains was generated. The main goal was to assign a function to every open reading frame (ORF). Based on the acquired whole-genome sequence of *S. cerevisiae* (Goffeau *et al.*, 1996), every potential ORF was deleted from start to stop codon. Deletion strains were analyzed for growth defects under various conditions (Winzeler *et al.*, 1999). In 2002, Giaever *et al* published a functional profiling of the *S. cerevisiae* genome using a bar-coded gene deletion set. The deletion strains were screened on several stress conditions and their relative fitness compared to the wild type was quantified. Thereby, genes contributing to buffer a certain stress condition were identified (Giaever *et al.*, 2002). In total, four deletion collections are available so far: haploids of both mating types, homozygous diploids for non-essential genes and heterozygous diploids comprising of non-essential and essential ORFs (http://www-sequence.stanford.edu/group/yeast_deletion_project/).

The yeast knock-out collection has been widely used for phenotypic screenings, to investigate the effect of various stress conditions and the mode of action of drugs, their targets and the corresponding target pathways (Parsons *et al.*, 2004; Tucker and Fields, 2004; Bharucha and Kumar, 2007; Ericson *et al.*, 2008). The principle of screening is fairly simple, since loss of a defined gene alters the growth abilities of a mutant strain under certain conditions when compared to its wild type. In other words, genes whose deletions render cells hypersensitive to a certain drug, are required to counteract drug-induced effects. In this way, genes or pathways affected by the drug are identified, thereby deciphering the mechanisms of action of the drug. Compounds that render a similar set of deletion mutants sensitive, might act in the same pathway. By collecting and comparing screening data sets, compound-specific profiles and chemical-genetic interactions can be generated (Giaever *et al.*, 2004).

Transcriptional profiling of stress responses

Likewise, microarray profiling using whole-genome DNA microarrays can yield conclusive insights into the mode of action of a drug or the genetic networks modulated by comparing untreated to drug-exposed cells (Hughes *et al.*, 2000). Due to rapidly changing environmental conditions, yeast has developed several mechanisms for adapting to drastic changes, including fluctuations in nutrition availability, temperature, osmolarity, radiation or drug treatment. Every cell establishes a distinct transcription profile dependent on the external conditions. For example, microarray profiling for a set of different stresses and environmental conditions identified an extensive transcriptional network underlying cellular stress responses (Gasch *et al.*, 2000), but also enables the discovery of direct as well as off-targets of bioactive compounds (Parsons *et al.*, 2006; Ericson *et al.*, 2008). Genes, whose transcription levels change upon various stresses, are involved in the so called ‘environmental stress response’ (Gasch *et al.*, 2000; Gasch and Werner-Washburne, 2002). This general stress response encompasses remodeling processes at all cellular stages and compartments. Thereby, physiological processes can be transiently arrested until cells have adjusted to the new conditions. Additionally, cells may specifically adapt to a specific stress condition. For instance, lack of a certain nutrient would cause induction of specific transporters, mediating import of this nutrient. In parallel, the cell would shut-down or silence exactly those non-essential mechanisms

consuming this nutrient. Consequently, a cell has to simultaneously control uptake, silencing and reconstruction of its intracellular homeostasis (for review see (Gasch and Werner-Washburne, 2002)).

Fine tuning of essential but dangerous metal ions

Cells constantly adapt to changes in their environment. For example, they accurately control uptake of essential nutrients or ions. Maintenance of the cellular ion homeostasis plays a crucial role for survival, as well as adaptation, since many ions are sometimes essential but as well toxic at higher concentrations. Therefore, cells have to strike a balance between uptake, usage and storage in intracellular compartments to avoid cell damage (Radisky and Kaplan, 1999). This toxicity is mainly based on the versatility of the transition metals, since they can produce free radicals in redox reactions. For uptake of transition metals, yeast has both a high affinity uptake system and low affinity transporters. High affinity transporters are specific for certain ions and regulated according to requirements for this specific ion. In contrast, low affinity transporters are less responsive to metal needs and can transport different ions. By establishing a dual layer uptake system, cells ensure adequate ion acquisition under conditions of either metal depletion or excess (Johnson *et al.*, 1985; Hentze *et al.*, 2004; Jin *et al.*, 2008; Eide, 2009).

Pumping iron

Iron is essential to almost all known organisms, since it is important for oxygen exchange and oxidizing processes. With its high affinity for oxygen, iron is involved in many cellular redox reactions, as well as being incorporated in heme, thereby acting as electron transporter. The ability of electron transport can cause production of harmful superoxide anion and hydroxyl radicals in the presence of oxygen. Thus, cells have to coordinate free intracellular iron either by strictly regulating iron uptake or by intracellular iron storage through proper sequestration (Kaplan and Kaplan, 2009).

In yeast, intracellular iron concentrations are mainly regulated by plasma membrane iron transport systems. Yeast has both high affinity and low affinity transport systems, as well as cell wall mannoproteins that bind siderophore-bound iron. The high affinity transport system is composed of a ferroxidase (Fet3) (Askwith *et al.*, 1994) and a transmembrane

permease (Ftr1) (Stearman *et al.*, 1996). The theory is that Fet3 oxidizes Fe(II) to Fe(III), which is in turn transported across the membrane by the permease Ftr1. Fet3/Ftr1-dependent iron transport requires oxygen. Under anaerobic conditions, Fet4 and Smf1, the low affinity transporters with broad transition metal specificity, import iron into the cells (Dix *et al.*, 1994; Supek *et al.*, 1996). Additionally, the ARN family of transporters specifically recognizes and imports siderophore-bound iron chelates (Yun *et al.*, 2000). In any case, reduction of ferric to ferrous iron happens at the cell surface through the heme-containing metalloreductases Fre1 and Fre2 (for review see (Radisky and Kaplan, 1999; Kaplan and Kaplan, 2009).

Under iron-replete conditions, the low-affinity transporters Fet4 and Smf1 import most of the required iron into cells. Iron is incorporated in heme and iron sulfur clusters, whereas excess iron is stored in the vacuole, from where it can be recovered if necessary. In contrast, under iron-limiting conditions, the low affinity transporters are not sufficient to provide suitable iron levels. Therefore, cells have to remodel enzymatic activities and metabolic pathways and activate the high affinity iron uptake machinery (Hausmann *et al.*, 2008).

Iron depletion causes transcriptional activation of a small set of about 20 genes, referred to as the iron regulon (Fig.3B, (Rutherford *et al.*, 2003; Courel *et al.*, 2005; Philpott and Protchenko, 2008)), which is regulated by the transcription factors Aft1 (Yamaguchi-Iwai *et al.*, 1995) and Aft2 (Blaiseau *et al.*, 2001). Low iron is sensed by the Aft1 transcription factor, which shuttles between the cytoplasm and the nucleus depending on the cellular iron availability (Yamaguchi-Iwai *et al.*, 2002). Aft2 is an Aft1 paralogue, which can bind to promoter elements of iron transport genes. However, its deletion does not cause any effects on iron transporters, whereas deletion of *AFT1* renders cells hypersensitive to iron depletion.

Low-iron conditions are not directly sensed by Aft1. Instead, they are transmitted by signals coming from the mitochondrial iron sulfur cluster (ISC) biosynthesis (Hausmann *et al.*, 2008). Due to a lack of iron, the synthesis of ISC decreases, resulting in transcriptional activation of iron transport genes independent of cytosolic iron levels (Chen *et al.*, 2004). However, maturation of Fe-S clusters in the nucleus or mitochondria is not required for low-iron sensing by Aft1/Aft2 (Rutherford *et al.*, 2005). So far, the model for low iron

sensing in yeast suggests that under iron depletion the decreased ISC levels are interpreted by a cytosolic complex of glutaredoxins Grx3 and Grx4 and the two cytosolic proteins Fra1 and Fra2, resulting in the nuclear translocation of Aft1 (Fig.3A, (Ojeda *et al.*, 2006; Pujol-Carrion *et al.*, 2006; Kumanovics *et al.*, 2008)).

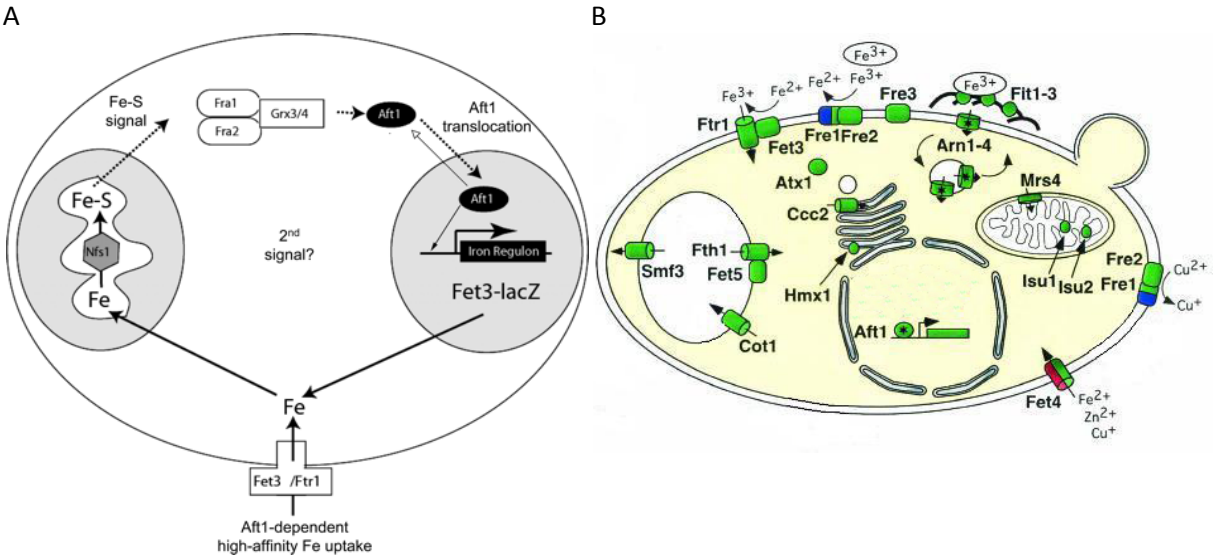

Figure 3: Low-iron sensing in yeast. A. Model for the regulation of low-iron sensing in yeast (Kumanovics *et al.*, 2008). B. Regulation of iron transport machinery under iron-limiting conditions, modified from (Rutherford and Bird, 2004).

Transcriptional activation of the iron regulon by Aft1/Aft2 causes responses by several metabolic processes. First, iron transporters at the plasma membrane are induced, ensuring the import of iron into cells. Second, intracellular iron stores are rapidly mobilized. Third, non-essential processes consuming iron are repressed to establish an iron-saving metabolism. For example, cells switch from biotin synthesis to biotin import, thereby saving iron that would be incorporated into the biotin synthase, which is an ISC-containing enzyme. Furthermore, genes involved in amino acid, nitrogen and tricarboxylic acid metabolism, as well as respiratory pathways change under iron-deplete conditions. Consequently, cells shift their metabolism from an iron-dependent to a parallel iron-independent mode (Shakoury-Elizeh *et al.*, 2004).

Zinc uptake in yeast

Zinc is an essential element for the cell, which, in contrast to iron or copper, is not redox-reactive. It is an important cofactor binding to proteins to establish their structure, conformational change and activity (MacPherson *et al.*, 2006). A prominent example for the importance of zinc in terms of protein conformation and function is the group of zinc-finger transcription factors (Krishna *et al.*, 2003). Although zinc is often referred to as a

trace element, cells actually carry high zinc concentrations. The so called 'zinc quota' refers to the total zinc content of a cell required to maintain its optimum growth (10^7 atoms /cell),(Outten and O'Halloran, 2001). Zinc is mainly bound by proteins because free zinc is highly toxic to cells. The main zinc binding proteins are Cu/Zn superoxide dismutase Sod1, the alcohol dehydrogenase Adh1 and the ribosome (Eide, 2006). Beside these high-affinity zinc binding proteins, zinc also binds to other proteins, as well as to DNA or small cellular compounds such as glutathione. Furthermore, excess zinc is stored in organelles such as the mitochondria, endoplasmic reticulum and the vacuole (Simm *et al.*, 2007).

Similar to the iron uptake systems, there are several zinc transporters regulating zinc homeostasis in yeast. Yeast expresses low-affinity and high-affinity zinc importers at the plasma membrane, as well as zinc transporters in the vacuolar membrane (Fig.4). Interestingly, no plasma membrane zinc exporters have been reported yet. First, the high affinity zinc transporter Zrt1 is expressed due to zinc limitation and specifically imports zinc into the cytoplasm (Zhao and Eide, 1996a). Under zinc-replete conditions, this transporter is endocytosed and degraded (Gitan and Eide, 2000). Second, the low-affinity transporter Zrt2 is active when zinc is abundant (Zhao and Eide, 1996b). Third, due to the fact that there is no zinc exporter, the main site for zinc storage and detoxification is the vacuole. Zrt3 is expressed under zinc shortage conditions to replenish cytoplasmic zinc. In contrast, Zrc1 and Cot1, vacuolar zinc transporters, import zinc into the vacuole for zinc sequestration (MacDiarmid *et al.*, 2000). Expression of zinc transporters is regulated by the transcription factor Zap1. During zinc deficiency, Zap1 transcriptionally activates the plasma membrane zinc transporters, as well as Zrt3 to mobilize zinc stored in the vacuole. Zap1 induces its own transcription under zinc-limiting conditions. Furthermore, if zinc levels are replete, Zap1 activity is repressed (Zhao and Eide, 1997).

Wild type yeast cells can grow on media containing millimolar ranges of zinc. As mentioned before, in yeast, no zinc export system has been identified yet. Therefore, the vacuole is the main site for zinc detoxification and sequestration in yeast. Mutants defective in vacuolar biogenesis or acidification have been shown to be zinc-hypersensitive (Ramsay and Gadd, 1997). Therefore, a functional V-ATPase is required to import zinc into the vacuole. Most likely, the established proton gradient across the vacuolar membrane drives zinc import into the vacuole. Depending on the cellular zinc

status, vacuolar zinc levels can reach up to 100mM zinc (i.e., $7x10^8$ zinc atoms per cell in the vacuole) (Simm *et al.*, 2007). Such enormous storage capacities provide even following yeast generations with sufficient zinc under changing nutrient conditions.

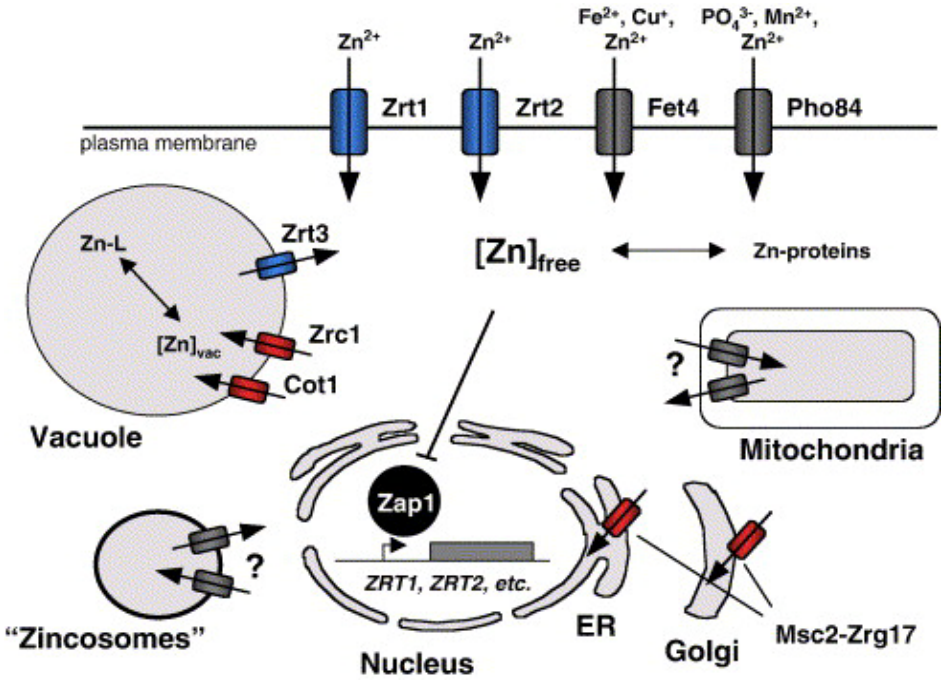

Figure 4: Scheme of proteins regulating zinc homeostasis in yeast, including plasma membrane and vacuolar zinc transporters, zincosomes as well as the zinc-responsive transcription factor Zap1 (Eide, 2006).

4. AIMS

This study aimed to decipher the mode of action of the antiviral drug PDTC, as well as potential target genes for PDTC. As PDTC shows antifungal activity, we applied a chemical genetic approach using the yeast *Saccharomyces cerevisiae* as simple eukaryotic model organism by combing transcriptional profiling and genome-wide phenotypic screenings. Target genes identified in yeast may help to ascertain structural and sequence homologues in mammalian genomes.

To analyze the transcriptional response and the kinetics of yeast cells to sublethal concentrations of PDTC, we performed whole-genome DNA microarray-based expression profiling. The microarray data sets were analyzed by extensive bioinformatics and verified by Northern blotting and immunoblotting. Clustering and Gene Ontology enrichment identified the functional categories and pathways involved in the transcriptional response to PDTC. Since expression profiling misses genes whose mRNA levels do not change upon drug treatment, the transcriptomics were complemented by a functional genomic screen.

The EUROSCARF yeast deletion strain collection, representing haploid viable single deletions representing some 4800 yeast genes, were subjected to robotic screening to identify genes mediating PDTC resistance. By systematically screening the entire yeast gene deletion collection, it is possible to identify all non-essential yeast genes that can modulate PDTC susceptibility.

Finally, genes and pathways identified by transcriptomics or phenotypic screening were further investigated by biochemical, genetic, physiological and proteomic studies.

Taken together, the eukaryotic model system baker's yeast and its genetic tractability were exploited to pursue several approaches to identify cellular targets of the antiviral drug PDTC, but also to study the mechanisms of its toxicity and resistance.

5. MATERIALS AND METHODS

Chemicals and reagents

Pyrrolidine dithiocarbamate (PDTC) was purchased from Alexis Biochemicals, Lausen, Switzerland, dissolved in H_2O and a 500mM stock solution was stored at -20°C.

Media and growth conditions

All media and buffers were prepared according to Karl Kuchler standard laboratory protocols.

Yeast media and growth

Rich medium (YPD) and synthetic medium (SC) were prepared essentially as described elsewhere (Kaiser, 1994). All media were autoclaved, heat sensitive substances were sterile-filtered and added to the media afterwards. For solid media, 250 ml of 4% agar were added to 250 ml of 2x medium. All yeast strains were routinely grown at 30°C unless otherwise indicated. For growth inhibition tests, exponentially growing cells were adjusted to OD_{600} of 0.2, serially diluted to $2x10^{-4}$ and equal volumes were spotted onto YPD plates containing different substances and concentrations. *S. pombe* was grown on YES medium as described in (Moreno *et al.*, 1991). For viability assays, cells were grown in liquid medium supplemented with PDTC and/or metal ions for 24h. Afterwards, cells were plated onto YPD plates and colony-forming units were determined after 48h incubation. Stressed cells were normalized to untreated wild type cells.

Rich medium (YPD)

50ml of 20% sterile glucose was added to 450ml 1x YPD to prepare liquid medium with a final concentration of 2% glucose. YPD plates contained glucose at a final concentration of 2% and 2% agar.

	1x YPD	2x YPD
Yeast extract	10g/l	20g/l
Peptone	20g/l	20g/l
Glucose (w/v)	2%	4%

Minimal medium

Minimal medium (MM) was prepared with 2x YNB without amino acids and glucose was added at a final concentration of 2%. MM solid media contained 2% glucose and 2% agar.

1x MM

Bacto-YNB w/o aa 6.7g/l
Glucose (w/v) 2%

Drop-out media

SC medium (500ml) was prepared with 2xSC medium and 250ml sterile H_2O and glucose were added to a final concentration of 2%. 5ml of the required amino acids from 100x stocks were added. SC solid media contained 2% glucose and 2% agar.

2x SC

Bacto-YNB w/o aa and $(NH_4)_2SO_4$ 3.4g/l
Ammonium sulfate 10.0g/l
Amino acid mix 2.86g/l

YES medium (Fission yeast medium)

5g/l yeast extract

30g/l glucose

supplements: 225mg/ml adenine, histidine, leucine, uracil, and lysine hydrochloride.

Sterile stock solutions:

Glucose: 20%, Agar: 4%

100x URA: 4g/l L-uracil in H_2O
100x HIS: 6g/l L-histidine in H_2O
100x LEU: 26g/l L -leucine in H_2O
100x TRP: 8g/l L-tryptophane in H_2O (filter-sterilized, 4°C)
Amino acid mix (per 29g):
0.4g L-arginine 0.6g L-tyrosine
0.6g L-isoleucin 8.0g L-serine
1.0g L-phenylalanine 2.0g L-glutamic acid
2.0g L-aspartic acid 3.0g L-valine
3.0g L-methionine 3.6g L-lysine
4.0g L-threonine 0.8g adenine

Sporulation media

250ml	2x
KAc	5g
Bacto-Yeast extract	0.5g
glucose	0.25g
Bacto agar	10g

E. coli media

For LB solid media, 2% agar was added to 2x LB. For selective media, e.g. LB-amp plates, 100µg/ml ampicillin (100mg/ml stock, H_2O) were added.

	1x LB	2x LB	SOC
Tryptone	10g/l	20g/l	20g/l
Yeast extract	5g/l	10g/l	5g/l
NaCl	10g/l	20g/l	10mM
KCl	-	-	2.5mM
$MgCl_2$	-	-	20mM

Bacterial strains

DH5α *F-, λ-, endA1, hsdR17(rk-, mk+), supE44, thi-1, recA, gyrA96,relA1, Φ80lacZΔM15* (Hanahan, 1983)

TOP10 F- *mcr*A Δ(*mrr-hsd*RMS-*mcr*BC) ϕ80*lac*ZΔM15 Δ*lac*X74 *rec*A1 *ara*D139 Δ(*araleu*)7697 *gal*U *gal*K *rps*L (StrR) *end*A1 *nup*G Invitrogen

Mating of yeast strains

To generate a *sod1*Δ *sod2*Δ double deletion strain, we mated the BY4742 *sod1*Δ and the BY4741 *sod2*Δ strains, followed by selecting the diploids. Afterwards cells were forced to undergo sporulation, followed by tetrad dissection. For tetrad dissection, cells were resuspended in water and treated with 1µl zymolyase (20mg/ml) for 5 minutes at RT to remove the cell wall. Spores were physically separated with the needle of the micromanipulator (Singer MSM) and placed one by one on a YPD plate.

Yeast strains used in this study

Name	Genotype	Reference
BY4741	*MAT***a**; *his3Δ1*; *leu2Δ0*; *met15Δ0*; *ura3Δ0*	(Brachmann *et al.*, 1998)
BY4742	*MAT*α ; *his3Δ1*; *leu2Δ0*; *lys2Δ0*; *ura3Δ0*	(Brachmann *et al.*, 1998)
BY4743	*MAT***a**/α *his3Δ1/his3Δ1 leu2Δ0/leu2Δ0 LYS2/lys2Δ0 met15Δ0/MET15 ura3Δ0/ura3Δ0*	(Brachmann *et al.*, 1998)
EUROSCARF yeast deletion collection	http://web.uni-frankfurt.de/fb15/mikro/euroscarf/index.html	
W303-1A	*MAT***a**, *leu2-3,112 trp1-1 can1-100 ura3-1 ade2-1 his3-11,15*	by Rodney Rothstein and Stephan Bartsch
AMP1600	*MATa RIMI-531::TRP1, rme1Δ5::LEU2, IME2-5-lacZ::URA3, ura3, leu2::hisG, trp1::hisG, lys2, ho::LYS2*	(Li and Mitchell, 1997)
AMP1603	*MATa RIMI-HA2 rim13-1 arg6, rme1Δ5::LEU2, IME2-5-lacZ::URA3, ura3, leu2::hisG, trp1::hisG, lys2, ho::LYS2*	(Li and Mitchell, 1997)
AMP1604	*MATa RIMI-HA2 arg6, rme1Δ5::LEU2, IME2-5-lacZ::URA3, ura3, leu2::hisG, trp1::hisG, lys2, ho::LYS2*	(Li and Mitchell, 1997)
AMP1605	*MATa rim1Δ12 arg6, rme1Δ5::LEU2, IME2-5-lacZ::URA3, ura3, leu2::hisG, trp1::hisG, lys2, ho::LYS2*	(Li and Mitchell, 1997)
AMP1606	*MATa arg6 his3, rme1Δ5::LEU2, IME2-5-lacZ::URA3, ura3, leu2::hisG, trp1::hisG, lys2, ho::LYS2*	(Li and Mitchell, 1997)
DY1457	*MAT*α, ura3-52, leu2-3, trp2-1, his3-11, can1-100(oc), ade6	(Chen *et al.*, 2004)
OCY355	*MAT*α, ura3-52, leu2-3, trp2-1, his3-11, can1-100(oc), ade2, ho::*FET3*LacZ	(Kumanovics *et al.*, 2008)
ATCC2001	*C. glabrata* wild type strain available at www.atcc.org	
Sc5314	*C. albicans* wild type strain	(Gillum *et al.*, 1984)
K11217	*S. pombe* wild type strain	Kindly provided by K. Nasmyth
YCG31	Isogenic to W303-1A, *ARN4*-Cit::*LEU2*	Kindly provided by C. Gregori
YCG31Δr	Isogenic to YCG31, *rim101*Δ::*kanMX4*	Kindly provided by C. Gregori
YCG31Δa	Isogenic to YCG31, *aft1*Δ::*kanMX4*	Kindly provided by C. Gregori
YCG14	Isogenic to W303-1A, *STL1*-Cit::*TRP1*	Kindly provided by C. Gregori
YCG12	Isogenic to W303-1A, *MLP1*-Cit::*URA3*	Kindly provided by C. Gregori
YCG12Δs	Isogenic to YCG12, *slt2*Δ::*kanMX4*	Kindly provided by C. Gregori
YNLSS12	Isogenic to BY4741, *sod1*Δ:: *kanMX4, sod2*Δ:: *kanMX4*	This study

Table 1: Yeast strains used in this study.

General methods of molecular biology

Standard methods like agarose gelelectrophoresis , determination of DNA concentration and PCR, as well as general cloning techniques including restriction analysis, dephosphorylation and ligation were performed as described in (Sambrook, 2001). For purification and elution of DNA fragments from agarose gels, the Peqlab gel extraction kit was used according to the manufacturer's recommendations. For restriction digestions

and dephosphorylation, Fermentas enzymes were used according to the manufacturer's recommendations.

For plasmid preparation, the STET minipreparation protocol adapted from Holmes and Quigley was used (Holmes and Quigley, 1981). 2ml of bacterial overnight culture were harvested by centrifugation at 6000rpm for 3 min in a table-top centrifuge. The pellet was resuspended in 500µl of STET buffer and 20µl of lysozyme (20mg/ml) were added. After inverting the tube several times, it was incubated on ice for 5 minutes. For lysis, the sample was incubated on 95°C for 70 seconds and immediately put on ice afterwards. After centrifugation for 10 minutes at 13000 rpm, the white pellet was removed and 500µl of isopropanol were added. The mixture was centrifuged at 13000rpm for 15 minutes, the pellet was washed with 70% ethanol and resuspended in 100µl of TE buffer. Finally, RNaseA was added to a final concentration of 50µg/ml (Karl Kuchler standard laboratory protocol).

STET-buffer (100ml): 8g Saccharose
0.5ml Triton X-100
10ml 0.5M EDTA
5ml 1M Tris/HCl pH 8.0
0.45µm filter-sterilize (Millipore)

Isolation of RNA from yeast

Total yeast RNA was isolated by the hot phenol method (Sambrook, 2001). 50ml of a yeast culture were harvested at 3000rpm, for 5min, at 4°C and washed with ice-cold water. The pellet was resuspended in 400µl of 50mM sodium acetate (pH 5.3) plus 10mM EDTA (pH 8). 40µl of 10% SDS and 400µl of acid phenol (pH 4.3) were added and the sample was incubated at 65°C for 15 minutes followed by rapid chilling on ice. The sample was centrifuged at 13000 rpm for 5 minutes at RT and the aqueous phase was used for PCI extraction, followed by two times chloroform extraction. For RNA precipitation, 1/10 volume of 3M sodium acetate (pH 5.3) and 2.5 volumes of ice cold 100% ethanol were added to the sample. After centrifugation (15min, 4°C, 13000rpm), the pellet was washed with 70% ethanol, dried at 55°C and resuspended in 100µl of TE buffer. RNA concentration was measured at 260nm in TE, pH 7, (Karl Kuchler standard laboratory protocol).

Northern Blot Analysis

About 20µg of total RNA were separated on a 1.4% agarose gel and transferred to nylon membranes (Amersham Biosciences). Methylene blue staining was used as control for equal RNA loading. Northern blots were pre-hybridized for 3h at 65°C. PCR-amplified probes were radiolabeled by incorporation of [-32P]dCTP using a MegaPrime labeling kit (Amersham Biosciences). The radiolabeled probes were added to the prehybridization solution after purification on a NICK column (Amersham Biosciences). Membranes were washed at 65 °C three times in 2x SSC, 1% SDS, and three times in 1x SSC, 1% SDS, and then exposed to x-ray films at -80 °C, (Karl Kuchler standard laboratory protocol).

Pre-hybridization solution:	2ml 50x Denhardt reagent
	1ml 20x SSC
	500µl 20% SDS
	6.5ml sterile water
	40µl ssDNA (10mg/ml)
50x Denhardt Reagent:	1% (w/v) Ficoll 400
	1% (w/v) Polyvinylpyrrolidone
	1% (w/v) Bovine Serum Albumine

DNA Microarray Experiments

Microarrays (Yeast 6.4K Arrays) were ordered from the Microarray Centre, University Health Network, Toronto (www.microarrays.ca). 50ml cultures of BY4741 or *aft1*Δ were grown in YPD to an OD_{600} of about 0.4. PDTC was supplemented, untreated control cells and PDTC treated cells were harvested after 1, 3 and 5 hours, washed with ice-cold water and frozen immediately. Total RNA was prepared by the hot phenol method and 20µg were used for cDNA synthesis using 200 units of Superscript II reverse transcriptase (Invitrogen) with either Cy3-dCTP or Cy5-dCTP. Labeled cDNAs were pooled, and RNA was hydrolyzed for 20 min in 50mM NaOH at 65 °C, followed by neutralization with acetic acid and probe clean-up with CyScribe GFX purifiaction kit (Amersham Biosciences).

Hybridization to whole genome cDNA microarrays was done in DigEasyHyb (Roche Applied Science) solution at 37°C overnight with 70µg of salmon sperm DNA/ml as a carrier. Microarrays were washed three times in 1x SSC, 0.1% SDS at 50 °C, followed by a 1-min wash in 1x SSC at room temperature. Glass slides were spun dry for 5 min at 500rpm in a tabletop centrifuge, scanned on an Axon 4000B scanner (Molecular Devices).

All microarray experiments were carried out with three independent RNA preparations and at least one technical replicate using dye-swaps. Microarray data sets are MIAME-compliant.

Computational analysis of microarray data and screening results

Gridding and spot identification on microarrays were performed using the Gene Pix Pro 4.1 software (Axon). For preprocessing, the background was subtracted and subsequently normalized, using the print-tip loess method of the limma Bioconductor/R package (Wettenhall and Smyth, 2004). To identify differentially expressed genes, a linear model and empirical Bayesian-moderated F-statistics were used with cut-off values of 0.001 for the adjusted p-value and a 2-fold expression change, as well as A-values ≥7 (Smyth, 2004).

Genes identified either on the microarrays or in the functional screening were grouped by gene ontology enrichment according to the predicted biological process using the GO Termfinder program provided by the *Saccharomyces* Gene Database (www.yeastgenome.org). Clustering of differentially expressed genes was performed using the MEV software using the linkage method and Euclidean distance (Saeed *et al.*, 2003; Saeed *et al.*, 2006).

Preparation of yeast cell extracts and immunoblotting

For immunoblotting, total cell-free protein extracts were prepared by the trichloroacetic acid (TCA) method. About 5 OD_{600} equivalents of cells were harvested. The pellet was resuspended in 1ml ice-cold water and supplemented with 150µl YEX lysis buffer. After 10 minutes incubation on ice, proteins were precipitated by adding 150µl of 50% TCA. Samples were centrifuged at 13000 rpm and the pellet was resuspended in sample buffer.

YEX lysis buffer:	1.85M NaOH 7.5% β-mercaptoethanol
Protein sample buffer:	40mM Tris–HCl pH 6.8 8M urea 5% sodium dodecyl sulfate (SDS) 0.1mM EDTA 0.1g/l bromophenol blue 1% β-mercaptoethanol

SDS-polyacrylamide gel electrophoresis (SDS-PAGE)

Cell lysates equivalent to 0.5 OD_{600} units were resolved by SDS–polyacrylamide gel electrophoresis gels and blotted onto nitrocellulose membranes.

7.5% running gel:	4.5% stacking gel:
5ml H_2O	6ml H_2O
2.5ml 1.5 M Tris pH 8.8	2.5ml 0.5M Tris pH 6.8
2.5ml acrylamide (30%)	1.5ml acrylamide (30%)
50µl SDS (20%)	50µl SDS (20%)
10µl TEMED	10µl TEMED
100µl APS (10%)	100µl APS (10%)

Protein running buffer: 1.5g Tris
7.2g glycine
4.0g SDS

To investigate PDTC-dependent changes in Rim101 processing and CoxIV protein levels, we performed immunoblotting using the monoclonal mouse anti-HA 12CA5 (Roche) and the mouse anti-CoxIV antisera (kindly provided by Andreas Hartig), respectively. Polyclonal anti-Swi6 antibodies (kindly provided by Kim Nasmyth) were used to verify equal loading.

Proteins were transferred to a nitrocellulose membrane by blotting for 1h at 25V in a Trans-Blot semidry transfer cell (Biorad), followed by blocking of unspecific binding with Blotto (TBS-T, 5% milk powder) shaking for 1h at RT. The primary antibodies, usually diluted 1:1000 or according to the manufacturer's recommendations, were incubated over night shaking at 4°C. The membrane was washed 3 times with 1x TBS-T followed by incubation with the secondary antibody conjugated to horse radish peroxidase (HRP) (1:7500) for 45 minutes. The membrane was washed again 3 times with 1xTBS-T, then equilibrated with Super Signal West Pico Chemiluminescent Substrate (Pierce, VWR) and exposed to CL-Xposure films (Pierce) (Karl Kuchler standard laboratory protocol).

Anode buffer 1: 0.3M Tris
20% methanol (v/v)
Anode buffer 2: 25mM Tris
20% methanol (v/v)
Cathode buffer: 25mM Tris
40mM 6-amino-n-hexanoic acid

If desired, blots can be stripped by shaking 15min in 50ml stripping buffer in a 50°C water bath and reused again for detection with another antibody

Stripping buffer: 100mM ß-mercaptoethanol
2% SDS
62.5mM Tris/HCl pH 6.7

Beta-galactosidase assays

Cells containing a genomically integrated *FET3*-LacZ reporter construct (OCY355) were grown in YPD medium to an OD_{600} of about 0.6. Cultures (50ml) were harvested after incubation with 100µM PDTC or being left untreated for 3 hours. Cells were resuspended in 250µl of breaking buffer plus protease inhibitor. Glass beads were added and crude cell extracts were prepared using a Fast Prep (FastPrep (2 × 15″, speed 5, Thermo Savant). The extract was clarified by centrifugation at 4°C 13000rpm for 15 minutes. Protein concentration of the extracts was determined using Coomassie Plus (Bradford) Protein Assay (Pierce) according to the manufacturer's recommendations.
Enzyme measurements were carried out by adding 10-100µl of cell extract to 0.9ml of Z-buffer and adjusting the volume to 1ml with breaking buffer. After incubating the mixture at 28°C for 5 minutes, the reaction was initiated by adding 200µl ONPG solution and further incubation at 28°C. The exact time was measured until the mixture turned to a pale yellow color. The reaction was terminated by adding 0.5ml of Na_2CO_3 stock solution. Finally optical density at 420nm was measured and normalized. The specific activity of the extract was expressed according to the formula:

$$\frac{OD_{420} \times 1.7}{0.0045 \times \text{protein (mg/ml)} \times \text{extract volume (ml)} \times \text{time (minutes)}}$$

OD_{420} is the optical density of the product o-nitrophenol, at 420nm. The factor 0.0045 is the OD of 1nmol/ml solution of o-nitrophenol. The factor 1.7 corrects for the reaction volume. Specific activity is expressed as nmoles/minute/mg protein (Kaiser, 1994).

Breaking buffer: 100mM TrisCl pH8
1mM dithiothreitol (DTT)
20% Glycerol

Z-buffer: 16.1g $Na_2HPO_4*7H_2O$
5.5g $NaH_2PO_4*4H_2O$
0.75g KCl
distilled water to adjust to a final volume of 1l
ONPG stock solution: 4mg/ml in Z-buffer

Fluorescent detection of zinc influx into yeast cells

About 2x 10^8 cells of a *pdr5*Δ *pdr12*Δ double deletion strain (laboratory strain collection) were loaded with 30µM mag-fura-2 (Molecular Probes, Invitrogen) for 30 minutes in 1xTBS; cells were washed three times and finally resuspended in 10ml TBS. Experiments were performed with constant agitation in 3ml silica cuvettes containing 2ml aliquots of cell suspensions. Intracellular zinc accumulation was monitored in real-time kinetics over a 500 second-period using a spectrofluorimeter LS-55 (Perkin-Elmer) by continually alternating the excitation wavelengths of 340 and 380nm in 20ms intervals and recording the emission at 509nm. Moreover, 10µM $ZnSO_4$, 10µM $CaCl_2$ or 10µM $CuSO_4$, and 100µM PDTC and 50µM EDTA were added to cell suspensions at indicated time points.

Phenotypic screening of the EUROSCARF deletion collection

For large scale phenotypic profiling, the 4800 haploid viable single gene deletion strains of the EUROSCARF deletion collection (http://web.uni-frankfurt.de/fb15/mikro/euroscarf/) were grown on YPD plates in 96-well format. For transferring strains to PDTC-containing plates and control YPD plates, we used the RoToR HDA robot (Singer Ltd., Roadwater, UK). Growth was inspected after 2 days incubating at 30°C. After incubation, plates were scanned with an HPScanjet G3010, using the Adobe Photoshop CS3 software. All strains displaying PDTC-sensitivity strains identified in the first screening were manually re-spotted for confirmation. Therefore, equal volumes of serial dilutions of exponentially growing cells ranging from an OD_{600} of 0.2 to $2x10^{-4}$ were spotted onto PDTC-plates and control plates.

Detection of reactive oxygen species

For detection of accumulated reactive oxygen species after incubation with PDTC, we stained yeast cells with H_2DCF-DA, dihydroethidium (DHE) and dihydrorhodamine (DHR).

Dyes were ordered from Invitrogen Molecular Probes, Oregon. Yeast cells were stressed for 15-30 minutes with PDTC or H_2O_2 as control, washed with 1xPBS and resuspended in PBS. Dyes were added and samples were incubated at 30°C for 10 minutes and directly used for FACS analysis. Chemiluminescence was measured using a FACS Calibur, PD Biosciences.

Dyes were used to a final concentration of:

DHR: 5µg/ml
H_2DCF-DA: 10µg/ml
DHE: 2µM

Analyis of PDTC response using promoter-tagged reporter strains

Promoter-tagged reporter strains were inoculated in YPD pH 4 and grown over night at 30°C, shaking. Cultures were diluted to an OD_{600}~0.2 in YPD pH 4, 6.5, and 9, respectively. After three hours cells were stressed or left untreated for two hours, washed with 1xPBS and resuspended in 1xPBS to a final concentration of $1x10^6$ cells/ml). Fluorescence was detected using a FACS Calibur, PD Biosciences or pictures were taken using the Olympus Cell R Live Cell Imaging Unit.

The promoter tagged-reporter strains for the Rim101 pathway (*ARN4*-Cit wild type, *ARN4*-Cit *rim101*Δ, *ARN4*-Cit *aft1*Δ) carried a genomically integrated *ARN4*-citrine construct (1kb of the *ARN4* promoter, citrine, 500bp of the ARN4 terminator). Additionally, we used reporter strains for the PKC-pathway (*MLP1*-Cit wild type, *MLP1*-Cit *slt2*Δ), as well as the HOG-pathway (*STL1*-Cit wild type). All reporter strains were kindly provided by Christa Gregori.

Vacuolar staining with fluorescent dyes

For carboxy-DCFDA vacuolar staining, yeast cells were grown to an OD_{600} of 0.8 before adding PDTC. After 2 hours incubation at 30°C with shaking, the fluorescent dye was added and cells were incubated at room temperature for another 15 minutes. Cells were washed with 50mM natrium citrate buffer, pH 7.5, 2% glucose, resuspended in buffer and kept on ice for microscopy. For vacuolar staining with FM4-64, cells were stained with FM4-64 for 15 minutes at 30°C, washed and resuspended in rich medium. Cells were either stressed or left untreated for the indicated time points, washed, resuspended in

PBS and used for microscopy. The cells were examined using an Olympus Cell-R Live Imaging Unit.

Carboxy-DCFDA (Invitrogen, Molecular Probes, C369) in DMSO, 10mM stock, stored at -80°C.

FM4-64 (Invitrogen, Molecular Probes, T3166) in DMSO, 3.2µM stock, stored at RT.

Buffers and solutions

TAE (50x stock solution):	2M Tris/HCl pH8 1M acetic acid 50mM EDTA
Electrophoresis buffer:	1xTAE
DNA Loading buffer:	1.2ml 10xTAE 0.6ml 5% bromphenol blue 0.6ml 5% xylene cyanol 4.8ml 100% glycerol 4.8ml H_2O
1M DTT	dissolved in 0.01M NaOAc pH 5.2
PBS, pH 7.4	87.7g NaCl 2.6g NaH_2PO_4 22.5g Na_2HPO_4

1000x Ampicillin 120mg/ml

G418 in H20, 200mg/ml 1000x stock

20x SSC (1l)	876.5g NaCl 441g NaCitrat pH 7.0
TE	100mM Tris-HCl pH7.5 10mM EDTA pH 8.0
10x TBS	1.44M NaCl 0.5% Tween 20 250mM Tris-HCl pH 7.5

6. RESULTS

PDTC shows antifungal activity

The effect of PDTC on growth of *Saccharomyces cerevisiae*, *Candida albicans*, *Candida glabrata* and *Schizosaccharomyces pombe* was analyzed by growth inhibition assays on agar plates (Fig.5). Serial dilutions of yeast cultures were spotted onto PDTC-supplemented plates. Cell growth was inhibited in a dose-dependent manner in both non-pathogenic and pathogenic yeast species, although not to the same degree. Namely, *S. cerevisiae*, *C. albicans* and *S. pombe* were sensitive at 30µM PDTC, whereas *C. glabrata* was more resistant to PDTC, growing up to a concentration of 75µM. However, it is known that *C. glabrata* shows increased tolerance to a variety of compounds including antifungals such as azoles (Pfaller and Diekema, 2004).

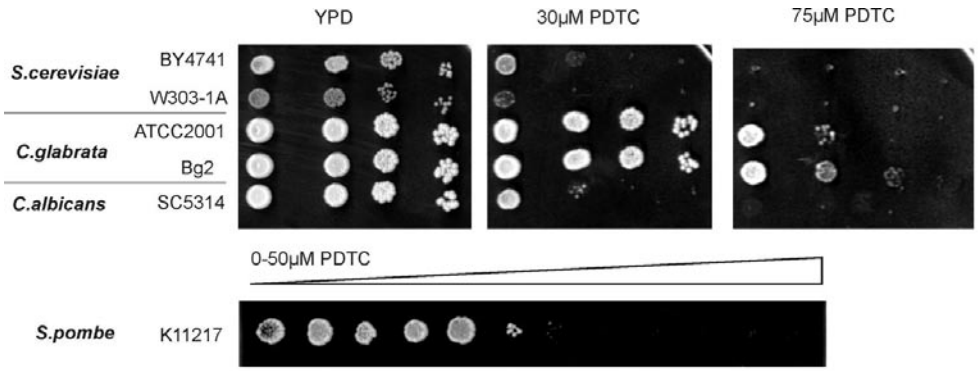

Figure 5: Spot assays of various yeast species to show PDTC-sensitivity. Cells were spotted in serial dilutions ranging from OD_{600} 0.2 to 2x 10^{-4} onto PDTC containing plates and grown at 30°C for 2 days. *S. pombe* requires YES medium and was therefore spotted onto a gradient plate ranging from 0 to 50µM PDTC (OD_{600} of 0.2).

In addition, we performed growth curves and viability assays with *S. cerevisiae* wild type cells to investigate the PDTC tolerance in liquid culture. Cells were grown in rich medium supplemented with increasing concentrations of PDTC, monitoring OD_{600} over time (Fig.6A). The growth curves showed a dose-dependent growth inhibition. At low concentrations (25µM), PDTC-treated cells responded with an elongated lag-phase and a delayed period to reach the stationary phase. At higher concentrations (100µM), PDTC caused complete growth inhibition. For testing viability, we treated cells with 100 to 325µM PDTC for 24h in liquid culture, determined colony forming units on YPD plates and set them relative to unstressed cells (Fig.6B). Remarkably, we found that PDTC lead to growth inhibition rather than killing of cells. The antifungal activity suggested using yeast

as a model system by exploiting well-established large-scale screening techniques to identify putative PDTC target genes.

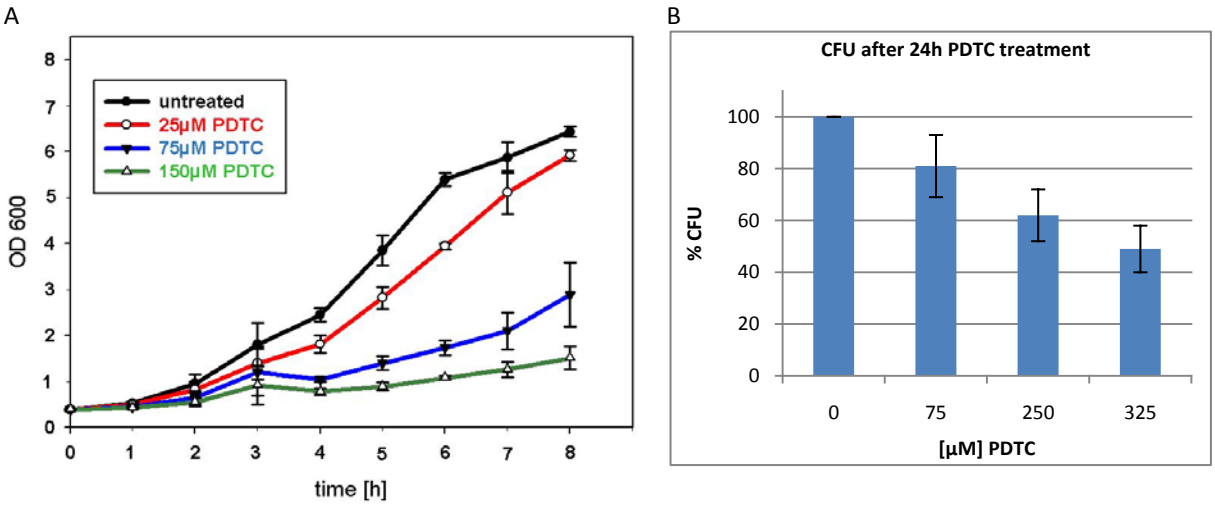

Figure 6: PDTC caused dose-dependent growth inhibition in yeast. A. Cells were grown in YPD medium supplemented with increasing concentrations of PDTC, monitoring OD_{600} over time. B. Viability assays. Cells were grown in liquid YPD medium with different concentrations of PDTC. After 24 hours of PDTC treatment, cells were plated on YPD plates. CFU was determined and normalized to untreated cells.

To characterize the genes involved in PDTC response, we screened by two types of genome-wide analysis. First, transcriptional changes were measured by whole-genome DNA microarrays. Second, we functionally screened the EUROSCARF yeast gene deletion collection.

Expression profiling in response to PDTC treatment

To examine the regulatory effects and kinetics of PDTC exposure on the yeast transcriptome, we performed whole-genome DNA microarray analysis. Therefore, wild type yeast cells were grown to the mid-logarithmic growth phase in rich medium, and treated with PDTC for 1, 3 or 5 hours. Transcript data of three independent biological and one technical replicate were generated comparing PDTC-treated versus untreated cells. Microarray results were statistically evaluated considering changes more than two-fold as significant and confirmed at RNA level by Northern blot analysis.

The PDTC transcriptome consisted of more than 200 differentially expressed genes, indicating a major transcriptional shift in yeast. Gene ontology (GO) enrichment of the microarray data using the *Saccharomyces* Gene Database GO Termfinder revealed that the main functional categories comprised of the iron regulon, aerobic respiration and general metabolic changes (Table 2).

Categories	Gene names	N° of Genes
Iron regulon Aft1/Aft2 targets	*FTH1, SIT1, FTR1, ARN1, ARN2, CTR2, FRE1, CCS1, FET3, ENB1, FIT1, FIT2, FIT3, YLR126C, ISU2, ISU1, FTR1*	17
Carboxylic acid metabolic process	*CYS3, GCV3, SHM1, CHA1, SFA1, GLT1, GCV1, ARO3, HOM3, MET6, LPD1, ARO9, POT1, ELO1, FBA1, FAS1, ILV5, ILV2, GCV2, LEU4, LYS9, LEU9, HIS3, GDH1, CAR1, GLN1, SHM2, URA1, GTT1, URA4*	30
Purine biosynthetic process	*ADE1, ADE8, ADE5,7, ADE13, ADE17, ADE3, ADE12*	7
Stress response to drug / toxin	*AAD3, RPN4, UBC5, YCF1, SNF1, AAD6, AAD16, YML131W, DDR48, HOR7, LAP3, GRE2, TIR2, OYE3, HSP31, SFP1, OYE2*	17
Response to oxidative stress	*YDL124W, CTA1, TRR1, YPR1, GRX2, TRX2, STB5, SOD1, CCP1, TRX1, AHP1, ZWF1, ATX1, GLR1, PEP4*	15
Hexose transport	*HXT10, HXT4, HXT5, HXT8, GAL2, HXT11, HXT12*	7
Respiration & citric acid cycle	*COX6, COX5A, COX9, COX13, IDH1, ACO1, RIB3, POR1, QCR7*	9
Heme	*HEM13, YHB1, YCP4*	3
Transport	*STP22, TRS23, INH1, VHT1, TOM6, HNM1, MUP1, TPO1, DIC1, SFH5*	11
Ergosterol biosynthesis	*ERG3, ERG1, ERG27, ERG11*	4
Telomere maintenance	*YGL039W, NMD2, CST6, HCR1, LST7, SWD1, PNC1*	7
Transcription/ translation	*MRP8, EFB1, GCD2, RLI1, GAT1, ERB1, UTP23, SSZ1, RLP7, TUF1*	10
DNA replication/ repair	*RNR2, RNR4, DON1, WTM1, YPL033C, NNF1, RFA2, SIM1*	8
Oxidoreductase activity	*ADH7, YDR541C, DLD3, YGL157W, ADH6, YNL134C*	6
Other	*PHO5, PHO11, PHO86, IRC7, IZH1, FRM2, MFA1, EMI2, AGA2, KOG1, BAR1, BNR1, MSG5, LAP4, AIM46, RIB4, SLA1, EHD3, FLO9, NDE1, SNC2, PAC11, TEC1, PEX5, UGP1, RMD6, AIM18, PMI40, SCW4, CWP1, SRP40, EMI1, VHS1, YRO2, PRE8, MRH1, APT2, TIP1, LRG1, CNS1, WWM1, RPN6, DPH5, FRQ1, FMP43*	45
Unknown	*YAL065C, YMR173W-A, YCR102C, YJL217W, YER156C, YGR146C, YDR476C, YOR285W, YKL088W, YDR154C, YKL030W, YPL067C, YKL066W, YLL044W, YDR271C, YBR053C, YJL068C, YFR024C, YHR213W, YAR073W, YKL171W, YEL033W, YDR119W, YLR460C, YNL208W, YCR074C*	26

Table 2: Functional categories of differentially expressed genes during PDTC treatment. Genes that were at least 2-fold (p-value ≤ 0.05) differentially expressed on our microarrays were categorized using the *Saccharomyces* Gene Database Gene Ontology termfinder (www.yeastgenome.org).

PDTC induced an immense stress response in yeast by changing expression levels of hundreds of genes. To identify the regulatory associations of the differentially expressed genes, we clustered the genes with YEASTRACT (Teixeira *et al.*, 2006). Thereby, differentially expressed genes identified through microarrays were grouped according to their transcription factors or potential regulators. Supporting the findings of the GO enrichment, the main transcription factors required for general and oxidative stress

response genes as well as proteasome and multidrug resistance genes were activated (Table 3). These included the transcriptional regulators Yap1, Msn2/4, Rpn4 and Sfp1 correlating with the activation of general stress response genes, as well as with repression of ribosomal genes (i.e. protein synthesis) under various conditions (Gasch *et al.*, 2000; Wu *et al.*, 2008).

Some 60 % of the genes are regulated by the Yap1 transcription factor (Table 3), which is required for oxidative stress tolerance (Lee *et al.*, 1999). Furthermore, the stress-responsive transcription factors Msn2 and Msn4, which are the main regulators of the environmental stress response program (Gorner *et al.*, 1998), were also found. Additionally, we found Pdr1, a transcription factor regulating multidrug resistance genes regulating about 28% of the PDTC-induced genes (Balzi *et al.*, 1987). Moreover, Rpn4, stimulating the expression of proteasome genes, and Gcn4, which is involved in amino acid biosynthesis, were also activated by PDTC (Xie and Varshavsky, 2001). Interestingly, the clustering specifically identified the iron-responsive transcription factor Aft1 (Yamaguchi-Iwai *et al.*, 1995) as one of the major responders.

The highest induced genes at least at one time point were *FIT1*, *HSP31*, *YNL134C*, *GRE2*, *FIT2*, *YLR460C* and *FIT3*. *HSP31* encodes a stress responsive protein probably acting as a chaperone. Gre2 is a metalloreductase involved in the high osmolarity glycerol (HOG)-pathway. *YNL134C* encodes a putative protein of unknown function that is induced upon DNA damage. *YLR460C* belongs to the quinone oxidoreductase family. Both, *YNL134C* and *YLR460C* are members of the medium-chain dehydrogenase/reductase (MDR) family. Many enzymes of the MDR family play roles in detoxification and environmental stress response coping with osmotic and oxidative stress. *FIT1*, *FIT2* and *FIT3* are cell wall mannoproteins involved in retention of siderophore-bound iron in the cell wall. Hence, among the 7 most induced genes, we identified three Aft1-regulated genes.

Transcription factor	%	ORF
Yap1	60.3	*EFB1, CYS3, ADE1, PHO11, IMD1, SLA1,* YBR053C, *YRO2, TIP1, PHO5, CNS1, FTH1, SHM1,* YCL026C-A, *YCP4,* YCR102c, *ADH7, AAD3, RPN4, RPN6, YDL124w, SFA1, GLT1, GCV1, MRH1, ARO3, EHD3, VBA4, YCF1,* YDR154c, *CTA1, DON1, TRR1, YPR1, FRQ1, ADE8, RIB3, GRX2, EMI2, HSP31, FIT1, DLD3, RMD6, PMI40, MET6,* YER156c, *GAT1, AAD6, AAD16, IRC7, PNC1, HNM1, MUP1, VHT1,* YGR146c, *ERG1, RNR4, ADE3, TRX2, YHB1, ARN1, ERG11, COX6, HXT4, HXT5, ARO9, CTR2, STB5, OYE2, KOG1, FMP22, FMP34, SIM1, HXT12, GTT1, RNR2, SOD1,* YKL030w, *FBA1,* YKL066w, *CWP1, LAP4, MRP8, FAS1, URA1, CCP1, SRP40, TPO1, TRX1, ERG3, SHM2, AHP1, DPH5, FRE1, ACO1, ILV5, SFP1, URA4,* YLR460c, *PRE8,* YML131w, *CCS1, ERB1, FET3, ADE17, DDR48,* YMR173w-a, *GCV2, HOR7, ADH6, LEU4,* YNL134c, YNL208w, *ADE12, LAP3, ZWF1, RFA2, RIB4, GRE2, HXT11, LEU9, ISU2, WTM1,* YOR285w, *GDH1, FIT3,* YPL067c, *GLR1, CAR1, PEP4, OYE3, GLN1*
Sfp1	47.0	*EFB1, GCV3, FLO9, IMD1, SLA1,* YBR053c, *CNS1, STP22,* YCL026c-a, YCR102c, *RPN4, RPN6, LRG1, GCV1, MRH1, HEM13, RLI1, VBA4, YCF1,* YDR154c, *TRS23, TRR1, YPR1, FRQ1, MFA1, PAC11, IZH1, HSP31, FIT1, SIT1, DLD3, PMI40, HOM3, FTR1,* YER156c, *HXT10, AAD16, AGA2,* YGL039w, YGL157w, *VHT1,* YGR146c, *ERG1, ADE3, YHB1, ARN1, ERG11, SSZ1, HXT4, CTR2, STB5, OYE2,* YHR213w, *BAR1, POT1, HXT12, RNR2,* YJL068c, *ELO1, NNF1, CWP1, FAS1, URA1, SRP40, ERG3, SHM2, GAL2, ERG27, AHP1, HCR1, ACO1, ILV5, SFP1,* YLR460c, YML131w, *ERB1, FET3, ILV2, ADE17,* YMR173w-a, *GCV2, HOR7, ADH6, RLP7, MSG5, LEU4,* YNL134c, *LAP3, ZWF1, RFA2, LYS9, RIB4, GRE2, ENB1, UTP23, LEU9, HIS3, ISU2, FIT2,* YPL067c, *CAR1, OYE3, GLN1*
Msn2	34.2	*EFB1, PHO11, SLA1,* YBR053c, *PHO5, RPN4,* YDL124w, *MRH1,* YDR154c, *CTA1, TRR1, APT2, EMI1, GRX2, EMI2, HSP31, MET6, FTR1, GAT1, AAD16, PNC1, HNM1,* YGL157w, *ADE5,7, MUP1, LST7, VHT1, ERG1, TRX2, YHB1, HXT4, HXT5, ARO9, CTR2, SIM1, POT1, GTT1, ACO2, REE1, SOD1, UGP1, FBA1, CWP1, LAP4, MRP8, CCP1, ERG3, AHP1,* YLR126c, *FRE1, ILV5,* YML131w, *ERB1, FET3, DDR48,* YMR173w-a, *HOR7, RLP7, IDH1, COX5a,* YNL134c, *LAP3, ATX1, RIB4, GRE2, UTP23, LEU9, HIS3, ISU2, WTM1,* YOR285w, *GDH1, FIT2, PEP4, OYE3*
Ste12	34.2	*EFB1, FLO9, ADE1, PHO11,* YBR053c, *YRO2, TIP1, TEC1,* YCL026c-a, *CHA1,* YCR102c, *SFA1, GLT1, LRG1, EHD3, HEM13, RLI1, APT2, MFA1, HSP31, RMD6, MET6, FTR1, LPD1, GAT1, IRC7, AGA2, PNC1,* YGL039w, YGR146c, *RNR4, YHB1, FMP43, SCW4, ARN1, ERG11, HXT4, HXT5, ARO9, OYE2, BAR1, CST6, SIM1, BNR1, POT1, HXT12, GTT1, SFH5, ELO1, ACO2, HXT8, CWP1, LAP4, TPO1, TRX1, GAL2, AHP1, ACO1, DIC1, URA4,* YLR460c, *CCS1, ERB1, ILV2, NDE1, DDR48, HOR7, MSG5, POR1,* YNL208w, *LYS9, TIR2, SNC2, GDH1, ISU1*
Sok2	30.1	*EFB1, FLO9,* YBR053c, *YRO2, TIP1, TEC1, CHA1, AAD3,* YDL124w, *SFA1, HEM13, APT2, IZH1, EMI2, HSP31, SIT1, DLD3, FTR1, AAD16, IRC7, AGA2, PNC1,* YGL157w, YGR146c, *RNR4, YHB1, SCW4, ERG11, HXT4, HXT5, OYE2, SIM1, HXT12, GTT1, RNR2, HXT8, CWP1, LAP4, FAS1, SRP40, TPO1, ERG3, SHM2, ACO1, ILV5,* YLR460c, YML131w, *NDE1, DDR48, HOR7, LEU4, ZWF1, LYS9, GRE2, HXT11, ENB1, TIR2, TUF1, WTM1, SNC2, GDH1, FIT3,* YPL067c, *ISU1, PEP4, OYE3*
Met4	28.8	*CYS3, GCV3, FLO9, IMD1,* YBR053c, *YRO2, SHM1, YCP4, AAD3, RPN4, INH1, GCV1, HEM13, UBC5, YCF1,* YDR154c, YDR476c, *RIB3, GRX2, QCR7, HSP31, SIT1, DLD3, MET6, HXT10, GAT1, AAD6, AAD16,* YFR024c-a, *PNC1, ADE5,7, MUP1, LST7, VHT1, ADE3, ARO9, BNR1, RNR2, PHO86, ACO2, REE1, SOD1, UGP1, MRP8, URA1, CCP1, TRX1, SHM2, SFP1, PRE8,* YML131w, *ERB1, NDE1, GCV2, MSG5,* YNL208w, *ADE12, LAP3, LYS9, HXT11, WTM1, FIT2, OYE3*
Rpn4	28.8	*GCV3, IMD1,* YBR053c, *YRO2, TIP1, PHO5, STP22,* YCL026c-a, *CHA1, YCP4,* YCR102c, *RPN4, RPN6, GCV1, MRH1, TRR1, FRQ1, FIT1, MTC7, DLD3, PMI40, HOM3, MET6, AAD6, AAD16, PNC1,* YGL039w, *TRX2, YHB1, FMP43, SCW4, ARN1, ARN2, HXT4, HXT5, ARO9, GTT1, UGP1, CWP1, LAP4, FAS1, URA1, ERG3, FRE1, DIC1,* YLR460c, *PRE8,* YML131w, *FET3, ILV2, ADE17, NDE1, GCV2, HOR7, IDH1, POR1, ENB1, TIR2,* YOR285w, *FIT2, FIT3, PEP4, GLN1*
Pdr1	27.9	*EFB1,* YAL065c, *PHO11,* YBR053c, *YRO2, TEC1, PHO5,* YCL026c-a, *ADH7, RPN4,* YDL124w, *TRR1, YPR1, IZH1, EMI2, HSP31, FIT1, SIT1, DLD3, HOM3, FTR1, AAD16, PNC1,* YGL039w, YGL157w, YGR146c, *FMP43, SCW4, HXT4, OYE2, HXT12, GTT1,* YKL030w, *UGP1, CWP1, FAS1, URA1, TPO1, ERG27, AHP1, ACO1, DIC1, ILV5,* YML131w, *FET3, NDE1, HOR7, ADH6,* YNL134c, *ZWF1, ATX1, LYS9, GRE2, HXT11, ENB1, HIS3, SNC2, FIT2, ISU1, PEP4, GLN1*
Aft1	25.6	*FLO9, YRO2, FTH1, YCP4, ADH7, AAD3, RPN4,* YDL124w, YDR154c, YDR271c, *HSP31, FIT1,* YDR541c, *SIT1, FTR1,* YER156c, *PNC1, COX13, VHT1,* YGR146c, *YHB1, FMP43, ARN1, ARN2, HXT4, HXT5, FMP22, GTT1, ELO1, SOD1, UGP1, LAP4, TPO1, ERG3, GAL2, AHP1, HCR1, FRE1,* YML131w, *FET3, NDE1, DDR48, GCV2, HOR7, IDH1, ZWF1, ATX1, HXT11, ENB1, TUF1, ISU2, FIT2, FIT3, ISU1, PEP4, OYE3*
Gcn4	24.7	*CYS3, GCV3, ADE1, PHO11, YRO2, PHO5,* YCL026c-a, *CHA1, COX9, GLT1, GCV1, ARO3, PEX5, ADE8, RIB3, EMI1, GRX2, HOM3, LPD1, GAT1, IRC7, PNC1, ADE5,7, VHT1, ADE3, YHB1, HXT5, ARO9, FMP34, ACO2, SOD1, NNF1, FBA1, CWP1, LAP4, ILV5, ADE13, ILV2, ADE17, DDR48, GCV2, IDH1, LEU4, ADE12, LAP3, ZWF1, LYS9, LEU9, HIS3, WTM1, GDH1, CAR1, ISU1, GLN1*
Pdr3	24.2	*EFB1,* YAL065c, *PHO11, SLA1, YRO2, PHO5,* YCL026c-a, YCR102c, *RPN4,* YDL124w, *MRH1, TRR1, IZH1, EMI2, HSP31, DLD3, HOM3, FTR1, AAD6, AAD16, PNC1,* YGL039w, YGL157w, *TRX2, YHB1, FMP43, SSZ1, HXT4, UGP1, LAP4, URA1, SRP40, TPO1, ERG27, DPH5, ACO1,* YLR460c, *ERB1, HOR7,* YNL134c, *GRE2, HXT11, ENB1, UTP23, TIR2, HIS3, ISU2, SNC2, FIT2, CAR1, ISU1, PEP4, OYE3*
Cin5	20.5	*GCV3, FLO9, ADE1,* YBR053c, *YRO2,* YCR102c, *SFA1, GLT1, MRH1, APT2, HSP31, RNR4, TRX2, ARN1, COX6, STB5, OYE2, SIM1, HXT12, GTT1, LAP4, MRP8, FAS1, CCP1, SHM2, GAL2, AHP1,* YLR126c, *FRE1, ACO1, ADE13,* YLR460c, YML131w, *CCS1, ADE17, DDR48,* YMR173w-a, *GCV2, ZWF1, GRE2, HXT11, WTM1,* YOR285w, *FIT2, GLN1*

Table 3: PDTC responsive genes grouped by transcription factor (TF) involved in their regulation. Microarray data sets were clustered using YEASTRACT (Teixeira *et al.*, 2006).

PDTC activates the iron regulon

Strikingly, among the highest induced genes, we identified several genes of the high-affinity iron uptake system (*FET3*, *ARN4*) as well as low-affinity iron-transporters (*FET4*) and cell wall mannoproteins (*FIT1*, *FIT2*, *FIT3*) required for iron retention of siderophore-bound iron. Interestingly, this set of the highest induced genes is referred to as the iron regulon which is activated under iron-limiting conditions. The iron regulon is mainly controlled by the transcription factors Aft1/ Aft2 (activator of ferrous transport 1/2) (Rutherford *et al.*, 2003). Aft1 mediates the response to the cellular iron status by trafficking into the nucleus upon iron deprivation and staying in the cytoplasm under iron-replete conditions. Nuclear shuttling of the Aft1 transcription factor induces a well-

regulated transcriptional remodeling program involving many cellular processes (Yamaguchi-Iwai *et al*., 2002). The primary response comprises of the up-regulation of the iron uptake machinery and the import of iron. In the second phase, intracellular iron storage is mobilized. Finally, the cells modulate and adapt their metabolic iron usage to the limitation switching to less iron-consuming pathways, shutting down non-essential pathways while preserving essential ones. Pathways regulated in response to iron changes are the biotin, glutamate and purine biosynthetic pathways, as well as the TCA cycle. Furthermore, genes involved in heme biosynthesis and in the respiratory chain are down-regulated (Hausmann *et al*, 2008). Recently, it has been shown that under low-iron conditions genes involved in biotin synthesis, glutamate metabolism and heme assembly are downregulated mediated through coordinated targeted mRNA degradation by Cth1/Cth2 (Tis11). By binding to certain mRNAs, Tis11 causes rapid degradation of these mRNAs, thereby reducing their expression level. These second wave targets complete the known multistage remodeling during iron deprivation (Table 4).

Upregulation of iron uptake genes	Genes either down-regulated or involved in downregulation of iron-consuming pathways
ARN1, *FIT2*, *FIT3*, *ARN2*, *FET3*, *FIT1*, *FTR1*, *ARN4*, *ARN3*, *FRE1*, *FTH1*, *ATX1*, ***CTR2***, ***CCS1***, ***ENB1***, **YLR126C**, ***ISU2***, ***ISU1***	***TIS11***, ***HMX1***, ***LEU1***, ***COR1***, ***RIP1***, ***COX6***, ***CYC1***, ***HEM15***, ***CCP1***, ***HEM13***, ***COX9***, ***RLI1***, ***RNR4***, ***BIO2***, ***RNR2***, ***ISA1***, ***SDH2***, ***COX8***, *COX5A*, *COX13*, *ACO1*

Table 4: List of genes differentially regulated in response to PDTC after 1, 3 or 5h treatment and iron deprivation. We compared our microarray data set to published data on iron deprivation (Puig *et al.*, 2005), overlapping genes are shown in bold.

The PDTC transcriptome compares to the transcriptional profile during iron deprivation

Hence, we compared the transcriptional profile of PDTC to published data on iron deprivation. Indeed, we found a significant overlap (p-values ≤ 0.005) between profiles reflecting iron deprivation or deletion of the iron sulfur complex (ISC) machinery and other stress conditions activating Aft1 (Fig.7). Consistent with the known cellular remodeling upon iron limitation, on the one hand, PDTC induced genes of the high-affinity and low-affinity iron import machineries, as well as sterol and fatty synthesis genes. On the other hand, genes of iron-consuming pathways were down-regulated. Many of these genes were known Tis11 target genes, indicating a secondary response after PDTC-induced activation of Aft1. Thus, PDTC triggered both the primary and secondary wave response genes involved in iron-dependent cellular remodeling (Table.4).

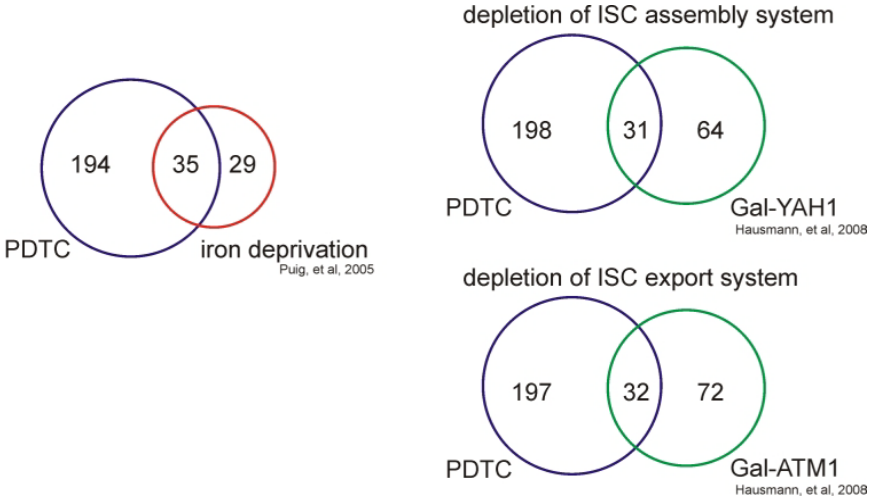

Figure 7: Venn diagrams of genes differentially expressed genes under iron-limited conditions and upon PDTC treatment (p-values ≤ 0.005).

PDTC causes strong induction of Aft1-target genes

To confirm the induction of the iron regulon in response to PDTC, we performed Northern analysis. As shown in Fig.8A, PDTC strongly induced the expression of *TIS11*, *GRE2* and *FIT3* when compared to untreated cells. The most upregulated genes (e.g. *FIT1*, *FIT2)* have several Aft1 binding sites in their promoter regions, explaining their enormous upregulation seen by microarray analysis and Northern blots (Fig.8B, (Yamaguchi-Iwai *et al.*, 1996)).

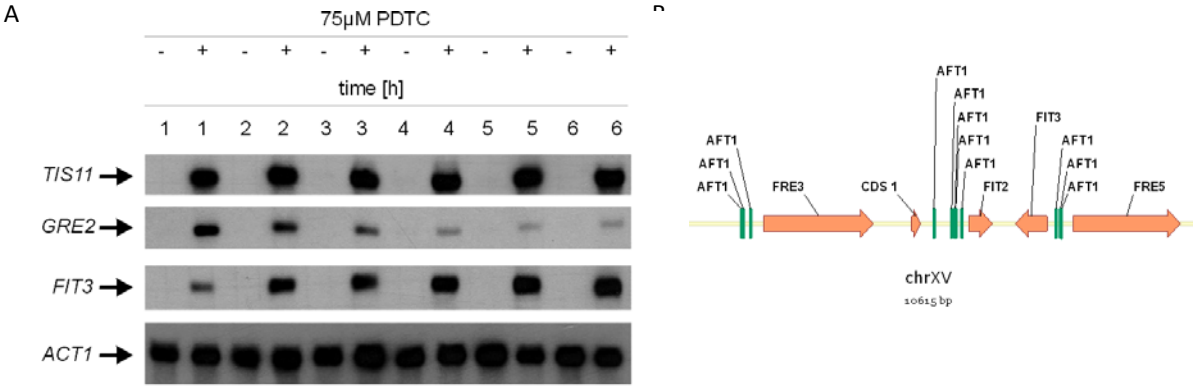

Figure 8: A. Northern blot analysis investigating induction of PDTC-induced genes. Cells were treated for 1 to 6h with PDTC. Untreated and PDTC-treated cultures were harvested and total RNA was isolated and transferred to a PVDF membrane. Radiolabeled probes were hybridized and the membrane was exposed to X-ray films. B. Cluster of Aft1 target genes in the subtelomeric region of chromosome XV.

The effect of PDTC on the iron regulon is Aft1-dependent

To investigate whether the increase in the expression levels of these genes is Aft1-dependent, we compared the transcript levels of wild type cells and those lacking the *AFT1* gene (Fig.9A). Activation of the iron regulon (*FIT2*, *FIT3*) upon PDTC exposure was fully Aft1-dependent, whereas *GRE2*, encoding a metalloreductase involved in the HOG pathway, served as control for Aft1-independent induction. Thus, in addition to the iron

regulon, other genes were differentially expressed, indicating additional regulatory mechanisms independent of Aft1. Furthermore, PDTC strongly induced the *FET3* promoter encoding the multicopper ferroxidase of the high-affinity iron uptake system as shown by a *FET3-lacZ* reporter assay (Fig.9B).

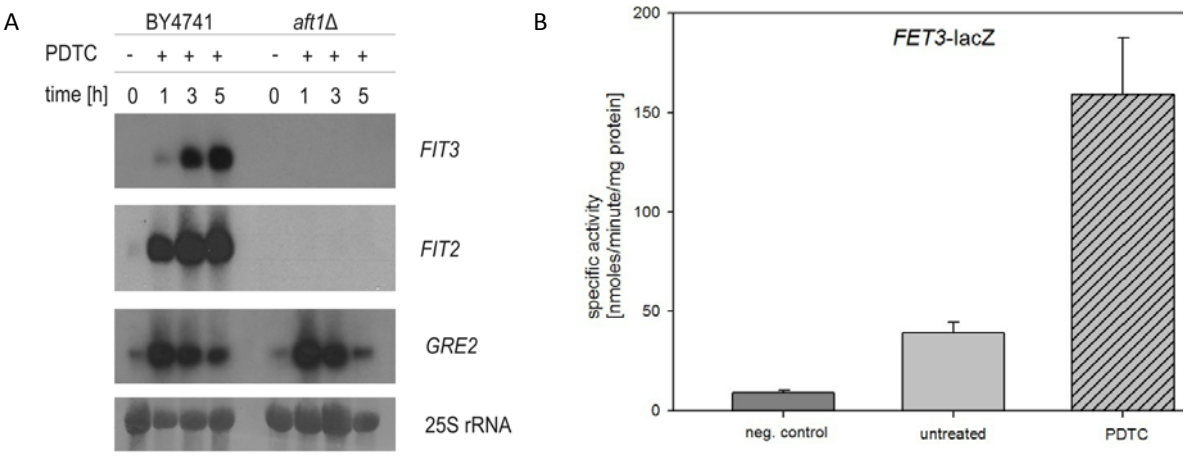

Figure 9: A. Northern blot analysis comparing gene expression in wild type and *aft1Δ* cells in the presence of PDTC. B. PDTC induced activation of the *FET3*-promoter. Cells containing an integrated lacZ-*FET3* reporter construct were grown to the logarithmic phase in YPD and treated with PDTC for 2 hours. Cells were harvested, crude extracts were prepared and β-galactosidase activity was determined.

PDTC causes down-regulation of the cytochrome c oxidase

Under iron-limited conditions, yeast cells switch to less-iron consuming pathways by post-transcriptional down-regulation of certain genes. Tis11 (Cth2) is a key player down-regulating genes related to respiration and citric acid cycle (Fig.10A, (Vergara and Thiele, 2008)). In cellular respiration, the cytochrome c oxidase (COX), a multisubunit enzyme and known target of Tis11, catalyzes the terminal step in the respiratory electron transport chain. Since several genes encoding subunits of the cytochrome c oxidase were downregulated during PDTC response, we confirmed downregulation of COXIV by immunoblotting using an anti COXIV antibody (Fig.10B).

A

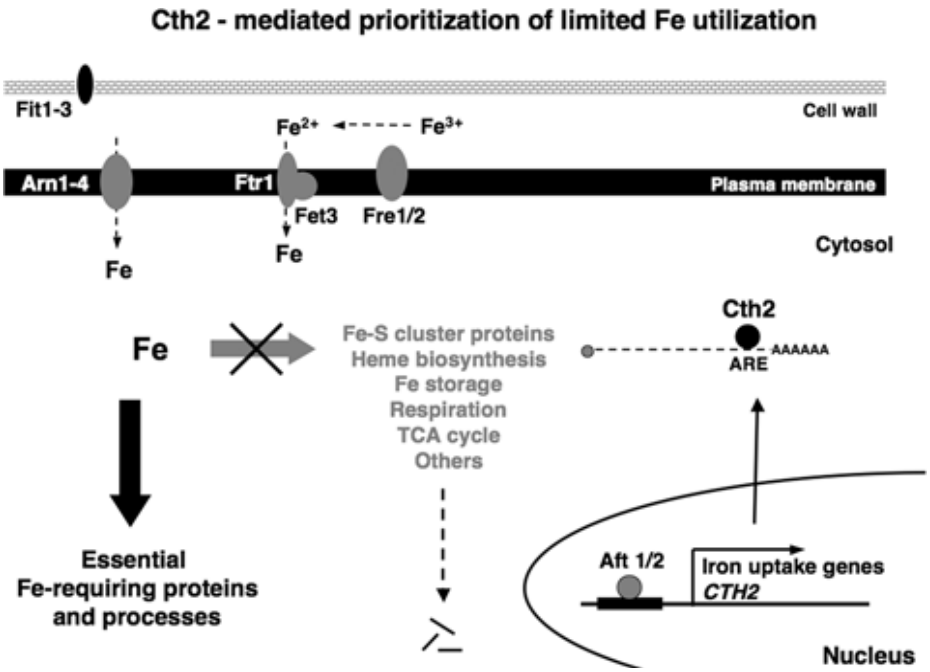

B

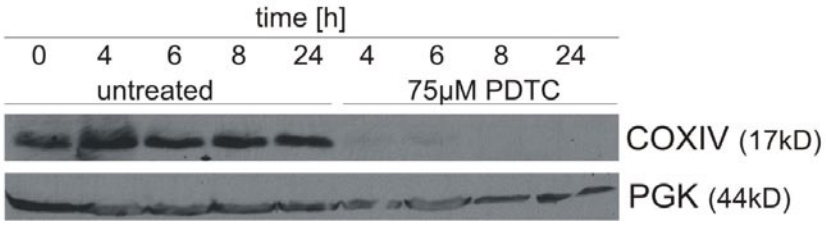

Figure 10: A. Schematic presentation of coordinated mRNA degradation by Cth2 in respone to iron deficiency to prioritize less-iron consuming pathways (Vergara and Thiele, 2008). B. PDTC caused down-regulation of COXIV. Cells were harvested at the indicated time points. 0.5 OD_{600} equivalents of TCA extracts were loaded per lane. Proteins were detected using an anti-COXIV and polyclonal anti-PGK antibodies as loading control.

Low-iron sensing genes are required during the PDTC response

Aft1 is required for growth under iron-limited conditions (Yamaguchi-Iwai *et al*., 1995), although Aft1 does not directly sense low-iron conditions. The signal is rather transmitted by mitochondrial iron-sulfur cluster (ISC) biosynthesis genes requiring a cytosolic complex of Grx3-Grx4-Fra1-Fra2 (Kumanovics *et al.*, 2008). Consistently, the *aft1*Δ, *fra2*Δ, and *grx3*Δ strains were hypersensitive to PDTC when compared to the corresponding wild type control. Iron-supplementation specifically rescued this sensitivity phenotype, thus showing that PDTC mimicked or caused a lack of iron availability (Fig.11A). Moreover, iron supplementation significantly reduced the induction of Aft1-target genes after PDTC treatment at the mRNA level (Fig.11B), whereas supplementation of calcium or copper failed to change mRNA levels of PDTC-induced genes (Fig.11C,D).

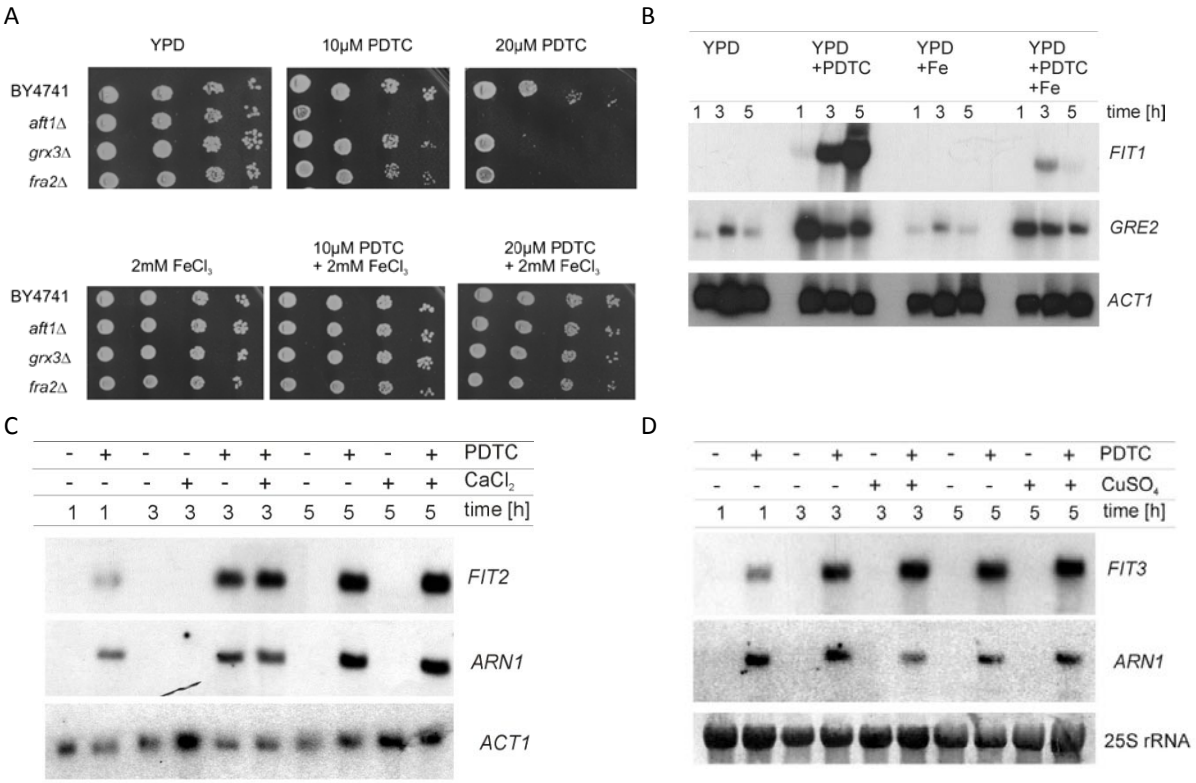

Figure 11: Iron supplementation rescued the PDTC-induced effects. A. Spot assays comparing wild type yeast growth to mutants of the iron sensing machinery. B: Northern blot analysis investigating the effect of iron supplementation during PDTC treatment. C, D. Calcium and copper failed to suppress the induction of PDTC-responsive genes.

Neither calcium nor magnesium could override the PDTC-induced effects

The *aft1*Δ strain is sensitive to a variety of stress conditions, including lack of iron, alkaline pH, hydroxyurea, excess zinc, nickel, cobalt and manganese (Fig.12, (Stadler and Schweyen, 2002; Serrano *et al.*, 2004; Dubacq *et al.*, 2006)). Consequently, we questioned whether supplementation of metal ions could influence growth and gene expression levels during PDTC treatment. Interestingly, except for iron, other ions such as Ca^{2+}, Mg^{2+}, Zn^{2+}, and Mn^{2+} failed to rescue the PDTC-dependent growth inhibition. Cd^{2+} supplementation even increased PDTC-sensitivity. Notably, copper supplementation rescued growth of the *aft1*Δ strain in the presence of PDTC, but impaired PDTC-tolerance of the wild type strain (Fig.12).

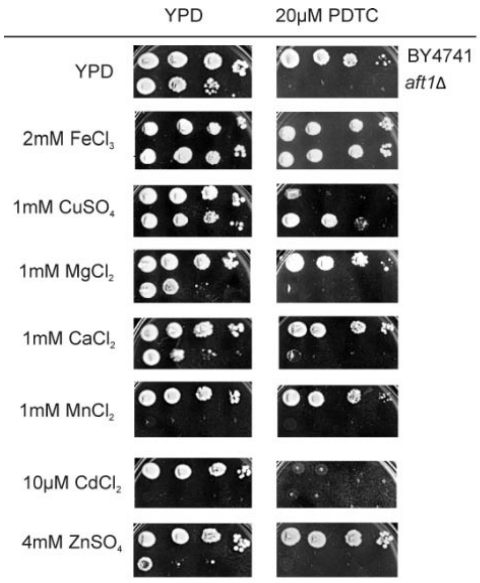

Figure 12: PDTC induced growth deficiency is iron-dependent. Growth inhibition assay with serial dilutions of wild type and *aft1*Δ cells on media containing PDTC and/or different ions.

PDTC induced stress-responsive genes in the *aft1*Δ strain

To identify Aft1-independet target genes of PDTC, we performed genome-wide microarray analysis with untreated and PDTC-stressed *aft1*Δ cells and compared these results to the transcriptional response in the wild type strain. We identified 47 genes differentially expressed upon PDTC treatment in the *aft1*Δ strain. As expected, upon deleting the main regulator of the iron regulon, no iron-responsive genes were induced. Comparison with the wild type PDTC data revealed an overlap of 31 genes including *GRE2*, *SOD1* or *STP22*. By functionally categorizing them, we mainly observed genes involved in response to stress, especially to toxin or oxidative stress (Table 5). However, we identified 16 genes that were exclusively differentially expressed in the *aft1*Δ strain upon PDTC treatment, including *CUP1*, *AAD4*, *HSP12, AAD10, DUG2, YGP1, GLK1, YOL150C, TFS1, TSA2, IRC14, IDH2, RPL5* and *HYR1*. *CUP1* encodes a metallothionein that binds to copper and mediates resistance to copper and cadmium (Winge *et al.*, 1985). Aad4 is a putative aryl-alcohol dehydrogenase involved in oxidative stress response (Dickinson *et al.*, 2003). The *HSP12* gene is induced upon several stress conditions such as heat shock, oxidative or osmotic stress, as well as glucose depletion or stationary phase entry (Sales *et al.*, 2000). *HYR1* encodes a thiol peroxidase sensing intracellular hydroperoxide levels and transducing a redox signal to the Yap1 transcription factor (Delaunay *et al.*, 2002). In summary, stress response genes and metallothioneins were the main gene sets regulated in the *aft1*Δ strain.

Categories	p-value	Genes names
response to stimulus	2.77e-09	*FRM2, YCR102C, AAD3, YDL124W, AAD4, TSA2, GRX2, HSP12, AAD6, AAD16, TRX2, YHB1, CUP1-1, CUP1-2, STB5, HYR1, SOD1, AAD10, YML131W, DDR48, HOR7, YGP1, GRE2, OYE3*
cellular aldehyde metabolic process	2.69e-07	*AAD3, AAD4, AAD6, AAD16, YJL068C, AAD10*
response to oxidative stress	3.86e-06	*YDL124W, TSA2, GRX2, HSP12, TRX2, STB5, HYR1, SOD1*
response to copper ion	0.00024	*YCR102C, CUP1-1, CUP1-2*

Table 5: Functional categories of differentially expressed genes during PDTC treatment in *aft1*Δ cells. Genes that were at least 2-fold (p-value ≤ 0.05) differentially expressed on our microarrays were categorized using the Saccharomyces Gene Database Gene Ontology termfinder (www.yeastgenome.org).

Metallothioneins are low-molecular weight proteins that bind ions, thereby regulating intracellular ion homeostasis and conferring resistance to certain ions. Since we observed the *CUP1* gene to be differentially regulated in the *aft1*Δ strain upon PDTC treatment, we confirmed its transcript levels by Northern analysis (Fig.13A). Moreover, in wild type cells supplementing both copper and PDTC was highly toxic, whereas copper rescued the *aft1*Δ sensitivity phenotype (Fig.13B). *CUP1* was highly induced in the *aft1*Δ strain, which might explain the increased copper-tolerance when compared to the wild type control.

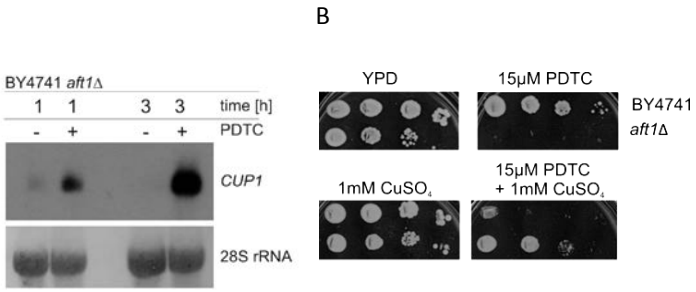

Figure 13: A. Northern analysis probing the metallothioneine gene *CUP1*. BY4741 *aft1*Δ cells were incubated with PDTC for 1 and 3 hours, respectively. After harvesting cells, total RNA was extracted and 15µg were blotted onto a PVDF membrane after agarose gel fractionation. B. Spot assays comparing growth of wild type and *aft1*Δ cells on YPD medium containing PDTC and copper sulfate, respectively.

PDTC interferes with intracellular zinc levels

On the one hand, PDTC caused strong induction of the iron uptake machinery. On the other hand, it was striking to note that PDTC also strongly altered expression of plasma membrane and vacuolar zinc transporters (Fig.14A). In detail, expression of the plasma membrane low-affinity zinc transporter Zrt2 and the vacuolar zinc exporter Zrt3 was strongly decreased upon PDTC treatment, whereas the transporter importing zinc into the vacuole, Cot1, was highly induced (Fig.14B). Transcript levels of the high-affinity zinc transporter Zrt1 stayed unchanged; however Zrt1 is regulated post-translationally via ubiquitination and endocytosis (Gitan and Eide, 2000). Although yeast lacks a cellular zinc exporter, free zinc concentrations are kept low because excess zinc is highly toxic for cells.

Spare zinc is bound to proteins or stored in vesicular compartments such as the vacuole as major site of storage and detoxification (Eide, 2009).

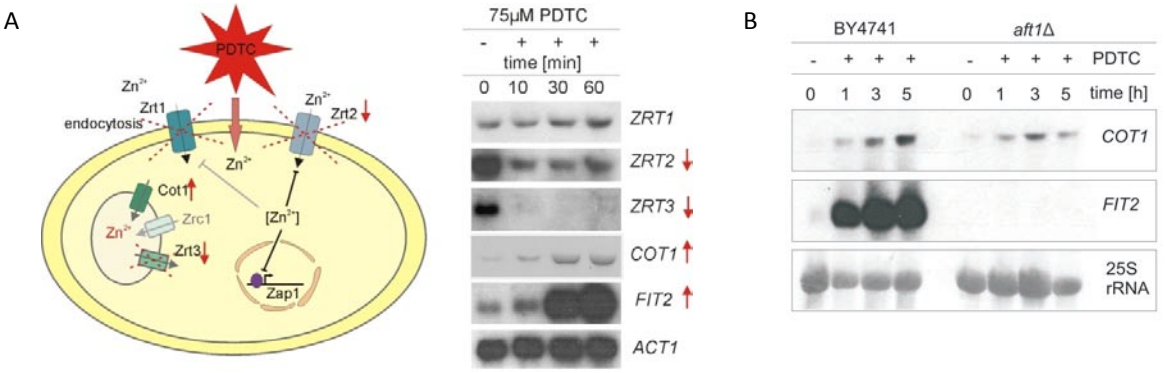

Figure 14: A. PDTC altered expression of zinc transporters. Cells were grown in YPD to an OD_{600} of ~0.8 and 75µM PDTC was supplemented. Cells were harvested at the indicated time points, total RNA was extracted and 15µg of each sample were used for Northern analysis. B: Induction of the *COT1* gene upon PDTC treatment was independent of Aft1.

Beside zinc sequestration in compartments, cells upregulate zinc-binding proteins like metallothioneins. In addition, large amounts of zinc are bound by the copper/zinc superoxide dismutase Sod1, as well as the alcohol dehydrogenase Adh1 and the ribosomes. Sod1, Adh1 and ribosomal zinc account for about 20% of the whole zinc quota per cell (Eide, 2006). Consistent with our notion of PDTC-mediated intracellular zinc excess, transcript levels of the major zinc-conserving proteins like alcohol dehydrogenases (ADHs) and superoxide dismutase 1 (Sod1) were increased. We confirmed the induction of the cytoplasmic superoxide dismutase *SOD1* gene by Northern blotting. In the *aft1*Δ strain, *SOD1* gene induction was even more pronounced than in the wild type control (Fig.15B).

Consistently, Sod1 deficiency led to increased PDTC, as well as zinc-sensitivity, whereas deletion of the manganese superoxide dismutase Sod2 had less severe effects (Fig.15A). Interestingly, iron supplementation failed to rescue the PDTC-induced growth defect of the *sod1*Δ strain. However, this failure might be due to a previously reported increase in iron demand of the *sod1*Δ mutant *per se* and its involvement in zinc detoxification (De Freitas *et al.*, 2000; Tarhan *et al.*, 2007). In this case, PDTC would worsen the lack of iron availability, thereby increasing the sensitivity of the *sod1*Δ strain. Taken together, the observed regulation of zinc homeostasis genes in response to PDTC indicates excess cytoplasmic zinc, leading to subsequent zinc detoxification by sequestration into the vacuole and by induction of zinc-binding proteins.

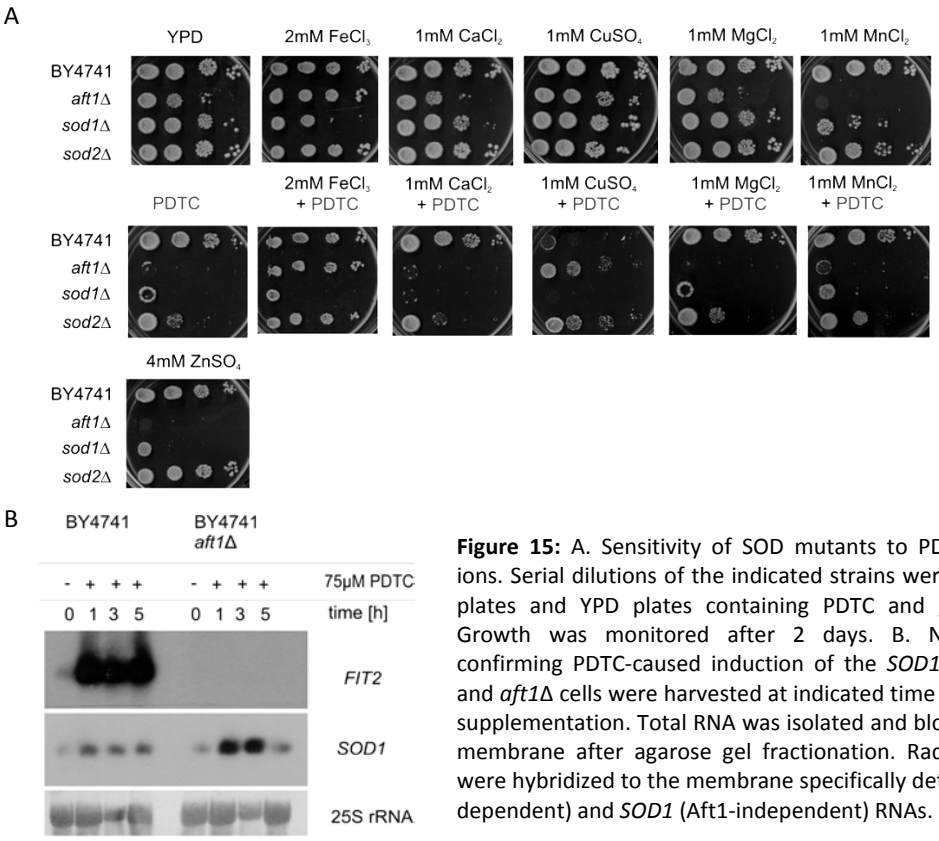

Figure 15: A. Sensitivity of SOD mutants to PDTC and different ions. Serial dilutions of the indicated strains were spotted on YPD plates and YPD plates containing PDTC and /or diverse ions. Growth was monitored after 2 days. B. Northern analysis confirming PDTC-caused induction of the *SOD1* gene. Wild type and *aft1*Δ cells were harvested at indicated time points after PDTC supplementation. Total RNA was isolated and blotted onto a PVDF membrane after agarose gel fractionation. Radiolabeled probes were hybridized to the membrane specifically detecting *FIT2* (Aft1-dependent) and *SOD1* (Aft1-independent) RNAs.

As PDTC induced Sod1, we further investigated the role of oxidative stress and accumulation of reactive oxygen species (ROS) in the PDTC response. Superoxide dismutases are required for detoxification by catalyzing the breakdown of superoxide anions into oxygen and hydrogen peroxide. In *S. cerevisiae,* there exist two types of superoxide dismutases, Sod1 and Sod2. The *SOD1* gene encodes a Cu/Zn superoxide dismutase localized to the cytoplasm and mitochondria (Lyons *et al.*, 2000), whereas Sod2, a manganese superoxide dismutase is found in the mitochondrial matrix (Luk *et al.*, 2005).

To investigate ROS accumulation in PDTC-treated cells, we labeled cells with dihydroethidium (DHE), dihydrorhodamine (DHR) and dichlorodihydrofluorescein diacetate (H_2DCFDA), respectively. DHE detects mitochondrial superoxide anion, DHR detects hydrogen peroxide, hypochlorous acid and peroxynitrite anion, whereas H_2DCFDA detects hydrogen peroxide, hydroxyl radical, peroxyl radical and peroxynitrite anion. Labeled wild type, *sod1*Δ, *sod2*Δ and *sod1*Δ *sod2*Δ cells were treated with PDTC and analyzed by FACS. We failed to detect ROS by using H_2DCFDA or DHR (data not shown). However, we detected a chemoluminsecent shift upon PDTC treatment in DHE-labeled *sod2*Δ cells (Fig.16C). Therefore, we suggest that PDTC only caused a weak ROS

generation in yeast cells. Indeed, we only managed to detect mitochondrial ROS accumulation in the *sod2*Δ strain (Fig.16). Probably, these ROS are rapidly dismutated in the wild type strain or cytoplasmic ROS levels were below the detection limit. Notably, microarray analysis indicated down-regulation of the *CCP1* gene encoding the mitochondrial cytochrome c oxidase, which is involved in ROS degradation in the mitochondria (Charizanis *et al.*, 1999). Repression of Ccp1 in the presence of PDTC might explain the increased ROS levels in the mitochondria.

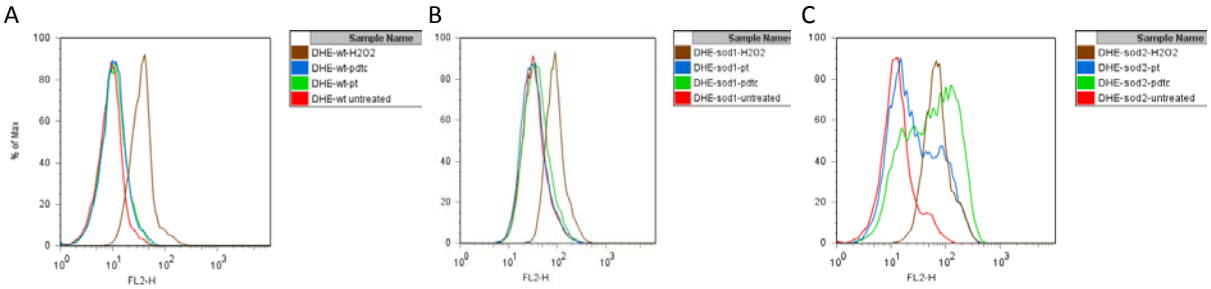

Figure 16: FACS analysis detecting mitochondrial ROS accumulation in wild type, *sod1*Δ, *sod2*Δ and *sod1*Δ *sod2*Δ cells using the fluorescent dye dihydroethidium (DHE).

Sod1 is required for oxidative stress defense, but it also links ROS response to metal ion homeostasis and pH sensitivity. For example, Sod1 requires the metallochaperone Ccs1 for copper loading *in vivo* (Culotta *et al.*, 1995). Moreover, Atx1, a metallochaperone for copper-dependent iron absorption, suppresses the superoxide sensitivity phenotype of mutants lacking superoxide dismutases. Atx1 can be induced by iron via Aft1, although it is not strictly Aft1-dependent (De Freitas *et al.*, 2000). Similar to *aft1*Δ, the *sod1*Δ strain shows increased sensitivity to zinc and cadmium excess, alkaline pH and hydroxyurea stress, all of which activate Aft1 and correspondingly the iron regulon.

PDTC causes immediate zinc influx into yeast cells

To directly monitor PDTC-induced zinc accumulation inside yeast cells in real time, we used the fluorescent dye mag-fura-2 (Molecular Probes). As the dye is normally effluxed from cells, all experiments were carried out in a strain lacking the ABC transporters Pdr5 and Pdr12 (Piper *et al.*, 1998; Holyoak *et al.*, 1999). The excitation wavelength of mag-fura-2 is shifted from 380 to 340 nm when binding bivalent cations (Raju *et al.*, 1989; Simons, 1993). After loading yeast cells with mag-fura-2, cells were extensively washed, and $ZnSO_4$, $CuSO_4$, $CaCl_2$ or $MgCl_2$, PDTC and EDTA were added at indicated time points. While adding $ZnSO_4$ had only minor effects on the fluorescent ratio, the supplementation

of PDTC caused a rapidly increasing signal as a readout for intracellular zinc accumulation (Fig.17). As expected, adding EDTA reduced the signal immediately. Other metal ions, including Mg^{2+}, Cu^{2+} and Ca^{2+}, had no effect on the fluorescent signal. Thus, PDTC caused an immediate influx of Zn^{2+} ions into yeast cells and elevated intracellular zinc levels.

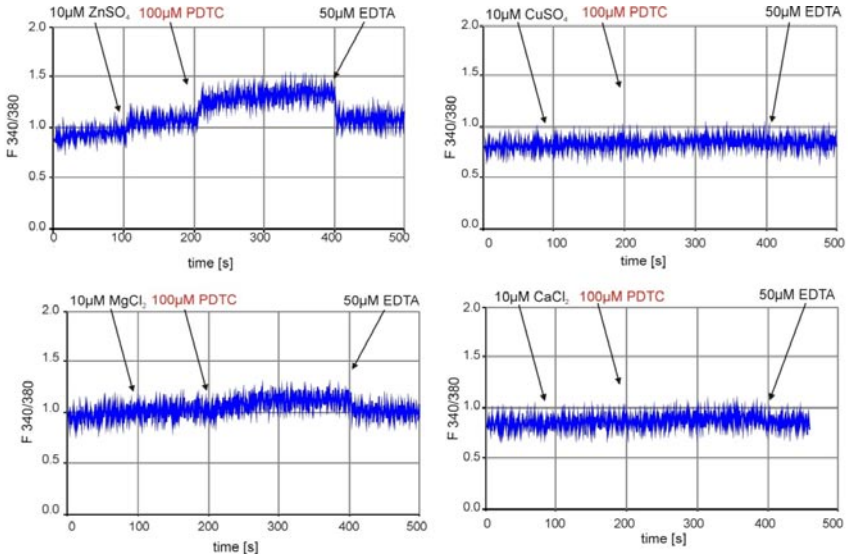

Figure 17: PDTC induces immediate influx of zinc ions into yeast cells. Cells were loaded with the mag-fura-2 dye and fluorescence was monitored in real-time after adding metal ions such as $ZnSO_4$, $CaCl_2$, $CuSO_4$, $MgCl_2$, PDTC and EDTA at the indicated time points. The excitation wavelength of mag-fura-2 is shifted by binding bivalent metal ions. Thus, change of the fluorescent ratio of F340/380nm following addition of zinc and PDTC, but not by calcium, magnesium or copper, show accumulation of intracellular labile zinc.

PDTC triggers a cross-talk between iron and zinc homeostasis

As both iron and zinc homeostasis were disturbed by PDTC, we aimed to investigate a thus potential cross-talk between the iron and zinc regulons. Supporting this notion, it was previously reported that zinc overload activates the iron regulon (Pagani *et al.*, 2007). In addition, *aft1*Δ cells are sensitive to high concentrations of extracellular zinc, which indicates that Aft1 is required to counteract the growth defect caused by excess zinc (Pagani et al., 2007). Hence, we performed viability assays with wild type and *aft1*Δ strains in the presence of PDTC, Zn^{2+} and Fe^{3+}, respectively (Fig.18). Colony forming units were determined after 24h stress treatment with 200µM PDTC in liquid medium and set relative to the untreated wild type. As expected, iron supplementation rescued the cytotoxic effect of PDTC in wild type and *aft1*Δ cells. In contrast, this effect was enhanced by excess zinc. Growth deficiency of *aft1*Δ cells on high excess zinc was rescued by iron supplementation. Strikingly, the combined effect of PDTC, iron and zinc was almost fully rescued in the *aft1*Δ background but not in the wild type strain (Fig. 18). These data suggest that in wild type cells, Aft1 also controls a yet unidentified cellular function counteracting zinc detoxification, at least in the presence of PDTC.

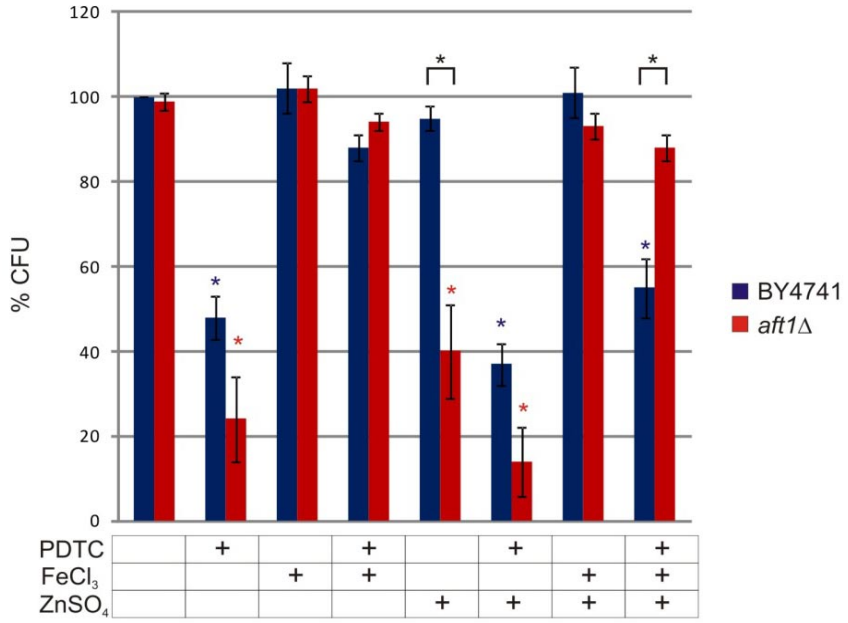

Figure 18: Cell viability assays to investigate the cross-talk between iron and zinc homeostasis. Wild type and *aft1*Δ were grown in liquid rich medium for 24h in the presence of PDTC, $ZnSO_4$ and $FeCl_3$, respectively. Afterwards, cells were plated on YPD and colony forming units (CFU) were determined after 2 days incubation at 30°C. Data are presented as percent CFU relative to the untreated wild type. Error bars represent ± 1 SD of three independent growth experiments; stars indicate significance of data valued by a student t-test.

Functional screening of the EUROSCARF deletion collection

Whole-genome transcriptome analysis undoubtedly yields important clues on changing gene expression levels. However, it will certainly miss all genes whose mRNA levels do not change during the PDTC response or inhibition by PDTC. This is particularly true for many signal transduction genes whose mRNA levels often do not significantly change. For example, kinase and phosphatase activites are often modulated by post-translational modifications (Theodosiou and Ashworth, 2002).

Genes involved in vacuolar maintenance and transport confer PDTC resistance

To identify genes that confer tolerance to PDTC, we screened the EUROSCARF deletion collection comprising of about 4800 haploid single knock-outs for altered growth in the presence of PDTC. Strains of the deletion collection were replicated on YPD and PDTC-containing plates and grown at 30°C for 6 days inspecting growth every day. The previously identified PDTC hypersensitivity of *aft1*Δ was used as a control in the screening procedure. Serial dilutions of mutants showing increased PDTC sensitivity were manually respotted on several PDTC concentrations to confirm the phenotype.

Among the about 4800 haploid single deletion strains, we identified 140 mutants as PDTC-sensitive. To categorize the PDTC-sensitive strains, we grouped them based on GO enrichment using the *Saccharomyces cerevisiae* Gene Database GO Termfinder (Fig. 19).

The main functional categories comprised of vacuolar acidification and vacuolar transport, protein modifications, mitochondrial organization and translation. Interestingly, many mutants related to membrane and vesicular trafficking and transport systems were also PDTC-sensitive [e.g., endosomal sorting complex required for transport (ESCRT); Golgi-associated retrograde protein complex (GARP); homotypic fusion and vacuole protein sorting (HOPS) complex]. Furthermore, mutants involved in the Rim101 pH sensing pathway were PDTC-sensitive. As the Rim101 pathway is connected to the ESCRT complexes, this might explain the overlapping sensitivity phenotypes (Hayashi *et al.*, 2005).

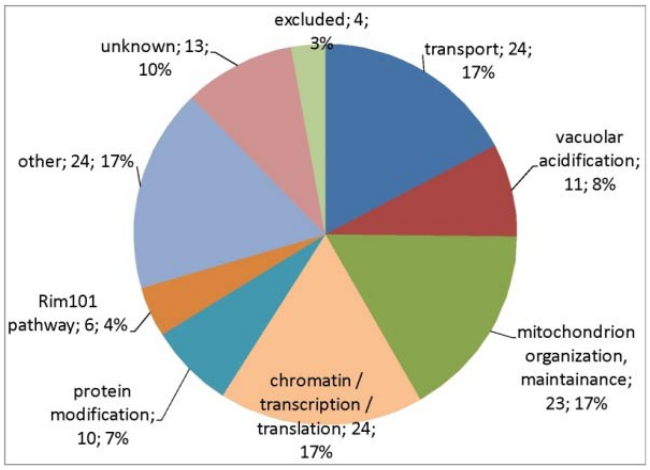

p-value ≤ 0.05

Figure 19: Functional screening identified processes mediating PDTC tolerance. The 4800 deletion strains were screened on YPD and PDTC-containing plates using a Singer RoTor HAD Robot. Growth was monitored every day for 6 days. Sensitive strains were verified by manual respotting and clustered into functional categories using the GO termfinder. The number of genes per category and the percentages of each category to the dataset are indicated.

The vacuole and a functional V-ATPase are crucial during PDTC treatment

Interestingly, mutants with impaired vacuolar trafficking and/or vacuolar proteins sorting, including *VPS4*, *VPS8*, *VPS18*, *VPS33*, *VPS41*, *VPS45*, as well as function and assembly of the V-ATPase such as *VMA8*, *VMA22*, *VMA2*, *TFP1*, *VMA21*, *VMA6*, and *PPA1* were PDTC-sensitive, suggesting that vacuolar function and maintenance is pivotal for cells responding to PDTC (Fig.20A,B). The sensitivity phenotype of these mutants towards PDTC was reversed by iron supplementation (Fig. 20B). The vacuole is the main compartment for storage and detoxification, osmoregulation, ion and pH homeostasis and macromolecular degradation. Several trafficking complexes coordinate specific transport of proteins, ions, amino acids, polyphosphates and other substances (for review see (Kane, 2006)). Thus, components involved in vacuolar biogenesis and trafficking are essential under various stress conditions. For example, a functional V-ATPase is crucial for establishing a proton gradient across the membrane to ensure vacuolar import of ions, especially for zinc sequestration (Fig.20B, (MacDiarmid *et al.*, 2002)).

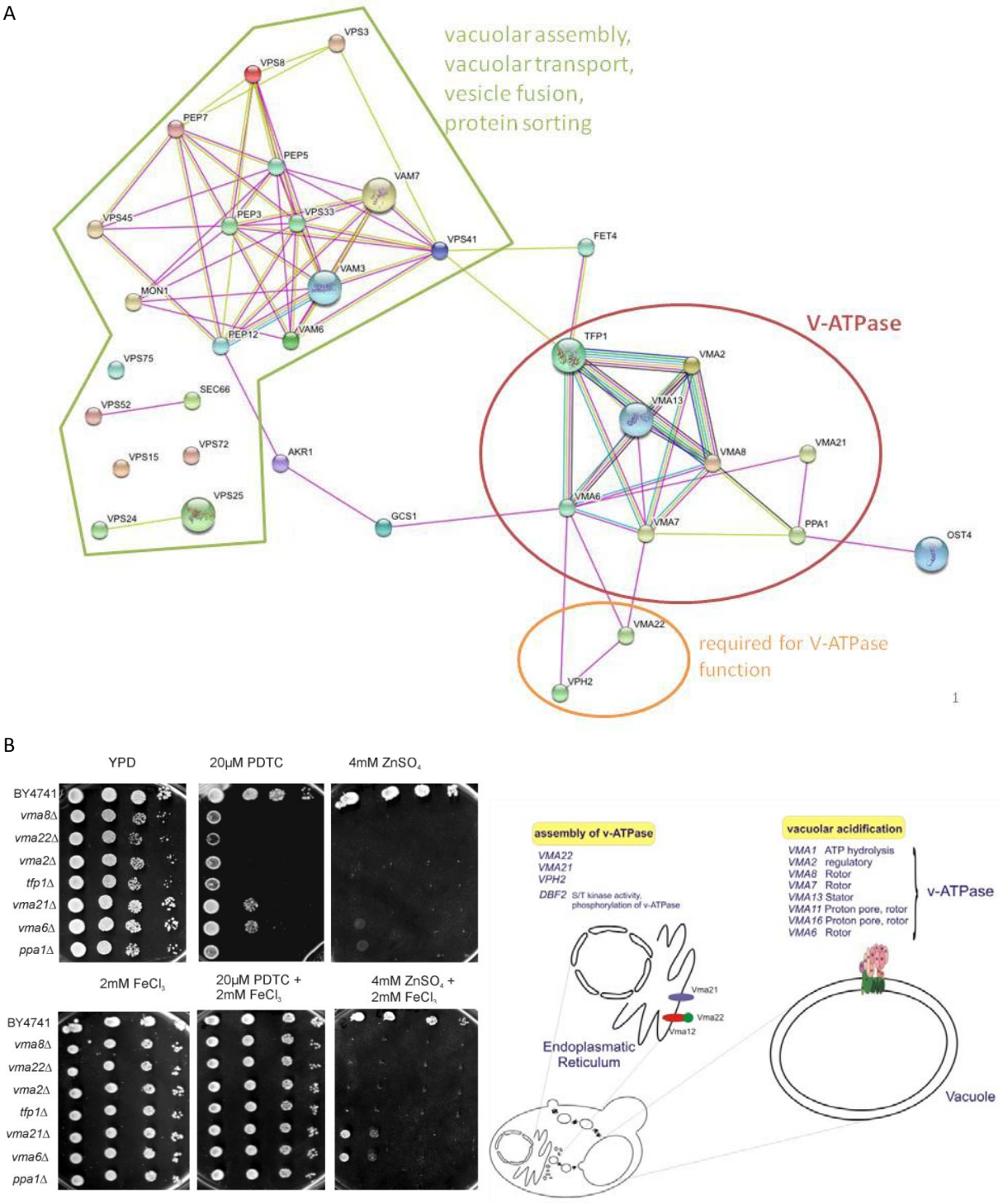

Figure 20: A functional V-ATPase is pivotal for PDTC-tolerance. Mutants disrupting assembly or biogenesis of the V-ATPase are PDTC-sensitive. A. Protein interaction network retrieved from the STRING database using the default parameters (von Mering *et al.*, 2007). Strong associations are represented by thicker connecting lines, whereas thin lines correspond to weaker associations. B. Mutants lacking a functional V-ATPase or restricted in vacuolar assembly or biogenesis are PDTC as well as zinc-sensitive. Mutants required for vacuolar protein sorting, the V-ATPase and its assembly were assayed for growth on YPD plates and plates containing PDTC and/or $FeCl_3$, $ZnSO_4$. Serial dilutions of the indicated strains were spotted and growth was monitored after 2 days.

'Complex' response to PDTC

In detail, vacuolar trafficking to and from the vacuole involves about 60 actors referred to as vacuolar protein sorting (*VPS*) genes. Protein sorting into multivesicular bodies (MVB)

is a pathway required for protein degradation, secretion and recycling, including class E Vps proteins as the main components. Proteins targeted for degradation are mainly passed through the ESCRT complexes (for review see (Raiborg and Stenmark, 2009)). ESCRT I, II and III are well-conserved multisubunit complexes that are subsequently acting on endosomal membranes, driving internalization of protein cargo into MVBs. ESCRT I (Vps23, Vps28, Vps37) recognizes ubiquitinated protein cargo. ESCRT II (Vps22, Vps25, Vps36) acts downstream of ESCRT I and is required for recruiting membranes to ESCRT III. ESCRT III (Did4/Vps2, Vps20, Vps24, Snf7/Vps32) concentrates protein cargo into MVB particles and coordinates MVB accessory factors like Vps4 or Doa4. Vps4, an AAA-type ATPase, catalyzes dissociation of the ESCRT complexes. Interestingly, several mutants lacking components of the ESCRT complexes were PDTC-sensitive (Fig. 21B).

Furthermore, we identified members of the CORVET, HOPS or GARP complexes as PDTC-sensitive (Fig.21A,B). The CORVET (class c core vacuole/endosome tethering) complex acts in cooperation with Rab GTPases as an endosomal tethering complex (Peplowska *et al.*, 2007). It captures endosomal vesicles and is required for transport between endosome and vacuole, as well as for endo-lysosomal biogenesis. The *S. cerevisiae* complex consists of Pep3, Pep5, Vps16, Vps3, Vps33, and Vps16. Mutants lacking the *PEP3*, *PEP5*, *VPS33* or *VPS8* genes are PDTC-hypersensitive. Some of them (*VPS33*, *VPS16*, *PEP3*, and *PEP5*) are part of the CORVET complex and the HOPS complex. The HOPS complex is involved in vacuolar protein sorting and vacuole fusion by binding to the vacuolar membrane (Wickner, 2010). In addition, we found mutants belonging to the GARP (Golgi-associated retrograde protein) complex, which is involved in recycling of proteins from endosomes to the late Golgi to be PDTC-sensitive (Fig 21.A,B).

A

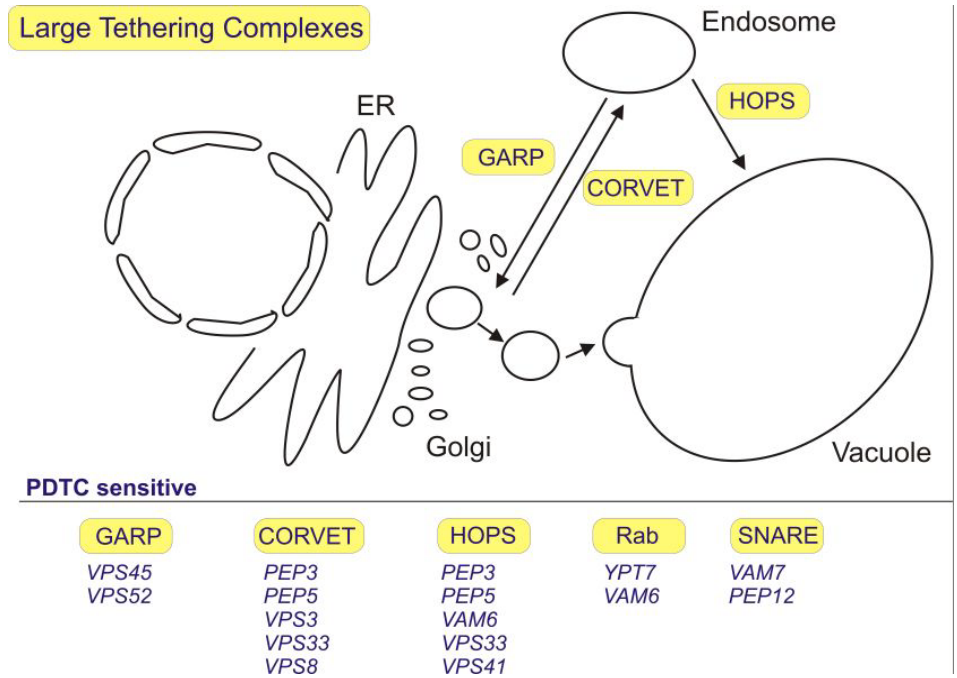

B

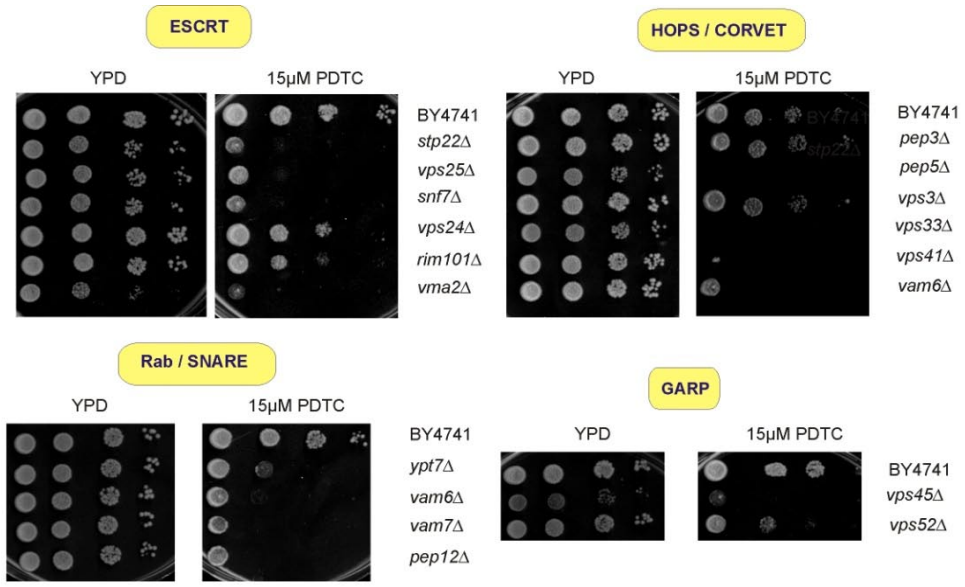

C

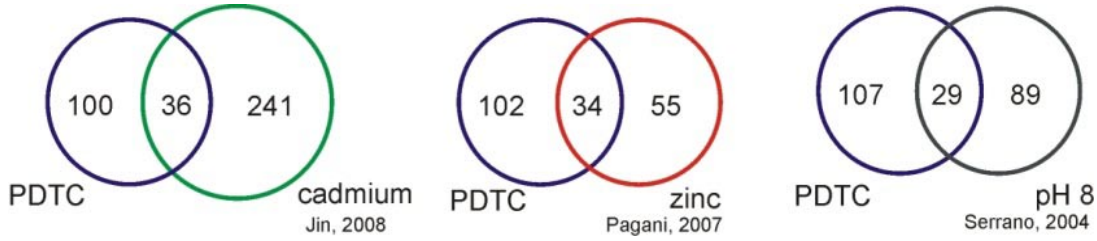

Figure 21: A. Several PDTC-sensitive mutants belong to protein complexes mainly involved in intracellular trafficking, which are indicated in the scheme. B. Deletion strains were re-tested by spotting serial dilutions on PDTC-containing plates. C. Venn diagram showing overlaps between PDTC-sensitive mutants and screening data on excess cadmium, zinc and alkaline pH (p-value ≤ 0.05).

As several PDTC-sensitive mutants have been grouped as multidrug resistance genes or genes involved in environmental stress response, we compared our data set with published large scale screenings (Fig. 21.C). Genes referred to as multidrug resistance genes show increased sensitivity to a variety of stress conditions as analyzed in (Hillenmeyer *et al.*, 2008). Remarkably, we found a significant overlap of PDTC-sensitive mutants and deletion strains sensitive to excess zinc, cadmium, oxidative stress, and alkaline pH ((Serrano *et al.*, 2004; Outten *et al.*, 2005; Pagani *et al.*, 2007; Jin *et al.*, 2008). For example, cadmium, nickel, zinc and alkaline pH interfere with the cellular iron homeostasis. The underlying mechanisms vary from decreased iron solubility at low pH, to competition at the level of uptake (zinc, cadmium) or competition at the level of iron-regulated enzymes (nickel) (Serrano *et al.*, 2004; Pagani *et al.*, 2007; Ruotolo *et al.*, 2008). Thus, PDTC tolerance requires several cellular processes and mechanisms to avoid collapse of cellular ion homeostasis.

Aberrant vacuole morphology in response to PDTC

Based on the involvement of genes encoding proteins implicated in vacuolar functions in response to PDTC, we asked whether PDTC caused changes in vacuolar morphology. Thus, we visualized the vacuole using three approaches. First, we took advantage of the W303-1A yeast wild type strain auxotrophic for adenine, which accumulates an endogenous fluorescent adenine-derived dye in its vacuole (Weisman *et al.*, 1987). Second, we investigated the vacuolar accumulation of cDCFDA in the absence or presence of PDTC. Third, we stained cells with FM4-64 to track endocytic intermediates from the plasma membrane to the vacuolar membrane (Vida and Emr, 1995).

In general, yeast vacuoles are highly dynamic organelles that rapidly change their morphology throughout the cell cycle. Typically, a large round-shaped vacuole fragments and is then separated into mother and daughter cells during cell division (Wickner, 2002). In contrast, in PDTC-stressed cells, we observed highly fragmented vacuoles and multiple vesicles surrounding the “main” vacuole (Fig.22).

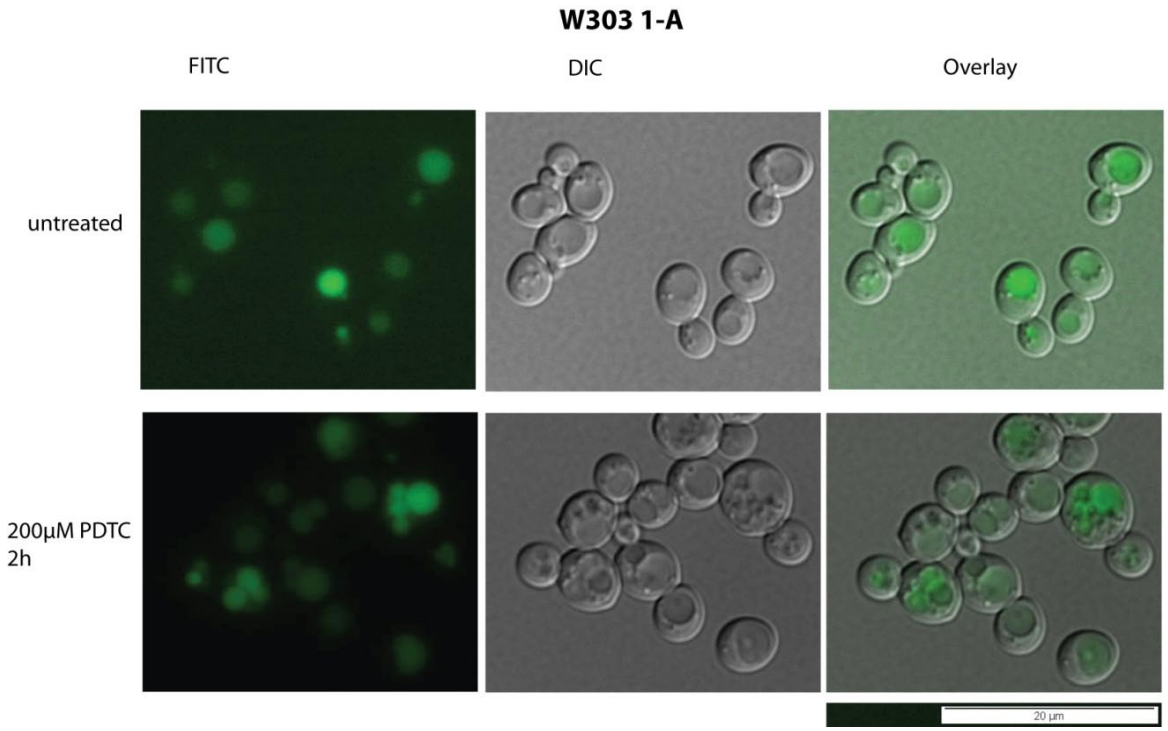

Figure 22: PDTC changes vacuolar morphology. W303-1A wild type cells were grown in rich medium to an OD_{600}~0.6 and stressed with 200µM PDTC for 2h or left untreated, washed and resuspended in 1xPBS. Pictures were taken using the Olympus Cell R Live Cell Image Microscope.

cDCFDA is a colorless compound that passively diffuses into cells, where the diacetate groups are cleaved by intracellular esterases to yield the fluorescent 5-(and-6)-carboxy-2',7'-dichlorofluorescein (cDCF), (Roberts *et al.*, 1991), which accumulates in the yeast vacuole. Interestingly, PDTC inhibited vacuolar accumulation of cDCF resulting in diffuse cytoplasmic fluorescence (Fig.23). This inhibitory effect was independent whether cells were stained with cDCFDA before or after PDTC treatment for two hours, thus indicating impaired vacuolar functions and vacuolar trafficking in the presence of PDTC.

Therefore, we aimed to investigate the endocytic trafficking to the vacuole by labeling the cells with FM4-64 tracking the fluorescent dye from the plasma membrane to vesicular intermediates and the vacuolar membrane. After staining, cells were washed, resuspended in rich medium and incubated with PDTC for the indicated time points or left untreated, washed and used for microscopy. In untreated cells, FM4-64 accumulated in small punctate intermediate compartments in the cytoplasm after 15 minutes, which disappeared concomitantly with staining of the vacuolar membrane after 45 minutes. Finally, FM4-64 specifically stained the vacuolar membrane. In contrast, in PDTC-treated cells, FM4-64 trafficking was impaired, leading to diffuse stained structures at 15 and 45 minutes and staining of multiple vesicles after two hours (Fig.24). Thus, PDTC caused

aberrant vacuolar morphology leading to fragmented vacuoles, comparable to the vacuolar maintenance of *vps* morphological group B mutants, e.g., *vps17*Δ (Vida and Emr, 1995), or preventing vacuolar fusion of endocytic vesicles.

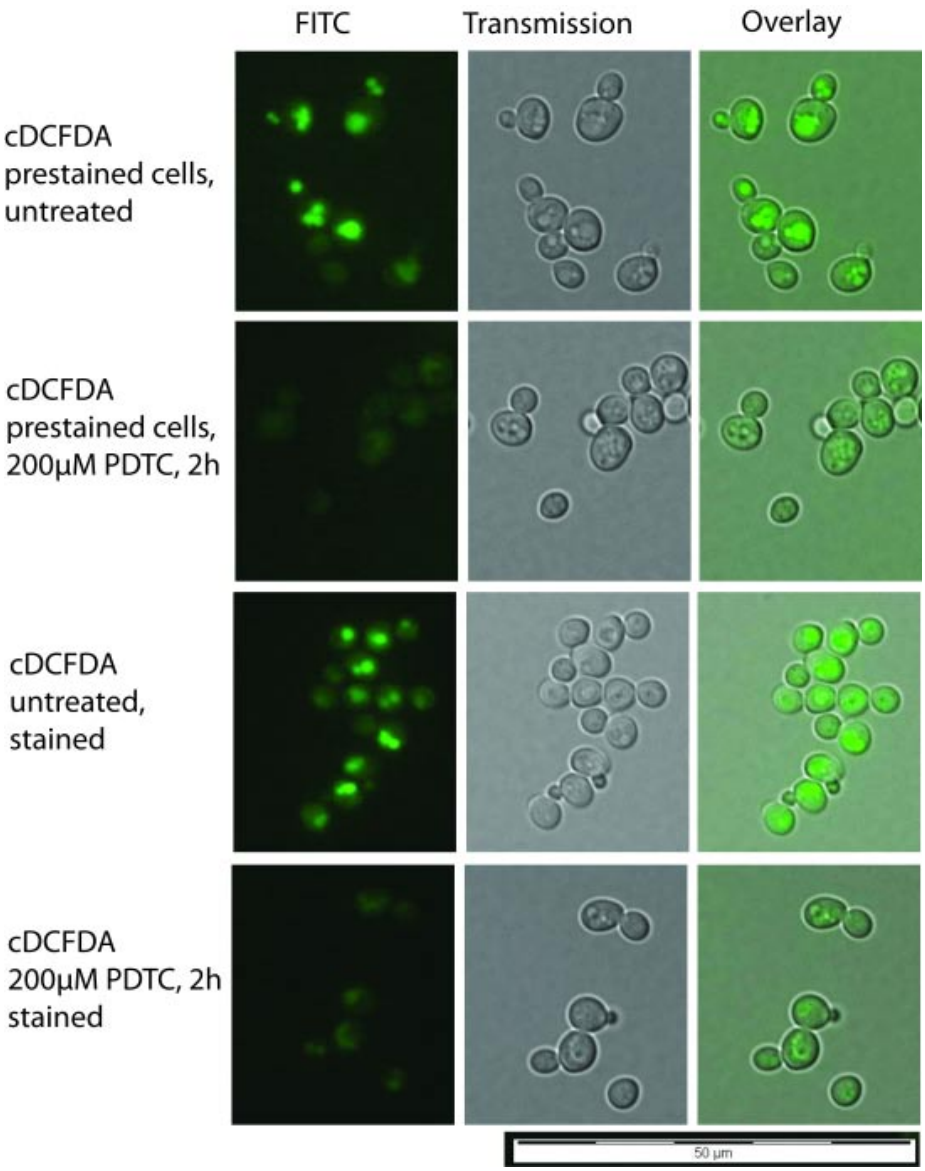

Figure 23: PDTC inhibits vacuolar accumulation of cDCFDA. BY4741 wild type cells were either pre-labeled with cDCFDA for 30 minutes, washed and stressed with 200µM PDTC or first stressed with PDTC, washed and stained with cDCFDA afterwards. Cells were washed with 1x PBS and resuspended in PBS. Pictures were taken using the Olympus Cell R Live Cell Imaging Microscope.

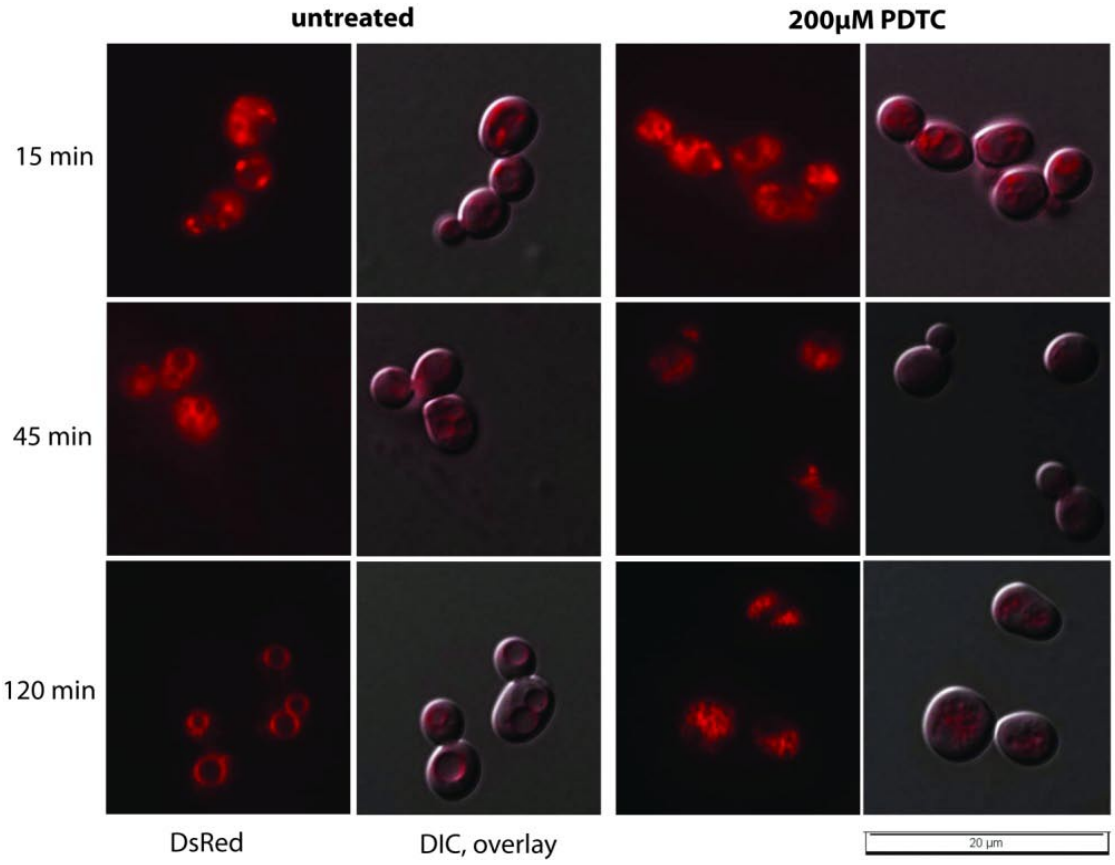

Figure 24: PDTC causes vacuolar fragmentation. Cells were labeled with FM4-64 for 15 minutes, washed, resuspended in rich medium and stressed with 200µM PDTC or left untreated. At the indicated timepoints, cells were intensely washed, and pictures were taken using the Olympus Cell R Live Cell Imaging Unit.

Mutants of pH-responsive genes and ESCRT complexes are PDTC-sensitive

Additional to vacuolar acidification, another important function of the vacuole is the maintenance of the intracellular pH in general. Changes in environmental pH are mainly interpreted by the Rim101 transcription factor. Activation of Rim101 depends on a proteolytic processing cascade that includes various components. Rim9, Rim21 (the pH sensors) and Rim8 are required for complex formation of Rim20-(Vps20-Snf7)-Rim13. Rim20 is the adaptor bringing the protease Rim13 into close proximity to its substrate Rim101. Notably, formation of the cleavage complex requires components of the ESCRT complexes, thereby linking multivesicular body sorting to alkaline pH response (Hayashi *et al.*, 2005). This link might be dependent on the requirement for a functional proton gradient during MVB sorting and its malfunction when disrupted. Under these conditions formation of the Rim101-activation complex would be promoted (Fig. 25) as proposed in (Hayashi *et al.*, 2005).

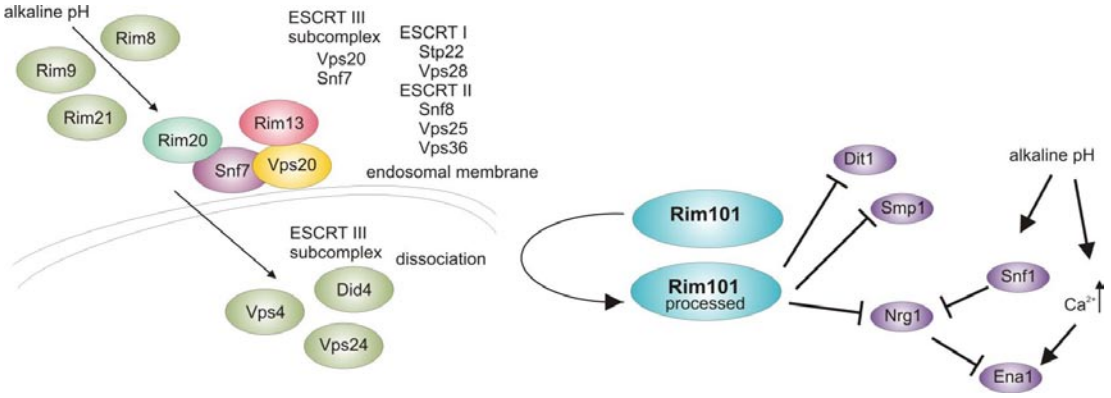

Figure 25: Proteolytic activation of Rim101 requires an activation cascade including components of the ESCRT complexes. Rim101 processing occurs at the endosomal membrane elicited by the Rim13 protease. Active Rim101 is a negative regulator of other transcription factors like Nrg1 or Smp1.

PDTC inhibits Rim101 processing

As the Rim101 pathway was required to cope with PDTC stress conditions, we investigated Rim101 activation in PDTC-treated cells. Strikingly, immunoblotting showed that PDTC inhibited proteolytic processing and thus activation of Rim101 in the AMP1604 strain carrying a genomic integrated Rim101-HA2 construct in a dose-dependent manner and independent of pH (Fig.26B,C). The processing was comparable to the cleavage pattern in the constitutive inactive control strain AMP1603 (Rim101-HA2, *rim13*Δ) lacking the protease Rim13 (Li and Mitchell, 1997).

Although growth defects of Rim101 pathway mutants were rescued by iron supplementation, the processing defect of Rim101 in the presence of PDTC remained unchanged. Hence, we investigated whether this inhibition required metal ions by comparing cell extracts of cells stressed in PBS with PDTC, $ZnSO_4$, $FeCl_3$, and combinations of those (Fig.26D). In PBS, PDTC failed to inhibit Rim101 cleavage. Zinc supplementation in combination with PDTC restored the inhibitory effect, whereas iron had no effect in Rim101 processing (Fig.26D). Neither magnesium, calcium or copper supplementation affected Rim101 processing in the presence of PDTC (data not shown). As a control for constitutive active Rim101, we used a strain expressing a mutated form of Rim101 (Rim101-HA2-531; AMP1600).

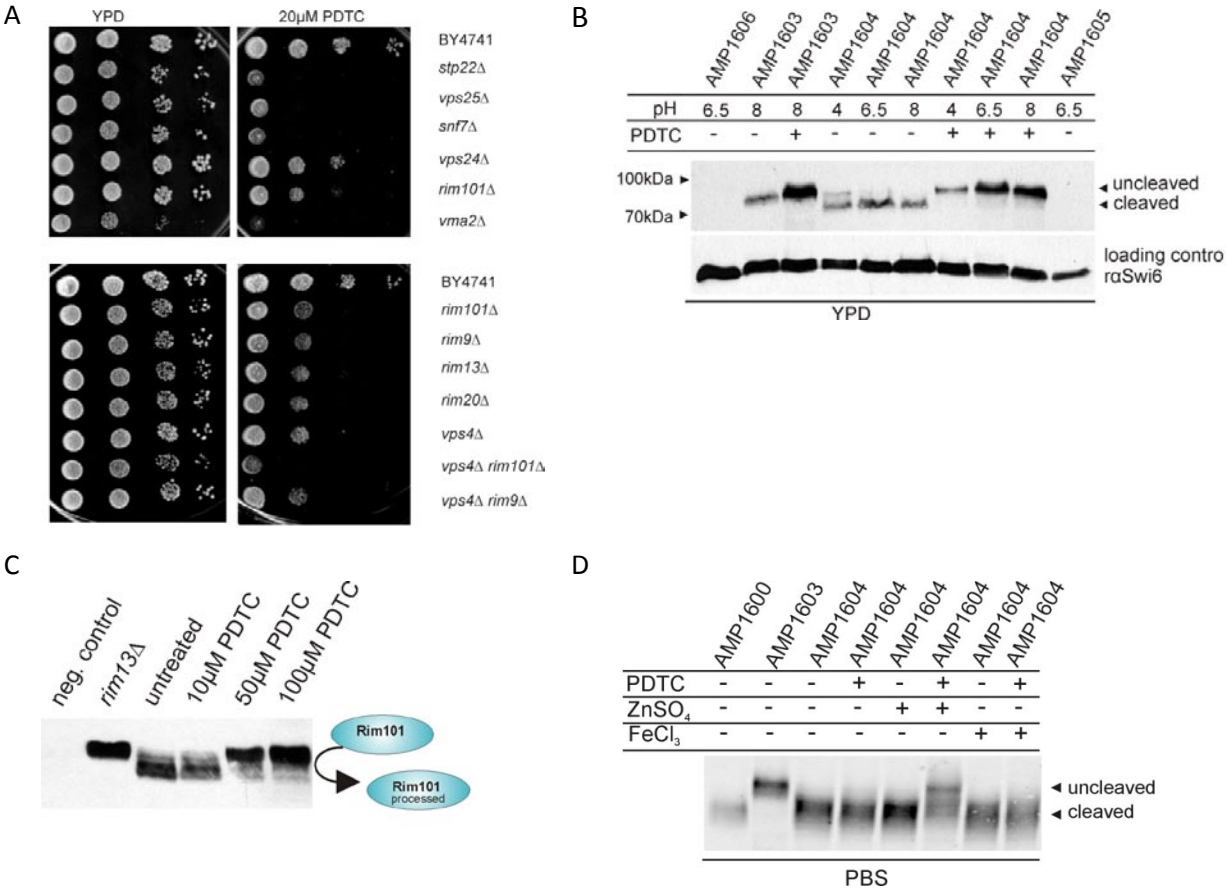

Figure 26: PDTC blocks Rim101 processing. A. *RIM101* pathway mutants and ESCRT deletion strains are PDTC-sensitive. Wild type and deletion strains were spotted in serial dilutions on YPD and PDTC-containing plates and grown at 30°C for 2 days. B. PDTC inhibits Rim101 cleavage at various pH. AMP1604 expresses a HA-tagged version of Rim101. AMP1603 was used as a constitutively inactive control strain, carrying the Rim101-HA2 construct, but lacking the Rim13 protease. AMP1600 carries a mutation that constitutively activates Rim101-HA2. AMP1605 and AMP1606 were used as untagged negative controls. C. PDTC-induced inhibition of Rim101-processing is dose-dependent. D. Inhibition of Rim101 processing by PDTC is strictly dependent on zinc ions in the medium. Cells were stressed in 1xPBS and supplemented with 200µM PDTC, 100µM $ZnSO_4$ or 1mM $FeCl_3$, respectively.

Thus, PDTC-induced inhibition of Rim101 cleavage strictly required zinc ions in the medium. Taken together, our data identified a potential host cell drug target for the antiviral drug PDTC. PDTC is to the best of our knowledge the first known small-molecule inhibitor of Rim101 processing in yeast, requiring zinc ions for exerting the inhibitory action.

As vacuolar functions and zinc storage during PDTC response were tightly connected, we aimed to identify an additional putative link to the Rim101 pathway. Therefore, we compared growth phenotypes and vacuolar morphology of single and double deletion strains lacking components of the *RIM101* pathway and ESCRT complex in the presence and absence of PDTC. By determining the inhibitory concentrations of PDTC, we observed a synergistic effect in the *rim101*Δ *vps4*Δ double deletion strain, whereas a *rim9*Δ *vps4*Δ strain showed the same sensitivity as the single deletion strains (Fig. 27.B). Therefore, we

focused on the impact of Vps4, an AAA-type ATPase involved in MVB sorting and disassembly of the ESCRT III complex (Davies *et al.*, 2009), on the Rim101 pathway in response to PDTC.

A

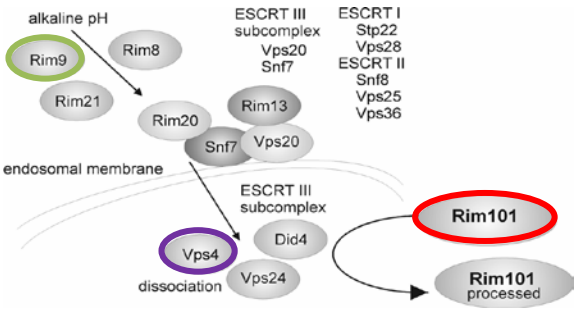

B

Yeast strains	PDTC IC_{50}
wild type	72
rim101Δ	41
vps4Δ	53
rim101Δ vps4Δ	28
rim9Δ	40
rim9Δ vps4Δ	43

Figure 27: A. Schematic presentation of components involved in the Rim101 processing cascade. B. We performed growth curves in the presence of various PDTC concentrations [µM] and determined the inhibitory concentrations of PDTC in the wild type and different deletion strains.

Mutants lacking Vps4 showed weak vacuolar membrane staining, but another intensely stained membrane-associated structure, comparable to *vps* morphological group E mutants (Vida and Emr, 1995). The punctate structure might be due to the failure of cells lacking Vps4 to disassemble the ESCRT III complex. Interestingly, deletion of Vps4 prevented vacuolar fragmentation in response to PDTC (Fig.28). Vacuolar staining in *rim101*Δ and *aft1*Δ cells was comparable to the wild type vacuolar morphology. However, in PDTC-treated *rim101*Δ cells, the dye accumulated in punctate structures rather than in fragmented vacuoles. In the double deletion strain, lacking both, Vps4 and Rim101, FM4-64 stained a membrane-enclosed structure similar to the Vps4 single deletion strain, which persisted during PDTC treatment. Thus, additional deletion of Vps4 suppressed the effect of the Rim101 deletion in response to PDTC. Hence, Vps4 might be an important player implicated in vacuolar trafficking and in the PDTC-dependent inhibition of Rim101 activation by PDTC.

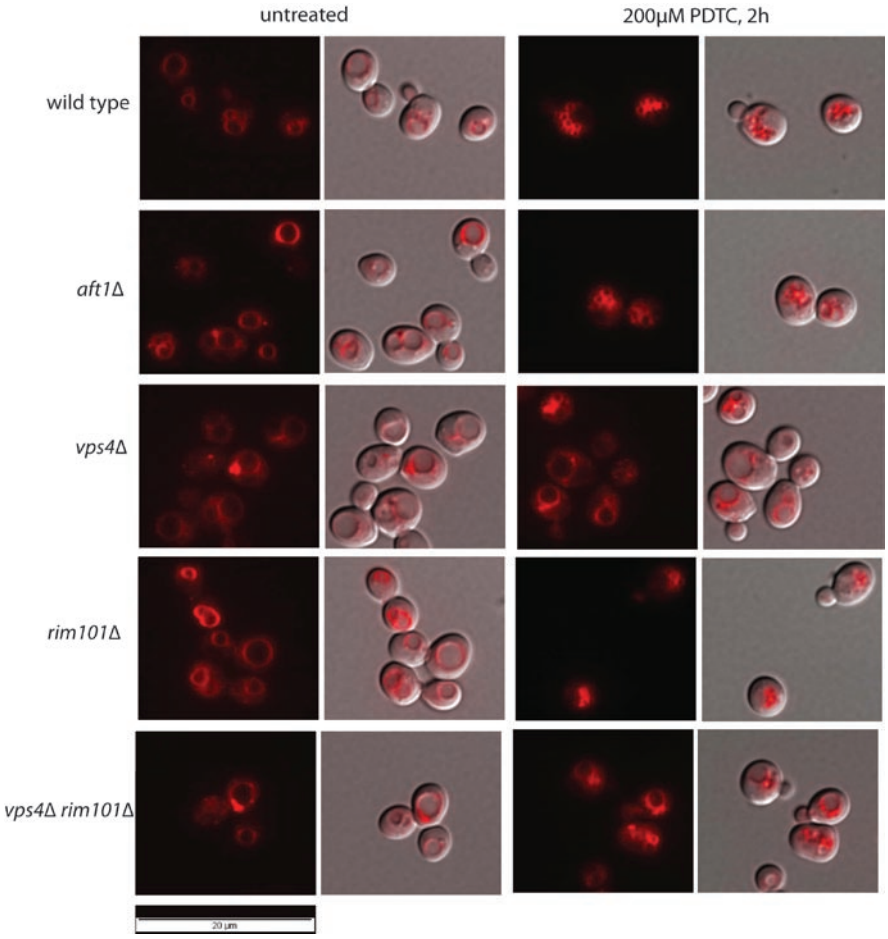

Figure 28: FM4-64 staining in wild type, *rim101*Δ, *vps4*Δ, and *rim101*Δ *vps4*Δ in response to PDTC. Cells were grown in YPD, stained with FM4-64 for 15 minutes, washed and resuspended in YPD. Cells were either stressed with PDTC for 2 hours or left untreated, washed and used for microscopy.

Deletion of Vps4 inhibited vacuolar fragmentation or fusion in response to PDTC. A similar phenotype has been observed in response to high osmotic stress. High salt concentrations cause vacuolar fragmentation, which is restored by disruption of the V-ATPase (Bonangelino *et al.*, 2002; Baars *et al.*, 2007). Thus, we asked whether ATPase activity was required to prevent changes in vacuolar morphology upon PDTC treatment. Consequently, we compared vacuolar morphology of cells lacking either Vps4, Vma2 or Stp22 to vacuoles in wild type cells (Fig.29). Deletion of Vma2, encoding the B subunit of the V-ATPase, results in the loss of vacuolar acidification (Kane, 2006). Stp22 is a component of the ESCRT-I complex involved in vacuolar protein sorting into the endosome (Katzmann *et al.*, 2001). In the wild type and in the *stp22*Δ strain, we observed regular vacuolar morphology as in untreated cells, which changed to multiple small vesicles upon PDTC treatment. In contrast, lack of the Vps4 ATPase activity at the endosomal membrane as well as vacuolar ATPase activity due to deletion of Vma2, resulted in large single vacuoles instead of multiple smaller vesicles in response to PDTC. Thus, as proton translocation by the V-ATPase is essential for vacuole fragmentation

(Baars *et al.*, 2007), the Vps4 ATPase activity might as well be implicated in this process, at least in response to PDTC.

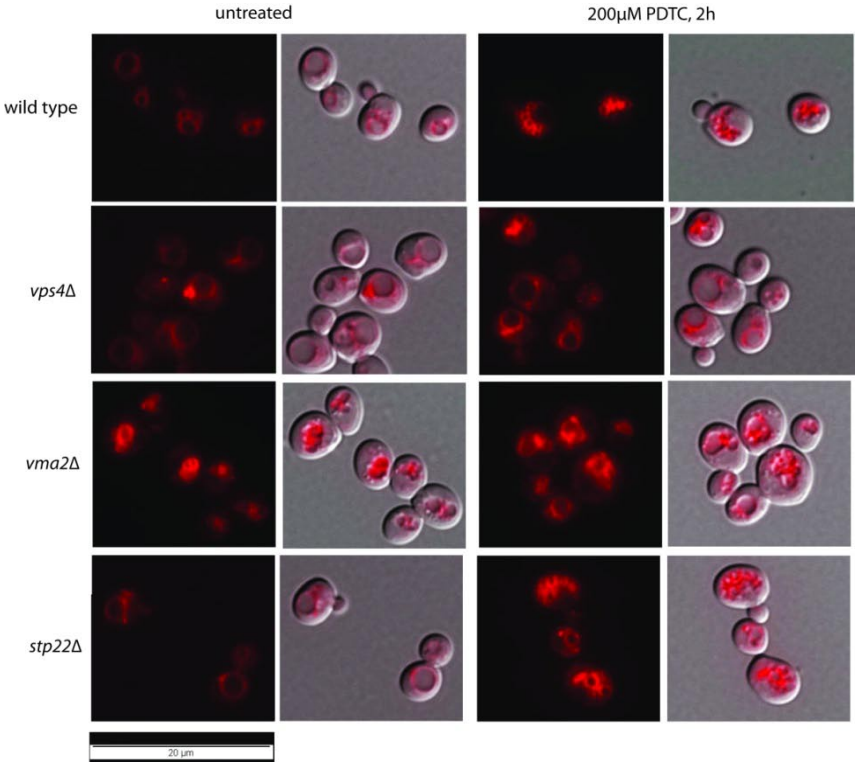

Figure 29: Lack of Vma2 and Vps4 inhibit vacuolar fragmentation in response to PDTC. Cells were grown to an OD_{600} ~0.6, labeled with FM4-64 for 15 minutes, washed with PBS, resuspended in YPD. After stressing the cells with PDTC for 2 hours, untreated control cells as well as PDTC-treated cells were washed with PBS and used for microscopy. Pictures were taken using the Olympus Cell R Live Cell Imaging Unit.

Moreover, we investigated the effect of genetically deleting Vps4, Rim101, as well as both on the transcriptional profile in untreated and PDTC-treated cells. As in the wild type, PDTC strongly affected the iron metabolism by activating genes of the Aft1-dependent iron regulon and stress responsive genes in these deletion strains (Fig.30). Rim101, a repressor of Nrg1 and Smp1, also regulates cell wall-related genes (e.g., *CWP1*, *KTR5*, YJR061W), as well as genes involved in the mating response (e.g., *AGA1*, *FUS1*, *BAR1*, *MFA1*). Interestingly, deletion of Rim101 already modulates iron and zinc transport genes (Fig.30, (Lamb and Mitchell, 2003)). In detail, lack of Rim101 induced genes involved in siderophore iron transport (*ARN1*, *ARN3*, *FIT2*, *FIT3*), as well as the high-affinity iron uptake system (*FET3*, *FTR1*), (Table 6). However, the endosomal ferric enterobactin transporter gene *ARN4* was downregulated in *rim101*Δ cells, whereas the high affinity zinc transporter gene *ZRT1* was induced. Strikingly, PDTC treatment reversed the effect by inducing *ARN4* and downregulating *ZRT1*. The activation of iron transport genes the absence of Rim101 indicates either changed iron availability upon varying pH levels or a potential cross-regulation with the iron-responsive transcription factor Aft1. Indeed, Rim101 and Aft1 have been recently suggested to act in parallel, since double deletion of

Rim101 and Aft1 causes synthetic sickness, which is ameliorated by iron supplementation (Berthelet *et al.*, 2010).

Gene name	fold wt vs wt PDTC	fold *rim101Δ* vs *rim101Δ* PDTC	fold *rim101Δ* vs wt	Description
FIT2	13,74	9,65	2,30	Mannoprotein that is incorporated into the cell wall via a glycosylphosphatidylinositol GPI anchor involved in the retention of siderophore-iron in the cell wall
FIT3	12,21	12,30	3,05	Mannoprotein that is incorporated into the cell wall via a glycosylphosphatidylinositol GPI anchor involved in the retention of siderophore-iron in the cell wall
FIT1	7,89	3,81	1,10	Mannoprotein that is incorporated into the cell wall via a glycosylphosphatidylinositol GPI anchor involved in the retention of siderophore-iron in the cell wall
ARN1	25,99	5,90	8,69	Transporter member of the ARN family of transporters that specifically recognize siderophore-iron chelates; responsible for uptake of iron bound to ferrirubin ferrirhodin and related siderophores
ARN2|TAF1	19,70	11,55	1,64	Transporter member of the ARN family of transporters that specifically recognize siderophore-iron chelates; responsible for uptake of iron bound to the siderophore
SIT1|ARN3	9,92	1,80	3,71	Ferrioxamine B transporter member of the ARN family of transporters that specifically recognize siderophore-iron chelates; transcription is induced during iron deprivation and diauxic shift; potentially phosphorylated by Cdc28p
ENB1|ARN4	5,66	6,82	-2,87	Endosomal ferric enterobactin transporter expressed under conditions of iron deprivation; member of the major facilitator superfamily; expression is regulated by Rcs1p and affected by chloroquine treatment
FET3	7,31	2,06	3,34	Ferro-O_2-oxidoreductase required for high-affinity iron uptake and involved in mediating resistance to copper ion toxicity belongs to class of integral membrane multicopper
FTH1	2,69	2,51	1,57	Putative high affinity iron transporter involved in transport of intravacuolar stores of iron; forms complex with Fet5p; expression is regulated by iron; proposed to play indirect role in endocytosis
FTR1	4,96	1,89	2,03	High affinity iron permease involved in the transport of iron across the plasma membrane; forms complex with Fet3p; expression is regulated by iron
FRE3	4,53	2,19	1,67	Ferric reductase reduces siderophore-bound iron prior to uptake by transporters; expression induced by low iron levels
FRE2	3,89	1,80	1,89	Ferric reductase and cupric reductase reduces siderophore-bound iron and oxidized copper prior to uptake by transporters; expression induced by low iron levels but not by low copper levels
ZRT1	-3,51	-9,19	4,92	High-affinity zinc transporter of the plasma membrane responsible for the majority of zinc uptake; transcription is induced under low-zinc conditions by the Zap1p transcription factor
ZRT2	-4,82	-5,03	1,27	Low-affinity zinc transporter of the plasma membrane; transcription is induced under low-zinc conditions by the Zap1p transcription factor
IZH1	-1,45	-2,17	-1,47	Membrane protein involved in zinc metabolism member of the four-protein IZH family; transcription is regulated directly by Zap1p expression induced by zinc deficiency and fatty acids; deletion increases sensitivity to elevated zinc
ZRC1|OSR1	-1,72	-2,60	1,58	Vacuolar membrane zinc transporter transports zinc from the cytosol into the vacuole for storage; also has a role in resistance to zinc shock resulting from a sudden influx of zinc into the cytoplasm
COT1	2,91	3,14	1,04	Vacuolar transporter that mediates zinc transport into the vacuole; overexpression confers resistance to cobalt and rhodium

Table 6: Genes related to iron or zinc transport that were differentially regulated in the *rim101Δ* strain compared to its wild type, as well as in response to PDTC. Upregulated genes (fold-change ≥ 2) are shaded in red, downregulated genes (fold-change ≤ -2) in green, (p-value ≤ 0.05).

***rim101Δ* vs wild type**

Upregulated genes

Gene Ontology term	Cluster frequency	P-value	Genes annotated to the term
iron ion homeostasis	5 out of 55 genes, 9.1%	0.00132	*CCC2, SIT1, ARN1, TIS11, FET3*
transition metal ion transport	5 out of 55 genes, 9.1%	0.00308	*CCC2, SIT1, ZRT1, ARN1, FET3*
siderophore transport	3 out of 55 genes, 5.5%	0.00501	*SIT1, ARN1, FIT3*

Downregulated genes

Gene Ontology term	Cluster frequency	P-value	Genes annotated to the term
sexual reproduction	9 out of 37 genes	2.34e-05	*FUS1, MFA1, EMI2, BAR1, PRM2, FAR1, CWP1, PRM1, AGA1*
response to chemical stimulus	8 out of 37 genes	0.00371	*FUS1, MFA1, HSP12, BAR1, FAR1, PRM1, AGA1, USV1*

Figure 30: Functional categories of genes differentially expressed in a *rim101Δ* strain compared to its corresponding wild type. Lack of Rim101 causes activation of the Aft1-dependent iron regulon as well as downregulation of sporulation-related genes.

Lack of Vps4 caused differential expression of genes mainly involved in amino acid metabolic process. The transcriptional profile of the *rim101Δ vps4Δ* double deletion strain was highly similar to the *rim101Δ* transcriptome. In the *vps4Δ* strain, PDTC treatment caused significant induction of genes related to the proteasomal turnover (Fig.31A), thus indicating a need for enhanced proteolytic activity if the ATPase activity of Vps4 at the endosomal membrane is abolished. Moreover, a strain lacking the proteasomal subunits Pre1 and Pre2 showed increased PDTC-sensitivity (Fig.31B), (Heinemeyer *et al.*, 1993). Hence, Vps4 might be involved in Rim101 processing because of a changed proteasomal activity in response to PDTC.

A

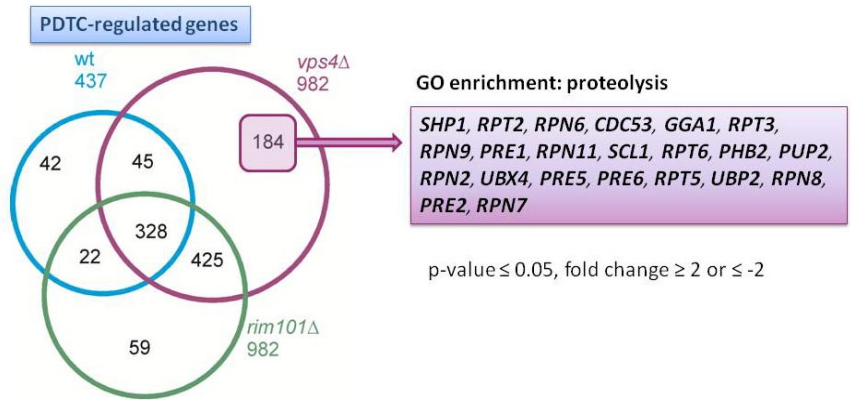

B

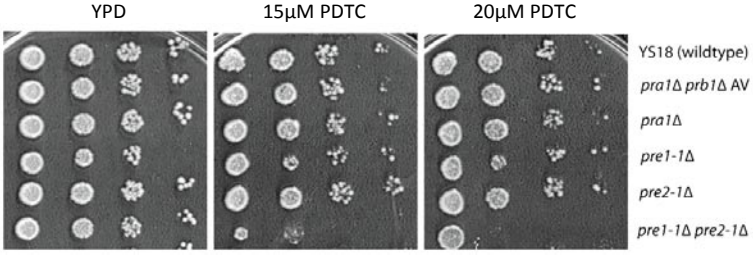

Figure 31: A. Venn diagramm of PDTC-regulated genes in the wild type, *rim101Δ* and *vps4Δ* strain. Strikingly, we identified proteasome-related genes upregulated specifically in the *vps4Δ* strain in response to PDTC. B. Lack of proteasomal subunits caused PDTC-sensitivity. Mutants lacking components of the proteasome were spotted in serial dilutions on YPD and PDTC-containing plates monitoring growth after two days.

To further investigate the impact of the Rim101 pathway on PDTC-induced disturbance of metal ion homeostasis, we used reporter strains expressing citrine under the control of the *ARN4* promoter. *ARN4* is downregulated in a *rim101*Δ strain, hence positively regulated by Rim101 in the wild type situation (Table 6, (Lamb and Mitchell, 2003)). Moreover, *ARN4* encoding the enterobactin siderophore iron transporter is a known target of Aft1 (Yamaguchi-Iwai *et al.*, 1996; Philpott and Protchenko, 2008). As Rim101 is activated upon alkaline pH stress, we performed experiments at pH 4, 6.5, and 9 with or without supplemented PDTC monitoring reporter fluorescence by microscopy (Fig.32A). In a control experiment, we verified that the fluorescent signal of citrine was stable and pH-independent using the *STL1*-citrine promoter-tagged strain (Fig. 32C), a reporter for the high osmolarity glycerol (HOG)-pathway inducible with salt stress. As expected, alkaline pH activated the *ARN4* promoter resulting in an increased fluorescent signal that was quantified by measuring average grey values of fluorescent cells (Fig.32B). Furthermore, PDTC treatment induced *ARN4* promoter activity at pH 4 and 6.5, which was additionally increased in combination with alkaline pH, leading to a contradictory observation. On the one hand, PDTC treatment induced *ARN4* expression, whereas on the other hand, PDTC inhibited cleavage of Rim101 in a zinc-dependent manner. Chromatin IP experiments investigating the Rim101 association state to various promoters revealed that Rim101 might only indirectly activate *ARN4* (Lamb and Mitchell, 2003). In agreement, deletion of Rim101 weakened the fluorescent signal, but the *ARN4* promoter was still activated upon alkaline pH and PDTC treatment. In context with the previously reported role of Rim101 in ion tolerance and the suggestion that Rim101 and Aft1 act in parallel, we expected that deletion of Aft1 prevented promoter activation of *ARN4.* Indeed, the promoter activity of *ARN4* was completely abolished in the *aft1*Δ strain, indicating that *ARN4* expression in response to PDTC is Aft1-dependent. However, due to an overall decrease in the fluorescence intensity in the *rim101*Δ strain (Fig.32A,B), our results might indicate a potential additive effect of Rim101 and Aft1.

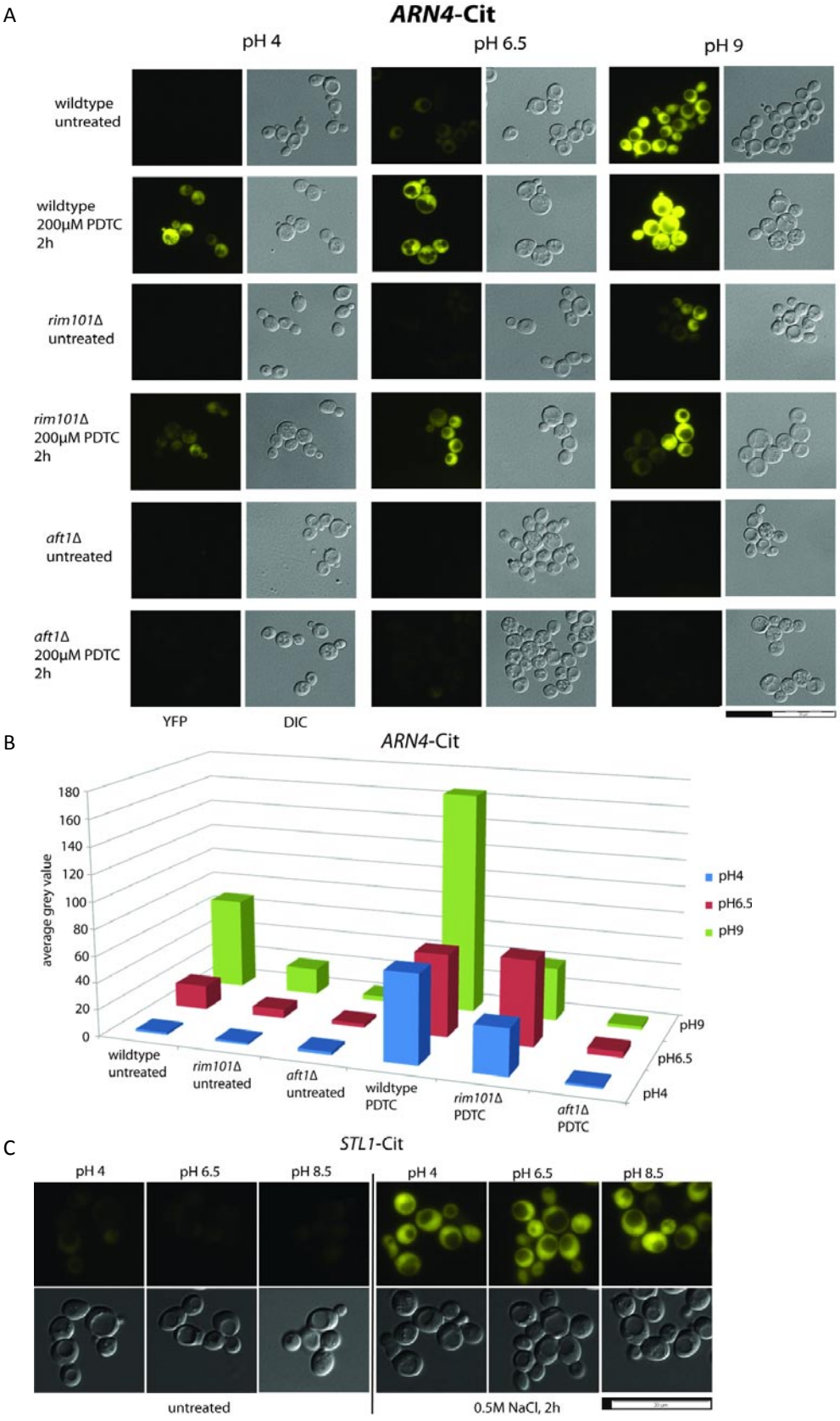

Figure 32: PDTC activates the *ARN4* promoter. A. Microscopy of *ARN4*-Cit promoter activity in the wild type, *rim101*Δ, and *aft1*Δ strain. Cells were grown in YPD adjusted to pH 4, 6.5 or 9, stressed with 200µM PDTC for 2h or left untreated. After extensive washing in PBS cells, were used for microscopy. Pictures were taken using the Olympus Cell R Live Cell Imaging Unit. B. Quantification of the fluorescent signal by measuring average grey values. Average values of at least 15 cells per strain are shown. C. *STL1*-Cit was used as control to ensure pH-independency of citrine fluorescence intensity. Therefore, we grew *STL1*-Cit at pH 4, 6.5, and 8.5. Activation of the *STL1* promoter was induced by 0.5M NaCl for 2h.

As PDTC caused inhibition of Rim101 processing in a zinc-dependent manner, and iron supplementation rescued the PDTC-caused growth defect of the Rim101 pathway and ESCRT complex deletion mutants, we investigated the effect of iron and zinc on *ARN4*-promoter activity. Activation of the *ARN4* promoter was dose-dependent as shown by FACS analysis (Fig.33A). In agreement with our suggested cross-talk between iron and zinc regulons, supplementing Zn^{++} also activated the *ARN4* promoter (Fig.33B). Iron supplementation inhibited the basal expression level of *ARN4*-citrine in rich medium, but failed to reverse PDTC-induced activation in the wild type and the *rim101*Δ strain (Fig.33C,D).

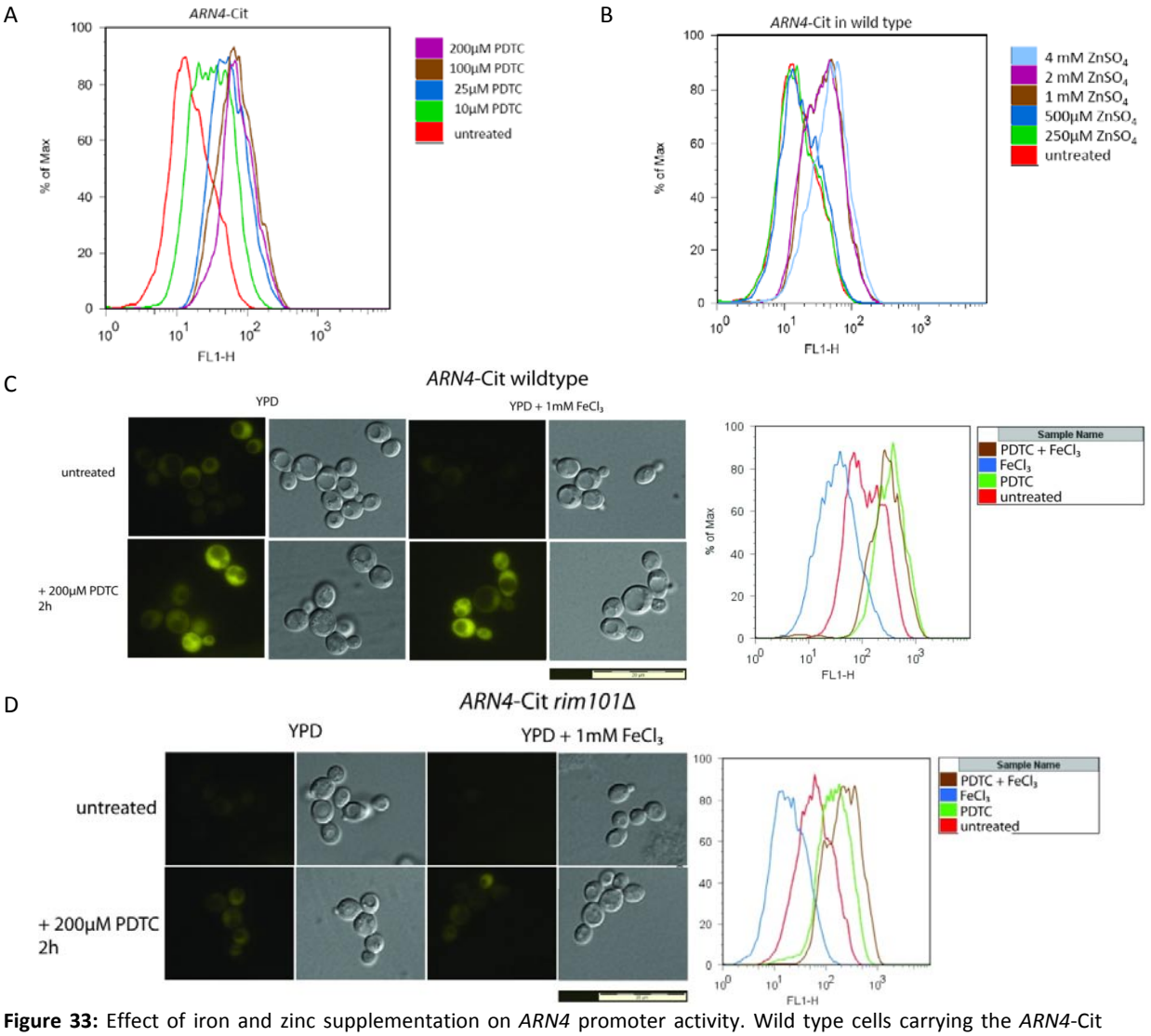

Figure 33: Effect of iron and zinc supplementation on *ARN4* promoter activity. Wild type cells carrying the *ARN4*-Cit reporter construct were grown to an OD_{600}~ 0.6 and stressed for 2 hours with various concentrations of PDTC, $FeCl_3$ and $ZnSO_4$, respectively, washed with PBS and fluorescence was monitored using a FACS Calibur. A. PDTC caused dose-dependent activation of *ARN4*-Cit. B. In agreement with the proposed cross-talk between zinc and iron regulon, zinc supplementation induced *ARN4* promoter activity. C. Iron supplementation abolished the basal activity of the *ARN4* promoter, but failed to compensate or decrease its activity in response to PDTC. D. In a *rim101*Δ strain carrying the *ARN4*-Cit promoter reporter construct, we observed the same activity pattern as in the wild type, however concomitant with an overall decrease in fluorescence.

Furthermore, we tested whether other stress conditions activated the reporter. In summary, the *ARN4* promoter was activated upon alkaline pH, PDTC, high excess zinc and MMS. Contrary, cell wall stress like SDS, calcofluor white and zymolyase failed to activate the *ARN4* promoter (Fig.34). Interestingly, PDTC activated the *MLP1* promoter, which was used as a reporter for the PKC pathway. A *MLP1*-citrine reporter strain lacking the MAPK Slt2 was used as control. Rim101 is a regulator of cell wall stress, thus PDTC might exert effects on the Rim101 pathway that are connected to the PKC pathway signaling.

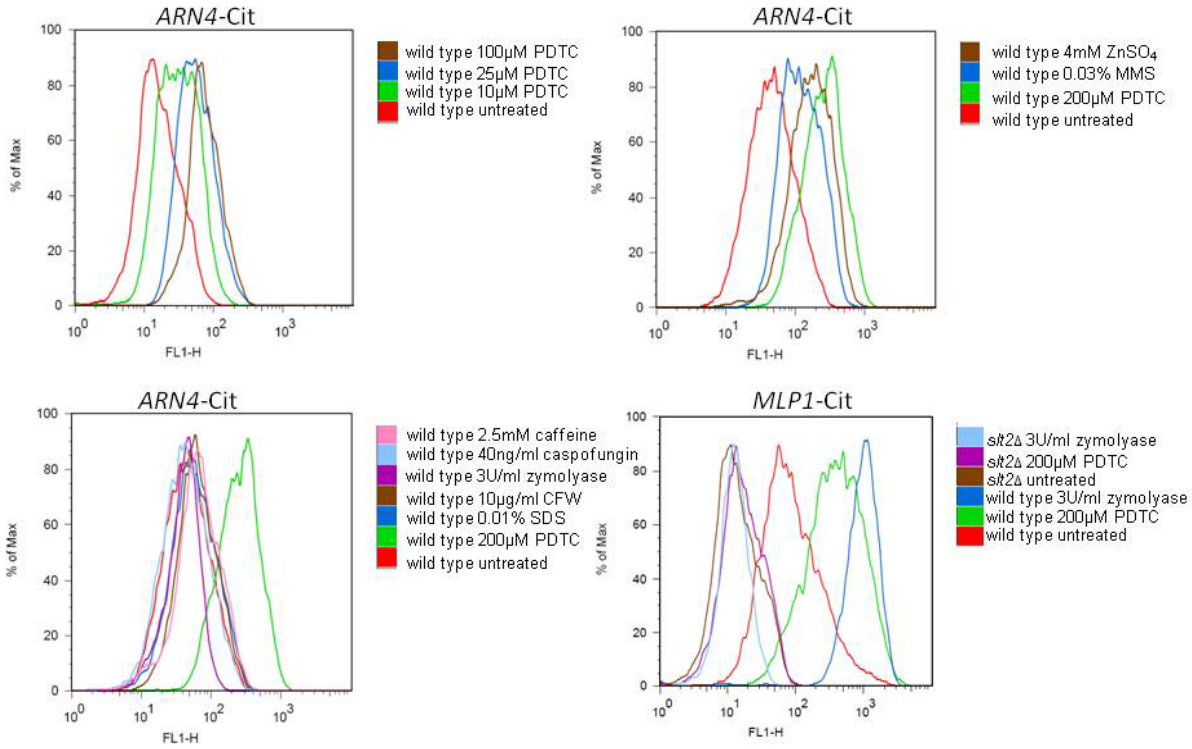

Figure 34: FACS analysis of *ARN4*-Cit. Upper left panel, PDTC caused dose-dependent activation of the *ARN4* promoter. Upper right panel, the *ARN4* promoter was activated upon excess zinc, MMS treatment and PDTC. Lower left, cell wall stress failed to activate the *ARN4* promoter. Lower right, the *MLP1* promoter was activated in response to PDTC.

In a nutshell, we propose that PDTC causes an immediate zinc influx into yeast cells, storage of the excess zinc in the vacuole and a zinc-dependent disruption of the iron homeostasis thereby activating the iron-dependent transcription factor Aft1 and interference with the Rim101 pathway. Strikingly, PDTC inhibited activation of Rim101 in a zinc-dependent manner. PDTC is to the best of our knowledge the first known small-molecule inhibitor of Rim101 processing in yeast, requiring zinc ions for exerting the inhibitory action. Furthermore, PDTC is known to inhibit cleavage of the eukaryotic translation initiation factor eIF4G (Gaudernak *et al.*, 2002), as well as activation the transcription factor nuclear factor kappa B (Meyer *et al.*, 1993). Taken together, our data

identify a potential host cell drug target for the antiviral drug PDTC, thereby linking our data found in yeast to the function of PDTC in higher eukaryotes. In essence, the results underscore the important role of cellular trafficking, ion homeostasis and the involvement of multiple pathways in response to stress.

7. DISCUSSION

In this study, we take advantage of a yeast genetic approach combining transcriptional profiling and genome-wide phenotypic screenings to identify potential cellular targets of the antiviral compound pyrrolidine dithiocarbamate (PDTC). The transcriptional profile indicates disturbance of metal ion homeostasis, including a strong induction of the iron regulon as well as regulation of zinc transport. The screening of the yeast gene deletion collection for mutants with increased PDTC susceptibility identifies numerous genes essential for PDTC tolerance, including those required for vacuolar functions and transport complexes. In more detail, this study provides data showing:

- PDTC has antifungal activity by inhibiting growth of various yeast species.
- The transcriptional profile, comprising of about 200 differentially expressed genes, reveals strong similarities to the transcriptional remodeling upon iron deprivation.
- The low-iron sensing genes including the iron-responsive transcription factor Aft1 as well as components of mitochondrial iron-sulfur complexes and glutaredoxins refer PDTC resistance.
- Iron supplementation rescues the PDTC-induced growth defect and abolishes activation of the iron regulon.
- PDTC, a zinc ionophore, causes immediate zinc influx into cells and changes the transcript levels of cellular zinc transporters driving vacuolar sequestration.
- Viability assays investigating the supplementary effect of zinc and iron on PDTC-treated cells indicate a cross-regulatory network linking zinc and iron homeostasis.
- Functionally screening of the yeast deletion collection identifies about 130 genes as PDTC-sensitive. The corresponding proteins are mainly involved in vacuolar assembly, biogenesis and vesicular and vacuolar transport and trafficking.
- PDTC causes ATPase-dependent vacuole fragmentation or a defect in fusion.
- *RIM101* pathway and ESCRT complex mutants are hypersensitive to PDTC. Strikingly, PDTC inhibits proteolytic cleavage of the Rim101 transcription factor.

Taken together, our data demonstrate that several cellular processes and regulatory networks tightly act together forming a complex and interdependent response to PDTC.

PDTC disrupts ion homeostasis causing massive cellular remodeling

Sudden stress conditions require quick responses and changes of yeast cells by activating signaling cascades, as well as initiating a stress-dependent gene expression program to adapt to changes in their environment. This adaptation process involves a precisely coordinated program of specific and general stress response mechanisms to promote a preferably positive outcome for cells, thus being cell survival. The main requirement following stress is to save energy. Thus, many genes involved in protein synthesis and cellular growth are shut down. Simultaneously, cells respond specifically to a certain stress inducing a genomic response dedicated to adaptation. Thereby, cells build up an additive response to many stresses which might strengthen the adaptation to the new stress environment (Gasch *et al.*, 2000; Gasch and Werner-Washburne, 2002).

PDTC treatment induces transcriptional changes of more than 2oo genes including general stress response genes but also specific adaptations. The general stress response genes are involved in growth related processes, RNA metabolism and repression of ribosomal protein genes. In contrast, the specific response indicates massive disturbance of metal ion homeostasis, including a strong induction of the Aft1-dependent iron regulon, as well as regulation of zinc homeostasis.

Activation of the iron regulon leads to induction of the iron uptake machinery, as well as several metabolic changes, including downregulation of various factors to switch to less iron-consuming pathways. Possibilities for activation of the iron regulon are i) inhibition of iron uptake, ii) interference with iron sensing, iii) competition with iron for protein binding sites, iiii) changes in iron utilization, iiiii) variations in copper availability. Beside iron deprivation, the iron regulon is activated by various stress conditions, ranging from changes in ion concentrations caused by excess zinc (Pagani *et al.*, 2007) or cobalt (Stadler and Schweyen, 2002), to physiological changes induced by lactic or acetic acid (Kawahata *et al.*, 2006), as well as glucose depletion occurring during the diauxic shift (Haurie *et al.*, 2003). Moreover, drugs such as the fungicide mancozeb (Santos *et al.*, 2009), chloroquine (Emerson *et al.*, 2002), hydroxyurea (Dubacq *et al*., 2006), or the anticancer drug cisplatin (Kimura *et al.*, 2007) trigger activation of the iron regulon.

Apart from environmental changes, genetic manipulations identified components whose deletion activates the iron regulon: Depletion of the mitochondrial ISC machinery

constitutively activates Aft1-dependent transcription (Hausmann *et al.*, 2008). Interestingly, deletion of the mediator tail component *SSN3* (also referred to as *CDK8* or *SRB10*) or inhibition of Med2 phosphorylation upregulates Aft1-dependent genes, linking the general transcription coactivator machinery to the iron-specific signaling cascade (van de Peppel *et al.*, 2005). Furthermore, the pH-responsive transcriptional regulator Rim101 has been implicated in iron transport (Lamb and Mitchell, 2003; Berthelet *et al.*, 2010), because iron transport genes are differentially expressed in a *rim101*Δ strain. Recently, iron-dependent down-regulation of genes at the level of regulatory metabolites provides another layer of adaptation (Ihrig *et al.*, 2009).

Like PDTC, the fungizide mancozeb is an ethylene-bis-dithiocarbamate that complexes manganese and zinc and also activates the iron regulon. Proteomic analysis suggests that mancozeb induces oxidative stress response genes, as well as genes involved in translation and protein degradation (Santos *et al.*, 2009). An important property of dithiocarbamates is their metal-chelating activity, thereby forming lipophilic dithiocarbamate-metal complexes able to enter cells. In detail, PDTC shows the highest affinity to zinc, although also chelating other ions such as copper or iron (Krenn *et al.*, 2005). Thus, PDTC or dithiocarbamates in general might complex significant amounts of extracellular iron or disturb the intracellular copper homeostasis activating the iron regulon. Moreover, PDTC causes zinc influx (Fig.17) and changes transcript levels of genes encoding zinc transporters (Fig.14).

Mutants sensitive to PDTC were also essential during excess zinc conditions (Fig.21). Thus, by changing the delicate ion balance in the cell, excess ions alter enzyme activities and metabolic functions. Since high zinc levels provoke activation of the iron regulon (Pagani *et al.*, 2007), PDTC-induced activation of the iron regulon might be an indirect effect due to increased intracellular zinc levels. This hypothesis is supported by the observation that the induction of the iron-responsive genes is delayed when compared to the transcriptional regulation of zinc transporters (Fig.14).

Metal ion homeostasis is a delicate system precisely monitored and controlled in yeast. Since diverse stimuli provoke activation of the iron regulon, interconnections between responses to different ions have been proposed due to overlapping regulatory networks. For instance, iron and copper are tightly connected as copper is the essential cofactor in

the high-affinity iron permease complex Ftr1/Fet3 (Gross *et al.*, 2000). Consequently, inhibition of copper uptake results in reduced iron uptake. Fet3 is a multicopper ferroxidase whose deletion renders cells highly sensitive to transition metal stress, alkaline pH and it causes impaired growth on ethanol and galactose/raffinose (Rutherford and Bird, 2004). Moreover, relationships between cobalt-iron (Stadler and Schweyen, 2002) and zinc-iron (Santos *et al.*, 2003; Pagani *et al.*, 2007) were identified. Notably, the vacuolar transporter Cot1, normally involved in zinc transport into the vacuole and cobalt accumulation, is induced under iron limitation (Li and Kaplan, 1998). High excess zinc disrupts iron homeostasis by altering the intracellular iron content and iron-dependent enzyme activities such as cytochrome c oxidase, and aconitase, linking zinc, iron and iron/sulfur cluster (ISC) metabolism (Santos *et al.*, 2003; Pagani *et al.*, 2007). Studies of the yeast *ionome*, as well as the interplay of alkaline pH stress and ion metabolism confirm a tight and dynamic co-regulation at genomic levels (Serrano *et al.*, 2002; Serrano *et al.*, 2004; Eide *et al.*, 2005). For instance, at alkaline pH conditions, copper loading of Fet3 is impaired due to reduced bioavailability of iron.

Here, we show the impact of various metal ions in combination with PDTC on the cellular ion homeostasis. For example, the *aft1*Δ strain is sensitive to nickel, calcium, manganese, cobalt, zinc and alkaline pH (Fig.12, (Stadler and Schweyen, 2002; Serrano *et al.*, 2004)). These growth defects can be compensated by the supplementation of high iron to the growth media, thereby increasing intracellular iron concentrations. In the case of glucose exhaustion, iron addition fails to rescue the growth defect, indicating two independent signals activating the iron regulon (Haurie *et al.*, 2003). In cells lacking the *AFT1* gene, the copper-binding metallothionein gene *CUP1* is highly induced by PDTC treatment, which might explain the increased copper-tolerance of the mutant when compared to the wild type (Fig.13). Consistent with the fact that PDTC is a zinc ionophore mediating zinc influx into HeLa cells (Krenn *et al.*, 2005), as well as into yeast cells, it triggers changes in transcript levels due to the intracellular ionic imbalance.

Genes involved in vacuolar maintenance & traffic confer PDTC tolerance

By functionally screening the yeast gene deletion collection for PDTC hypersensitivity, we identify genes encoding proteins involved in vacuolar functions and transport complexes that are also essential under other stress conditions such as alkaline pH and excess zinc

(Fig.21). Recently, a chemical genomic profile of yeast has uncovered a set of genes required for a variety of stress conditions classified as multidrug resistance (MDR) genes, encompassing functional categories such as endosomal transport, vacuolar degradation, and transcription (Hillenmeyer *et al.*, 2008). In context with their cellular processes, these factors build a complex system of endocytosis and vacuolar degradation, as well as synthesis of new proteins to adapt corresponding to changing conditions.

As the vacuole is the main site for intracellular detoxification, storage and maintenance of the cellular pH, lack of vacuolar biogenesis genes results in sensitivity phenotypes to various stress conditions. For example, vacuolar acidification, which is driven by a proton gradient across the vacuolar membrane through the V-ATPase, is required for vacuolar import of ions, especially for zinc sequestration (MacDiarmid *et al.*, 2002). The immense zinc storage capacity of the yeast vacuole is required to cope with PDTC-induced influx of zinc.

Maintenance of vacuolar functions and assembly also requires a complex regulation network modulating trafficking to and away from the vacuole. Thus, the vacuole is a highly dynamic structure undergoing constant fission and fusion throughout the cell cycle. Shape, size and numbers ranging from 1-5 vacuoles per cell vary dependent on the cell cycle state and in due course on adaptations in response to environmental changes. Due to constant fission and fusion, vacuoles are connected to endosomal transport and trafficking complexes permanently coordinating transport of proteins, amino acids and other substances (Wickner, 2002; Kane, 2006). As shown by microscopy, PDTC treatment causes aberrant vacuolar morphology (Fig.22) and inhibition of vacuolar accumulation of the fluorescent dye cDCF (Fig.23). By tracking the fluorescent dye FM4-64 from the plasma membrane along the endocytic pathway to the vacuolar membrane, we observe vacuolar fragmentation into multiple small vesicles (Fig.24). Fragmentation of vacuoles implies a defect in membrane fusion. For instance, vacuoles fragment into multiple vesicles due to disruption of microtubule polymerization in response to nocodazole treatment (Guthrie and Wickner, 1988). Furthermore, high osmotic stress also causes vacuolar fragmentation, a phenotype, which strictly requires proton translocation and that is inhibited by disruption of the V-ATPase (Bonangelino *et al.*, 2002; Baars *et al.*, 2007). Strikingly, mutants lacking Vps4 or Vma2 display large single vacuoles instead of

the vacuolar fragmentation phenotype in response to PDTC (Fig.29). Thus, lack of either the Vps4 ATPase activity at the endosomal membrane or the V-ATpase activity at the vacuole itself reinstates normal vacuolar morphology, indicating that vacuolar fragmentation is dependent on either ATPase activity. This observation is consistent with the suggested regulatory function of the V-ATPase in vacuolar morphology and membrane dynamics (Baars *et al.*, 2007). Thus, Vps4 ATPase activity might as well be implicated in this process, at least in response to PDTC. Proton translocation activity, establishing an electrochemical gradient across the membranes, is crucial for pH regulation, ion transport and intracellular flux. Fragmentation of vacuoles changes the surface-volume ratio, thus providing a complex regulatory mechanism, which, for instance, avoids vacuolar lysis due to water loss during high osmotic shock conditions (Bonangelino *et al.*, 2002).

Moreover, deletion of the copper-zinc superoxide dismutase Sod1 causes vacuolar fragmentation in yeast, which is oxygen-mediated and ameliorated by iron starvation, indicating that oxidative stress also changes iron homeostasis (Corson *et al.*, 1999). However, deletion of Sod1 leads to an increased intracellular iron content compared to its wild type, as well as induction of the high-affinity iron uptake gene *FET3*, indicating iron limitation in the *sod1*Δ strain (De Freitas *et al.*, 2000). Interestingly, the *SOD1* gene is induced in response to PDTC, and its deletion renders cells PDTC-sensitive, a growth defect which cannot be restored by iron supplementation (Fig.15). However, this failure might be due to an increase in iron demand of the *sod1*Δ mutant *per se* and its involvement in zinc detoxification as zinc-binding protein (De Freitas *et al.*, 2000; Tarhan *et al.*, 2007). In this case, PDTC would worsen the lack of iron availability, thereby increasing the sensitivity of the *sod1*Δ strain.

By disrupting metal ion homeostasis, PDTC induces a complex regulatory network, ranging from endocytic traffic to protein synthesis and degradation to vacuolar functions. ATPase activity establishes an electrochemical gradient, which might influence pH levels or pH-dependent processes such as transport of amino acids and ions across the vacuolar membrane (Baars *et al.*, 2007). The endocytic pathway, including the endosomal sorting complexes required for transport (ESCRT complexes), is tightly connected to both, vacuolar acidification, as well as pH regulation. First, several mutants involved in

endocytosis are synthetic lethal with *vma* mutants lacking V-ATPase activity (Munn and Riezman, 1994). Second, various components of the ESCRT complexes are required for proteolytic activation of the pH-responsive transcription factor Rim101.

PDTC inhibits proteolytic activation of the Rim101 transcription factor

Strikingly, PDTC also strongly interferes with the Rim101 pathway and ESCRT complexes by inhibiting the proteolytic activation of Rim101 (Fig.26). PDTC response involves metal ion homeostasis, inhibition of the Rim101 processing cascade, as well as vacuolar trafficking and functions. By comparing transcriptional profiles of *rim101*Δ, *vps4*Δ and the *rim101*Δ *vps4*Δ double deletion in response to PDTC, we identify a potential link between these pathways. Rim101 interferes with the cellular ion homeostasis, since it differentially regulates genes involved in metal ion homeostasis (Table 6, (Lamb and Mitchell, 2003)). Deletion of Rim101 induces genes of the iron regulon (*ARN1*, *ARN3*, *FIT2*, *FIT3, FET3*, *FTR1*). However, the endosomal ferric enterobactin transporter gene *ARN4* is down-regulated in a *rim101*Δ strain, whereas the high affinity zinc transporter gene *ZRT1* is induced. Strikingly, PDTC causes the vice-versa effect by inducing *ARN4* and downregulating *ZRT1*.

The activation of iron transport genes in a strain lacking Rim101 indicates either changed iron availability upon varying pH levels or a potential cross-regulation with the iron-responsive transcription factor Aft1. Accordingly, the genetic interaction network of Aft1 includes several components of the Rim101 pathway. For instance, double deletion of Rim101 and Aft1 causes synthetic sickness, which is ameliorated by iron supplementation (Berthelet *et al.*, 2010). Rim101 is involved in sporulation, pH response and cell wall assembly, thus its deletion causes increased sensitivity to cell wall stress and alkaline pH (Lamb *et al.*, 2001). Based on these observations and in context with the sensitivity of *aft1*Δ cells to cell wall-damaging agents such as calcofluor white (CFW) and caffeine, Rim101 and Aft1 are suspected to act in parallel (Berthelet *et al.*, 2010). By using promoter-tagged citrine reporter strains, we observe reduced fluorescent signal in a *rim101*Δ strain, but still activation of the promoter in response to alkaline pH and PDTC. Deletion of Aft1 inhibits *ARN4* promoter activity, thus indicating that *ARN4* is Aft1-dependent and may only be indirectly activated by Rim101 (Fig.32). This observation is in agreement with chromatin IP experiments suggesting indirect activation of *ARN4* gene

expression by Rim101 (Lamb and Mitchell, 2003). Furthermore, the *ARN4* promoter is activated upon alkaline pH, PDTC, high excess zinc and MMS, whereas cell wall stress such as SDS, calcofluor white and zymolyase fail to induce promoter activity. Consistent with an overall decrease in the fluorescent signal in a *rim101*Δ strain, we suggest an additive effect of Rim101 and Aft1 signalling in iron homeostasis and response to PDTC. Notably, based on our hypothesis of intracellular cross-talks, iron homeostasis is disturbed due to immense zinc influx into the cytoplasm in response to PDTC, which in turn prevents proteolytic activation of Rim101.

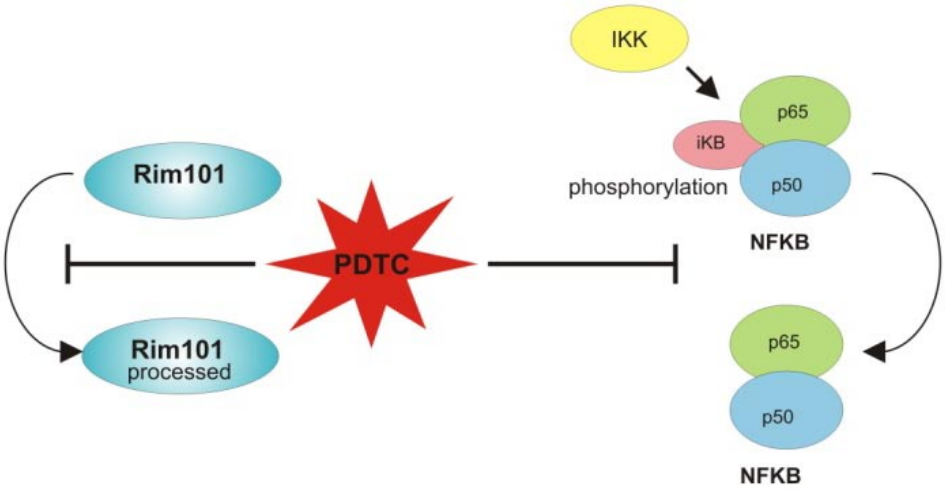

Figure 35: In yeast as well as in higher eukaryotic cells, PDTC causes zinc-dependent inhibition of a transcription factor. In yeast, PDTC inhibits the Rim101 processing cascade. Thus, the PDTC mode of action identified in yeast might provide an important linkage to higher eukaryotes, where PDTC is a known inhibitor of NF-κB activation.

Interestingly, in higher eukaryotes, PDTC is a known inhibitor of NF-κB activation, which requires ubiquitin/proteasome-dependent degradation of the inhibitory protein IκB (Fig.35,(Schreck *et al.*, 1992)). In both cases, inhibition of Rim101, as well as NF-κB activation, PDTC-caused zinc influx plays a vital role in the inhibitory activity of a transcription factor. Moreover, PDTC is known to inhibit cleavage of the eukaryotic translation initiation factor eIF4G in rhinovirus-infected HeLa cells, thus preventing virus-induced host-cell shut-off (Gaudernak *et al.*, 2002). PDTC prevents protein degradation by inhibiting an E3 ubiquitin ligase (Hayakawa *et al*., 2003) or the proteasome (Kim *et al*., 2004) in a zinc-dependent manner. In a *vps4*Δ strain, we observe induction of genes required for the proteasome function in response to PDTC (Fig.31), indicating an increased need for proteolytic processing in the absence of the Vps4 ATPase activity at

the endosomal membrane, which is also involved in Rim101 activation (Hayashi *et al.*, 2005). Thus, the zinc-dependent inhibition of Rim101 cleavage by PDTC is an important discovery. To date, and to the best of our knowledge, only genetic alterations have been shown to block Rim101 processing under activating conditions in yeast (Hayashi *et al.*, 2005). Furthermore, inhibition of a proteolytic cleavage cascade in yeast might indicate a conserved mechanism in the response to PDTC, which is mediated by zinc. Zinc has previously been shown to directly inhibit proteases. For instance, it blocks caspase-3 activity during apoptosis (Perry *et al.*, 1997). Hence, based on our data obtained in yeast and known effects of PDTC, we suggest that the antiviral activity of PDTC is primarily mediated by facilitation of zinc influx and a cumulative effect of zinc-dependent inhibitions of proteolytic activities, including the proteasome, protease-requiring activation cascades or maybe even by blocking the viral proteases 2A und 3C themselves directly.

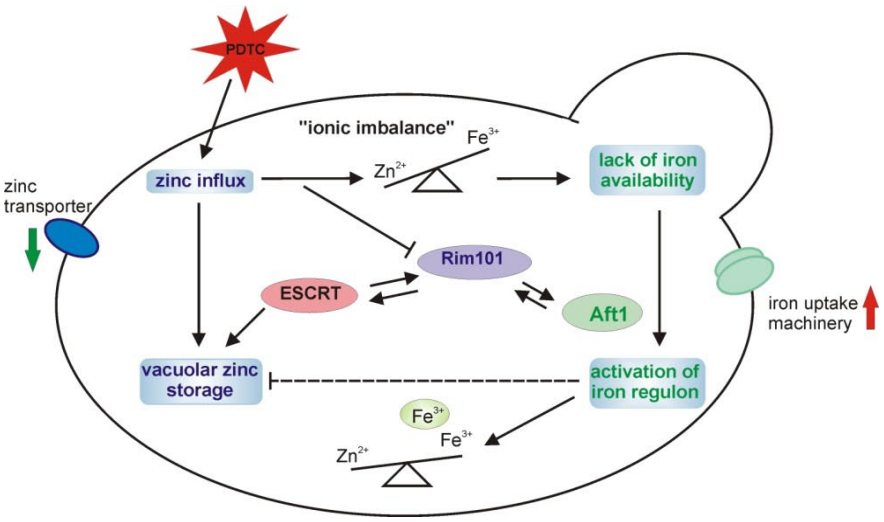

Figure 36: The ionic imbalance model. PDTC mediates intracellular zinc accumulation, leading to zinc detoxification by vacuolar sequestration, thereby causing a decrease in iron availability. Hence, the iron-responsive transcriptional factor Aft1 activates the iron regulon, stimulating cellular remodeling as under iron-limited conditions. Moreover, PDTC prevents proteolytic activation of the Rim101 transcription factor, requiring zinc ions to exert the inhibitory action. Consequently, PDTC links intracellular disturbance of iron and zinc homeostasis to other cellular processes, including vacuolar and vesicular transport, as well as pH regulation.

In summary, based on our data, we propose the "*ionic imbalance*" model for the cellular response to PDTC exposure and the PDTC mechanism of action (Fig.36). Viability assays investigating the supplementary effect of zinc and iron on PDTC-treated cells as well as transcriptome data point towards a cross-regulation of networks linking zinc and iron homeostasis (Fig.18). Iron supplementation rescues the PDTC-induced growth defects in both wild type and *aft1*Δ cells. In contrast, additional zinc in combination with PDTC is highly toxic. By investing the cumulative effect of zinc plus iron in combination with PDTC,

the *aft1*Δ mutant was rescued, whereas the wild type was hypersensitive. This cross-regulation with Aft1 as a central player is required to maintain the proper yeast *ionome*. Furthermore, this drastic modulation of metal ion homeostasis has a significant impact on cellular trafficking, intracellular pH as well as on vacuolar functions, including zinc-dependent inhibition of the Rim101 activation cascade, vesicular transport, and the endocytic trafficking pathway leading to fragmented vacuoles. Thus, cells establish a multilayer regulatory adaptation network to cope with PDTC-induced environmental changes.

Taken together, this work underscores the importance of yeast as a model system and its high potential for drug target identification. By combining transcriptional profiling datasets and genome-wide phenotypic screening, it is possible to identify complex and highly dynamic regulatory networks to disclose various biological processes involved in the response to a single drug. Notably, apart from deciphering specific drug targets by expression and sensitivity profiling of drugs, large-scale screenings in yeast can uncover off-targets, which are important for the understanding of unwanted side effects.

8. REFERENCES

Askwith, C., Eide, D., Van Ho, A., Bernard, P.S., Li, L., Davis-Kaplan, S., Sipe, D.M., and Kaplan, J. (1994). The *FET3* gene of *S. cerevisiae* encodes a multicopper oxidase required for ferrous iron uptake. Cell *76*, 403-410.

Baars, T.L., Petri, S., Peters, C., and Mayer, A. (2007). Role of the V-ATPase in regulation of the vacuolar fission-fusion equilibrium. Mol Biol Cell *18*, 3873-3882.

Balzi, E., Chen, W., Ulaszewski, S., Capieaux, E., and Goffeau, A. (1987). The multidrug resistance gene PDR1 from *Saccharomyces cerevisiae*. J Biol Chem *262*, 16871-16879.

Berthelet, S., Usher, J., Shulist, K., Hamza, A., Maltez, N., Johnston, A., Fong, Y., Harris, L.J., and Baetz, K. (2010). Functional Genomics Analysis of the *Saccharomyces cerevisiae* Iron Responsive Transcription Factor Aft1 Reveals Iron-independent Functions. Genetics.

Bharucha, N., and Kumar, A. (2007). Yeast genomics and drug target identification. Comb Chem High Throughput Screen *10*, 618-634.

Blaiseau, P.L., Lesuisse, E., and Camadro, J.M. (2001). Aft2p, a novel iron-regulated transcription activator that modulates, with Aft1p, intracellular iron use and resistance to oxidative stress in yeast. J Biol Chem *276*, 34221-34226.

Bonangelino, C.J., Nau, J.J., Duex, J.E., Brinkman, M., Wurmser, A.E., Gary, J.D., Emr, S.D., and Weisman, L.S. (2002). Osmotic stress-induced increase of phosphatidylinositol 3,5-bisphosphate requires Vac14p, an activator of the lipid kinase Fab1p. J Cell Biol *156*, 1015-1028.

Borrello, S., and Demple, B. (1997). NF kappa B-independent transcriptional induction of the human manganous superoxide dismutase gene. Arch Biochem Biophys *348*, 289-294.

Brachmann, C.B., Davies, A., Cost, G.J., Caputo, E., Li, J., Hieter, P., and Boeke, J.D. (1998). Designer deletion strains derived from *Saccharomyces cerevisiae* S288C: a useful set of strains and plasmids for PCR-mediated gene disruption and other applications. Yeast *14*, 115-132.

Caruso, T.J., Prober, C.G., and Gwaltney, J.M., Jr. (2007). Treatment of naturally acquired common colds with zinc: a structured review. Clin Infect Dis *45*, 569-574.

Charizanis, C., Juhnke, H., Krems, B., and Entian, K.D. (1999). The mitochondrial cytochrome c peroxidase Ccp1 of *Saccharomyces cerevisiae* is involved in conveying an oxidative stress signal to the transcription factor Pos9 (Skn7). Mol Gen Genet *262*, 437-447.

Chen, O.S., Crisp, R.J., Valachovic, M., Bard, M., Winge, D.R., and Kaplan, J. (2004). Transcription of the yeast iron regulon does not respond directly to iron but rather to iron-sulfur cluster biosynthesis. J Biol Chem *279*, 29513-29518.

Corson, L.B., Folmer, J., Strain, J.J., Culotta, V.C., and Cleveland, D.W. (1999). Oxidative stress and iron are implicated in fragmenting vacuoles of *Saccharomyces cerevisiae* lacking Cu,Zn-superoxide dismutase. J Biol Chem *274*, 27590-27596.

Courel, M., Lallet, S., Camadro, J.M., and Blaiseau, P.L. (2005). Direct activation of genes involved in intracellular iron use by the yeast iron-responsive transcription factor Aft2 without its paralog Aft1. Mol Cell Biol *25*, 6760-6771.

Culotta, V.C., Joh, H.D., Lin, S.J., Slekar, K.H., and Strain, J. (1995). A physiological role for *Saccharomyces cerevisiae* copper/zinc superoxide dismutase in copper buffering. J Biol Chem *270*, 29991-29997.

Davies, B.A., Azmi, I.F., and Katzmann, D.J. (2009). Regulation of Vps4 ATPase activity by ESCRT-III. Biochem Soc Trans *37*, 143-145.
De Freitas, J.M., Liba, A., Meneghini, R., Valentine, J.S., and Gralla, E.B. (2000). Yeast lacking Cu-Zn superoxide dismutase show altered iron homeostasis. Role of oxidative stress in iron metabolism. J Biol Chem *275*, 11645-11649.
De Palma, A.M., Vliegen, I., De Clercq, E., and Neyts, J. (2008). Selective inhibitors of picornavirus replication. Med Res Rev *28*, 823-884.
Delaunay, A., Pflieger, D., Barrault, M.B., Vinh, J., and Toledano, M.B. (2002). A thiol peroxidase is an H2O2 receptor and redox-transducer in gene activation. Cell *111*, 471-481.
Dickinson, J.R., Salgado, L.E., and Hewlins, M.J. (2003). The catabolism of amino acids to long chain and complex alcohols in *Saccharomyces cerevisiae*. J Biol Chem *278*, 8028-8034.
Dix, D.R., Bridgham, J.T., Broderius, M.A., Byersdorfer, C.A., and Eide, D.J. (1994). The FET4 gene encodes the low affinity Fe(II) transport protein of *Saccharomyces cerevisiae*. J Biol Chem *269*, 26092-26099.
Dreschers, S., Dumitru, C.A., Adams, C., and Gulbins, E. (2007). The cold case: are rhinoviruses perfectly adapted pathogens? Cell Mol Life Sci *64*, 181-191.
Dubacq, C., Chevalier, A., Courbeyrette, R., Petat, C., Gidrol, X., and Mann, C. (2006). Role of the iron mobilization and oxidative stress regulons in the genomic response of yeast to hydroxyurea. Mol Genet Genomics *275*, 114-124.
Eide, D.J. (2006). Zinc transporters and the cellular trafficking of zinc. Biochim Biophys Acta *1763*, 711-722.
Eide, D.J. (2009). Homeostatic and adaptive responses to zinc deficiency in *Saccharomyces cerevisiae*. J Biol Chem *284*, 18565-18569.
Eide, D.J., Clark, S., Nair, T.M., Gehl, M., Gribskov, M., Guerinot, M.L., and Harper, J.F. (2005). Characterization of the yeast ionome: a genome-wide analysis of nutrient mineral and trace element homeostasis in *Saccharomyces cerevisiae*. Genome Biol *6*, R77.
Emerson, L.R., Nau, M.E., Martin, R.K., Kyle, D.E., Vahey, M., and Wirth, D.F. (2002). Relationship between chloroquine toxicity and iron acquisition in *Saccharomyces cerevisiae*. Antimicrob Agents Chemother *46*, 787-796.
Ericson, E., Gebbia, M., Heisler, L.E., Wildenhain, J., Tyers, M., Giaever, G., and Nislow, C. (2008). Off-target effects of psychoactive drugs revealed by genome-wide assays in yeast. PLoS Genet *4*, e1000151.
Erl, W., Weber, C., and Hansson, G.K. (2000). Pyrrolidine dithiocarbamate-induced apoptosis depends on cell type, density, and the presence of Cu(2+) and Zn(2+). Am J Physiol Cell Physiol *278*, C1116-1125.
Foury, F. (1997). Human genetic diseases: a cross-talk between man and yeast. Gene *195*, 1-10.
Gasch, A.P., Spellman, P.T., Kao, C.M., Carmel-Harel, O., Eisen, M.B., Storz, G., Botstein, D., and Brown, P.O. (2000). Genomic expression programs in the response of yeast cells to environmental changes. Mol Biol Cell *11*, 4241-4257.
Gasch, A.P., and Werner-Washburne, M. (2002). The genomics of yeast responses to environmental stress and starvation. Funct Integr Genomics *2*, 181-192.
Gaudernak, E., Seipelt, J., Triendl, A., Grassauer, A., and Kuechler, E. (2002). Antiviral effects of pyrrolidine dithiocarbamate on human rhinoviruses. J Virol *76*, 6004-6015.
Giaever, G. (2003). A chemical genomics approach to understanding drug action. Trends Pharmacol Sci *24*, 444-446.

Giaever, G., Chu, A.M., Ni, L., Connelly, C., Riles, L., Veronneau, S., Dow, S., Lucau-Danila, A., Anderson, K., Andre, B., Arkin, A.P., Astromoff, A., El-Bakkoury, M., Bangham, R., Benito, R., Brachat, S., Campanaro, S., Curtiss, M., Davis, K., Deutschbauer, A., Entian, K.D., Flaherty, P., Foury, F., Garfinkel, D.J., Gerstein, M., Gotte, D., Guldener, U., Hegemann, J.H., Hempel, S., Herman, Z., Jaramillo, D.F., Kelly, D.E., Kelly, S.L., Kotter, P., LaBonte, D., Lamb, D.C., Lan, N., Liang, H., Liao, H., Liu, L., Luo, C., Lussier, M., Mao, R., Menard, P., Ooi, S.L., Revuelta, J.L., Roberts, C.J., Rose, M., Ross-Macdonald, P., Scherens, B., Schimmack, G., Shafer, B., Shoemaker, D.D., Sookhai-Mahadeo, S., Storms, R.K., Strathern, J.N., Valle, G., Voet, M., Volckaert, G., Wang, C.Y., Ward, T.R., Wilhelmy, J., Winzeler, E.A., Yang, Y., Yen, G., Youngman, E., Yu, K., Bussey, H., Boeke, J.D., Snyder, M., Philippsen, P., Davis, R.W., and Johnston, M. (2002). Functional profiling of the *Saccharomyces cerevisiae* genome. Nature *418*, 387-391.

Giaever, G., Flaherty, P., Kumm, J., Proctor, M., Nislow, C., Jaramillo, D.F., Chu, A.M., Jordan, M.I., Arkin, A.P., and Davis, R.W. (2004). Chemogenomic profiling: identifying the functional interactions of small molecules in yeast. Proc Natl Acad Sci U S A *101*, 793-798.

Gillum, A.M., Tsay, E.Y., and Kirsch, D.R. (1984). Isolation of the *Candida albicans* gene for orotidine-5'-phosphate decarboxylase by complementation of *S. cerevisiae ura3* and *E. coli pyrF* mutations. Mol Gen Genet *198*, 179-182.

Gitan, R.S., and Eide, D.J. (2000). Zinc-regulated ubiquitin conjugation signals endocytosis of the yeast Zrt1 zinc transporter. Biochem J *346 Pt 2*, 329-336.

Goffeau, A., Barrell, B.G., Bussey, H., Davis, R.W., Dujon, B., Feldmann, H., Galibert, F., Hoheisel, J.D., Jacq, C., Johnston, M., Louis, E.J., Mewes, H.W., Murakami, Y., Philippsen, P., Tettelin, H., and Oliver, S.G. (1996). Life with 6000 genes. Science *274*, 546, 563-547.

Gorner, W., Durchschlag, E., Martinez-Pastor, M.T., Estruch, F., Ammerer, G., Hamilton, B., Ruis, H., and Schuller, C. (1998). Nuclear localization of the C2H2 zinc finger protein Msn2p is regulated by stress and protein kinase A activity. Genes Dev *12*, 586-597.

Gross, C., Kelleher, M., Iyer, V.R., Brown, P.O., and Winge, D.R. (2000). Identification of the copper regulon in *Saccharomyces cerevisiae* by DNA microarrays. J Biol Chem *275*, 32310-32316.

Guthrie, B.A., and Wickner, W. (1988). Yeast vacuoles fragment when microtubules are disrupted. J Cell Biol *107*, 115-120.

Hartsfield, C.L., Alam, J., and Choi, A.M. (1998). Transcriptional regulation of the heme oxygenase 1 gene by pyrrolidine dithiocarbamate. FASEB J *12*, 1675-1682.

Haurie, V., Boucherie, H., and Sagliocco, F. (2003). The Snf1 protein kinase controls the induction of genes of the iron uptake pathway at the diauxic shift in *Saccharomyces cerevisiae*. J Biol Chem *278*, 45391-45396.

Hausmann, A., Samans, B., Lill, R., and Muhlenhoff, U. (2008). Cellular and mitochondrial remodeling upon defects in iron-sulfur protein biogenesis. J Biol Chem *283*, 8318-8330.

Hayakawa, M., Miyashita, H., Sakamoto, I., Kitagawa, M., Tanaka, H., Yasuda, H., Karin, M., and Kikugawa, K. (2003). Evidence that reactive oxygen species do not mediate NF-kappaB activation. EMBO J *22*, 3356-3366.

Hayashi, M., Fukuzawa, T., Sorimachi, H., and Maeda, T. (2005). Constitutive activation of the pH-responsive Rim101 pathway in yeast mutants defective in late steps of the MVB/ESCRT pathway. Mol Cell Biol *25*, 9478-9490.

Hayden, F.G., Herrington, D.T., Coats, T.L., Kim, K., Cooper, E.C., Villano, S.A., Liu, S., Hudson, S., Pevear, D.C., Collett, M., and McKinlay, M. (2003). Efficacy and safety of oral pleconaril for treatment of colds due to picornaviruses in adults: results of 2 double-blind, randomized, placebo-controlled trials. Clin Infect Dis *36*, 1523-1532.

Heikkinen, T., and Jarvinen, A. (2003). The common cold. Lancet *361*, 51-59.
Heinemeyer, W., Gruhler, A., Mohrle, V., Mahe, Y., and Wolf, D.H. (1993). *PRE2*, highly homologous to the human major histocompatibility complex-linked *RING10* gene, codes for a yeast proteasome subunit necessary for chrymotryptic activity and degradation of ubiquitinated proteins. J Biol Chem *268*, 5115-5120.
Hentze, M.W., Muckenthaler, M.U., and Andrews, N.C. (2004). Balancing acts: molecular control of mammalian iron metabolism. Cell *117*, 285-297.
Hillenmeyer, M.E., Fung, E., Wildenhain, J., Pierce, S.E., Hoon, S., Lee, W., Proctor, M., St Onge, R.P., Tyers, M., Koller, D., Altman, R.B., Davis, R.W., Nislow, C., and Giaever, G. (2008). The chemical genomic portrait of yeast: uncovering a phenotype for all genes. Science *320*, 362-365.
Holmes, D.S., and Quigley, M. (1981). A rapid boiling method for the preparation of bacterial plasmids. Anal Biochem *114*, 193-197.
Holyoak, C.D., Bracey, D., Piper, P.W., Kuchler, K., and Coote, P.J. (1999). The *Saccharomyces cerevisiae* weak-acid-inducible ABC transporter Pdr12 transports fluorescein and preservative anions from the cytosol by an energy-dependent mechanism. J Bacteriol *181*, 4644-4652.
Hughes, T.R., Marton, M.J., Jones, A.R., Roberts, C.J., Stoughton, R., Armour, C.D., Bennett, H.A., Coffey, E., Dai, H., He, Y.D., Kidd, M.J., King, A.M., Meyer, M.R., Slade, D., Lum, P.Y., Stepaniants, S.B., Shoemaker, D.D., Gachotte, D., Chakraburtty, K., Simon, J., Bard, M., and Friend, S.H. (2000). Functional discovery via a compendium of expression profiles. Cell *102*, 109-126.
Ihrig, J., Hausmann, A., Hain, A., Richter, N., Lill, R., and Muhlenhoff, U. (2009). Iron regulation through the back door: Iron-dependent metabolite levels contribute to the transcriptional adaptation to iron deprivation in *S. cerevisiae*. Eukaryot Cell.
Jacoby, E. (2006). Chemogenomics: drug discovery's panacea? Mol Biosyst *2*, 218-220.
Jin, Y.H., Dunlap, P.E., McBride, S.J., Al-Refai, H., Bushel, P.R., and Freedman, J.H. (2008). Global transcriptome and deletome profiles of yeast exposed to transition metals. PLoS Genet *4*, e1000053.
Johnson, E.A., Tanford, C., and Reynolds, J.A. (1985). Variable stoichiometry in active ion transport: theoretical analysis of physiological consequences. Proc Natl Acad Sci U S A *82*, 5352-5356.
Kaiser, C., S. Michaelis & A. P. Mitchell. (1994). Methods in yeast genetics. A laboratory course manual. Cold Spring Harbor Laboratory Press, Cold Spring Harbor, NY.
Kane, P.M. (2006). The where, when, and how of organelle acidification by the yeast vacuolar H+-ATPase. Microbiol Mol Biol Rev *70*, 177-191.
Kaplan, C.D., and Kaplan, J. (2009). Iron acquisition and transcriptional regulation. Chem Rev *109*, 4536-4552.
Katzmann, D.J., Babst, M., and Emr, S.D. (2001). Ubiquitin-dependent sorting into the multivesicular body pathway requires the function of a conserved endosomal protein sorting complex, ESCRT-I. Cell *106*, 145-155.
Kawahata, M., Masaki, K., Fujii, T., and Iefuji, H. (2006). Yeast genes involved in response to lactic acid and acetic acid: acidic conditions caused by the organic acids in *Saccharomyces cerevisiae* cultures induce expression of intracellular metal metabolism genes regulated by Aft1p. FEMS Yeast Res *6*, 924-936.
Kim, C.H., Kim, J.H., Lee, J., and Ahn, Y.S. (2003). Zinc-induced NF-kappaB inhibition can be modulated by changes in the intracellular metallothionein level. Toxicol Appl Pharmacol *190*, 189-196.

Kim, I., Kim, C.H., Kim, J.H., Lee, J., Choi, J.J., Chen, Z.A., Lee, M.G., Chung, K.C., Hsu, C.Y., and Ahn, Y.S. (2004). Pyrrolidine dithiocarbamate and zinc inhibit proteasome-dependent proteolysis. Exp Cell Res *298*, 229-238.

Kimura, A., Ohashi, K., and Naganuma, A. (2007). Cisplatin upregulates *Saccharomyces cerevisiae* genes involved in iron homeostasis through activation of the iron insufficiency-responsive transcription factor Aft1. J Cell Physiol *210*, 378-384.

Krenn, B.M., Holzer, B., Gaudernak, E., Triendl, A., van Kuppeveld, F.J., and Seipelt, J. (2005). Inhibition of polyprotein processing and RNA replication of human rhinovirus by pyrrolidine dithiocarbamate involves metal ions. J Virol *79*, 13892-13899.

Krishna, S.S., Majumdar, I., and Grishin, N.V. (2003). Structural classification of zinc fingers: survey and summary. Nucleic Acids Res *31*, 532-550.

Kumanovics, A., Chen, O.S., Li, L., Bagley, D., Adkins, E.M., Lin, H., Dingra, N.N., Outten, C.E., Keller, G., Winge, D., Ward, D.M., and Kaplan, J. (2008). Identification of *FRA1* and *FRA2* as genes involved in regulating the yeast iron regulon in response to decreased mitochondrial iron-sulfur cluster synthesis. J Biol Chem *283*, 10276-10286.

Lamb, T.M., and Mitchell, A.P. (2003). The transcription factor Rim101p governs ion tolerance and cell differentiation by direct repression of the regulatory genes *NRG1* and *SMP1* in *Saccharomyces cerevisiae*. Mol Cell Biol *23*, 677-686.

Lamb, T.M., Xu, W., Diamond, A., and Mitchell, A.P. (2001). Alkaline response genes of *Saccharomyces cerevisiae* and their relationship to the *RIM101* pathway. J Biol Chem *276*, 1850-1856.

Lanke, K., Krenn, B.M., Melchers, W.J., Seipelt, J., and van Kuppeveld, F.J. (2007). PDTC inhibits picornavirus polyprotein processing and RNA replication by transporting zinc ions into cells. J Gen Virol *88*, 1206-1217.

Lee, J., Godon, C., Lagniel, G., Spector, D., Garin, J., Labarre, J., and Toledano, M.B. (1999). Yap1 and Skn7 control two specialized oxidative stress response regulons in yeast. J Biol Chem *274*, 16040-16046.

Li, L., and Kaplan, J. (1998). Defects in the yeast high affinity iron transport system result in increased metal sensitivity because of the increased expression of transporters with a broad transition metal specificity. J Biol Chem *273*, 22181-22187.

Li, W., and Mitchell, A.P. (1997). Proteolytic activation of Rim1p, a positive regulator of yeast sporulation and invasive growth. Genetics *145*, 63-73.

Lin, J.Y., Chen, T.C., Weng, K.F., Chang, S.C., Chen, L.L., and Shih, S.R. (2009). Viral and host proteins involved in picornavirus life cycle. J Biomed Sci *16*, 103.

Lissiman, E., Bhasale, A.L., and Cohen, M. (2009). Garlic for the common cold. Cochrane Database Syst Rev, CD006206.

Luk, E., Yang, M., Jensen, L.T., Bourbonnais, Y., and Culotta, V.C. (2005). Manganese activation of superoxide dismutase 2 in the mitochondria of *Saccharomyces cerevisiae*. J Biol Chem *280*, 22715-22720.

Lyons, T.J., Nersissian, A., Huang, H., Yeom, H., Nishida, C.R., Graden, J.A., Gralla, E.B., and Valentine, J.S. (2000). The metal binding properties of the zinc site of yeast copper-zinc superoxide dismutase: implications for amyotrophic lateral sclerosis. J Biol Inorg Chem *5*, 189-203.

MacDiarmid, C.W., Gaither, L.A., and Eide, D. (2000). Zinc transporters that regulate vacuolar zinc storage in *Saccharomyces cerevisiae*. EMBO J *19*, 2845-2855.

MacDiarmid, C.W., Milanick, M.A., and Eide, D.J. (2002). Biochemical properties of vacuolar zinc transport systems of *Saccharomyces cerevisiae*. J Biol Chem *277*, 39187-39194.

MacPherson, S., Larochelle, M., and Turcotte, B. (2006). A fungal family of transcriptional regulators: the zinc cluster proteins. Microbiol Mol Biol Rev *70*, 583-604.
McKinlay, M.A. (2001). Recent advances in the treatment of rhinovirus infections. Curr Opin Pharmacol *1*, 477-481.
Meyer, M., Schreck, R., and Baeuerle, P.A. (1993). H2O2 and antioxidants have opposite effects on activation of NF-kappa B and AP-1 in intact cells: AP-1 as secondary antioxidant-responsive factor. EMBO J *12*, 2005-2015.
Morais, C., Pat, B., Gobe, G., Johnson, D.W., and Healy, H. (2006). Pyrrolidine dithiocarbamate exerts anti-proliferative and pro-apoptotic effects in renal cell carcinoma cell lines. Nephrol Dial Transplant *21*, 3377-3388.
Moreno, S., Klar, A., and Nurse, P. (1991). Molecular genetic analysis of fission yeast *Schizosaccharomyces pombe*. Methods Enzymol *194*, 795-823.
Munn, A.L., and Riezman, H. (1994). Endocytosis is required for the growth of vacuolar H(+)-ATPase-defective yeast: identification of six new *END* genes. J Cell Biol *127*, 373-386.
Ojeda, L., Keller, G., Muhlenhoff, U., Rutherford, J.C., Lill, R., and Winge, D.R. (2006). Role of glutaredoxin-3 and glutaredoxin-4 in the iron regulation of the Aft1 transcriptional activator in *Saccharomyces cerevisiae*. J Biol Chem *281*, 17661-17669.
Otto, M.J., Fox, M.P., Fancher, M.J., Kuhrt, M.F., Diana, G.D., and McKinlay, M.A. (1985). In vitro activity of WIN 51711, a new broad-spectrum antipicornavirus drug. Antimicrob Agents Chemother *27*, 883-886.
Outten, C.E., Falk, R.L., and Culotta, V.C. (2005). Cellular factors required for protection from hyperoxia toxicity in *Saccharomyces cerevisiae*. Biochem J *388*, 93-101.
Outten, C.E., and O'Halloran, T.V. (2001). Femtomolar sensitivity of metalloregulatory proteins controlling zinc homeostasis. Science *292*, 2488-2492.
Pagani, M.A., Casamayor, A., Serrano, R., Atrian, S., and Arino, J. (2007). Disruption of iron homeostasis in *Saccharomyces cerevisiae* by high zinc levels: a genome-wide study. Mol Microbiol *65*, 521-537.
Parsons, A.B., Brost, R.L., Ding, H., Li, Z., Zhang, C., Sheikh, B., Brown, G.W., Kane, P.M., Hughes, T.R., and Boone, C. (2004). Integration of chemical-genetic and genetic interaction data links bioactive compounds to cellular target pathways. Nat Biotechnol *22*, 62-69.
Parsons, A.B., Lopez, A., Givoni, I.E., Williams, D.E., Gray, C.A., Porter, J., Chua, G., Sopko, R., Brost, R.L., Ho, C.H., Wang, J., Ketela, T., Brenner, C., Brill, J.A., Fernandez, G.E., Lorenz, T.C., Payne, G.S., Ishihara, S., Ohya, Y., Andrews, B., Hughes, T.R., Frey, B.J., Graham, T.R., Andersen, R.J., and Boone, C. (2006). Exploring the mode-of-action of bioactive compounds by chemical-genetic profiling in yeast. Cell *126*, 611-625.
Peplowska, K., Markgraf, D.F., Ostrowicz, C.W., Bange, G., and Ungermann, C. (2007). The CORVET tethering complex interacts with the yeast Rab5 homolog Vps21 and is involved in endo-lysosomal biogenesis. Dev Cell *12*, 739-750.
Perry, D.K., Smyth, M.J., Stennicke, H.R., Salvesen, G.S., Duriez, P., Poirier, G.G., and Hannun, Y.A. (1997). Zinc is a potent inhibitor of the apoptotic protease, caspase-3. A novel target for zinc in the inhibition of apoptosis. J Biol Chem *272*, 18530-18533.
Pfaller, M.A., and Diekema, D.J. (2004). Rare and emerging opportunistic fungal pathogens: concern for resistance beyond *Candida albicans* and *Aspergillus fumigatus*. J Clin Microbiol *42*, 4419-4431.
Philpott, C.C., and Protchenko, O. (2008). Response to iron deprivation in *Saccharomyces cerevisiae*. Eukaryot Cell *7*, 20-27.

Piper, P., Mahe, Y., Thompson, S., Pandjaitan, R., Holyoak, C., Egner, R., Muhlbauer, M., Coote, P., and Kuchler, K. (1998). The Pdr12 ABC transporter is required for the development of weak organic acid resistance in yeast. EMBO J *17*, 4257-4265.

Puig, S., Askeland, E., and Thiele, D.J. (2005). Coordinated remodeling of cellular metabolism during iron deficiency through targeted mRNA degradation. Cell *120*, 99-110.

Pujol-Carrion, N., Belli, G., Herrero, E., Nogues, A., and de la Torre-Ruiz, M.A. (2006). Glutaredoxins Grx3 and Grx4 regulate nuclear localisation of Aft1 and the oxidative stress response in *Saccharomyces cerevisiae*. J Cell Sci *119*, 4554-4564.

Radisky, D., and Kaplan, J. (1999). Regulation of transition metal transport across the yeast plasma membrane. J Biol Chem *274*, 4481-4484.

Raiborg, C., and Stenmark, H. (2009). The ESCRT machinery in endosomal sorting of ubiquitylated membrane proteins. Nature *458*, 445-452.

Raju, B., Murphy, E., Levy, L.A., Hall, R.D., and London, R.E. (1989). A fluorescent indicator for measuring cytosolic free magnesium. Am J Physiol *256*, C540-548.

Ramsay, L.M., and Gadd, G.M. (1997). Mutants of *Saccharomyces cerevisiae* defective in vacuolar function confirm a role for the vacuole in toxic metal ion detoxification. FEMS Microbiol Lett *152*, 293-298.

Roberts, C.J., Raymond, C.K., Yamashiro, C.T., and Stevens, T.H. (1991). Methods for studying the yeast vacuole. Methods Enzymol *194*, 644-661.

Ruotolo, R., Marchini, G., and Ottonello, S. (2008). Membrane transporters and protein traffic networks differentially affecting metal tolerance: a genomic phenotyping study in yeast. Genome Biol *9*, R67.

Rutherford, J.C., and Bird, A.J. (2004). Metal-responsive transcription factors that regulate iron, zinc, and copper homeostasis in eukaryotic cells. Eukaryot Cell *3*, 1-13.

Rutherford, J.C., Jaron, S., and Winge, D.R. (2003). Aft1p and Aft2p mediate iron-responsive gene expression in yeast through related promoter elements. J Biol Chem *278*, 27636-27643.

Rutherford, J.C., Ojeda, L., Balk, J., Muhlenhoff, U., Lill, R., and Winge, D.R. (2005). Activation of the iron regulon by the yeast Aft1/Aft2 transcription factors depends on mitochondrial but not cytosolic iron-sulfur protein biogenesis. J Biol Chem *280*, 10135-10140.

Saeed, A.I., Bhagabati, N.K., Braisted, J.C., Liang, W., Sharov, V., Howe, E.A., Li, J., Thiagarajan, M., White, J.A., and Quackenbush, J. (2006). TM4 microarray software suite. Methods Enzymol *411*, 134-193.

Saeed, A.I., Sharov, V., White, J., Li, J., Liang, W., Bhagabati, N., Braisted, J., Klapa, M., Currier, T., Thiagarajan, M., Sturn, A., Snuffin, M., Rezantsev, A., Popov, D., Ryltsov, A., Kostukovich, E., Borisovsky, I., Liu, Z., Vinsavich, A., Trush, V., and Quackenbush, J. (2003). TM4: a free, open-source system for microarray data management and analysis. Biotechniques *34*, 374-378.

Sales, K., Brandt, W., Rumbak, E., and Lindsey, G. (2000). The LEA-like protein HSP 12 in *Saccharomyces cerevisiae* has a plasma membrane location and protects membranes against desiccation and ethanol-induced stress. Biochim Biophys Acta *1463*, 267-278.

Sambrook, J., E. Fritsch & T. Maniatis,, . (2001). Molecular cloning: A laboratory manual. 3rd edition. Cold Spring Harbor, Press, New York.

Santos, P.M., Simoes, T., and Sa-Correia, I. (2009). Insights into yeast adaptive response to the agricultural fungicide mancozeb: a toxicoproteomics approach. Proteomics *9*, 657-670.

Santos, R., Dancis, A., Eide, D., Camadro, J.M., and Lesuisse, E. (2003). Zinc suppresses the iron-accumulation phenotype of *Saccharomyces cerevisiae* lacking the yeast frataxin homologue (Yfh1). Biochem J *375*, 247-254.

Schreck, R., Meier, B., Mannel, D.N., Droge, W., and Baeuerle, P.A. (1992). Dithiocarbamates as potent inhibitors of nuclear factor kappa B activation in intact cells. J Exp Med *175*, 1181-1194.

Serrano, R., Bernal, D., Simon, E., and Arino, J. (2004). Copper and iron are the limiting factors for growth of the yeast *Saccharomyces cerevisiae* in an alkaline environment. J Biol Chem *279*, 19698-19704.

Serrano, R., Ruiz, A., Bernal, D., Chambers, J.R., and Arino, J. (2002). The transcriptional response to alkaline pH in *Saccharomyces cerevisiae*: evidence for calcium-mediated signalling. Mol Microbiol *46*, 1319-1333.

Shakoury-Elizeh, M., Tiedeman, J., Rashford, J., Ferea, T., Demeter, J., Garcia, E., Rolfes, R., Brown, P.O., Botstein, D., and Philpott, C.C. (2004). Transcriptional remodeling in response to iron deprivation in *Saccharomyces cerevisiae*. Mol Biol Cell *15*, 1233-1243.

Simm, C., Lahner, B., Salt, D., LeFurgey, A., Ingram, P., Yandell, B., and Eide, D.J. (2007). *Saccharomyces cerevisiae* vacuole in zinc storage and intracellular zinc distribution. Eukaryot Cell *6*, 1166-1177.

Simons, T.J. (1993). Measurement of free Zn^{2+} ion concentration with the fluorescent probe mag-fura-2 (furaptra). J Biochem Biophys Methods *27*, 25-37.

Smyth, G.K. (2004). Linear models and empirical bayes methods for assessing differential expression in microarray experiments. Stat Appl Genet Mol Biol *3*, Article3.

Stadler, J.A., and Schweyen, R.J. (2002). The yeast iron regulon is induced upon cobalt stress and crucial for cobalt tolerance. J Biol Chem *277*, 39649-39654.

Stearman, R., Yuan, D.S., Yamaguchi-Iwai, Y., Klausner, R.D., and Dancis, A. (1996). A permease-oxidase complex involved in high-affinity iron uptake in yeast. Science *271*, 1552-1557.

Stockwell, B.R. (2000). Chemical genetics: ligand-based discovery of gene function. Nat Rev Genet *1*, 116-125.

Supek, F., Supekova, L., Nelson, H., and Nelson, N. (1996). A yeast manganese transporter related to the macrophage protein involved in conferring resistance to mycobacteria. Proc Natl Acad Sci U S A *93*, 5105-5110.

Takkouche, B., Regueira-Mendez, C., Garcia-Closas, R., Figueiras, A., Gestal-Otero, J.J., and Hernan, M.A. (2002). Intake of wine, beer, and spirits and the risk of clinical common cold. Am J Epidemiol *155*, 853-858.

Tarhan, C., Pekmez, M., Karaer, S., Arda, N., and Sarikaya, A.T. (2007). The effect of superoxide dismutase deficiency on zinc toxicity in *Schizosaccharomyces pombe*. J Basic Microbiol *47*, 506-512.

Teixeira, M.C., Monteiro, P., Jain, P., Tenreiro, S., Fernandes, A.R., Mira, N.P., Alenquer, M., Freitas, A.T., Oliveira, A.L., and Sa-Correia, I. (2006). The YEASTRACT database: a tool for the analysis of transcription regulatory associations in *Saccharomyces cerevisiae*. Nucleic Acids Res *34*, D446-451.

Theodosiou, A., and Ashworth, A. (2002). MAP kinase phosphatases. Genome Biol *3*, REVIEWS3009.

Tucker, C.L., and Fields, S. (2004). Quantitative genome-wide analysis of yeast deletion strain sensitivities to oxidative and chemical stress. Comp Funct Genomics *5*, 216-224.

Uchide, N., Ohyama, K., Bessho, T., Yuan, B., and Yamakawa, T. (2002). Effect of antioxidants on apoptosis induced by influenza virus infection: inhibition of viral gene replication and transcription with pyrrolidine dithiocarbamate. Antiviral Res *56*, 207-217.

van de Peppel, J., Kettelarij, N., van Bakel, H., Kockelkorn, T.T., van Leenen, D., and Holstege, F.C. (2005). Mediator expression profiling epistasis reveals a signal transduction pathway with antagonistic submodules and highly specific downstream targets. Mol Cell *19*, 511-522.

Vergara, S.V., and Thiele, D.J. (2008). Post-transcriptional regulation of gene expression in response to iron deficiency: co-ordinated metabolic reprogramming by yeast mRNA-binding proteins. Biochem Soc Trans *36*, 1088-1090.

Vida, T.A., and Emr, S.D. (1995). A new vital stain for visualizing vacuolar membrane dynamics and endocytosis in yeast. J Cell Biol *128*, 779-792.

Vizeacoumar, F.J., Chong, Y., Boone, C., and Andrews, B.J. (2009). A picture is worth a thousand words: genomics to phenomics in the yeast *Saccharomyces cerevisiae*. FEBS Lett *583*, 1656-1661.

von Mering, C., Jensen, L.J., Kuhn, M., Chaffron, S., Doerks, T., Kruger, B., Snel, B., and Bork, P. (2007). STRING 7--recent developments in the integration and prediction of protein interactions. Nucleic Acids Res *35*, D358-362.

Weisman, L.S., Bacallao, R., and Wickner, W. (1987). Multiple methods of visualizing the yeast vacuole permit evaluation of its morphology and inheritance during the cell cycle. J Cell Biol *105*, 1539-1547.

Wettenhall, J.M., and Smyth, G.K. (2004). limmaGUI: a graphical user interface for linear modeling of microarray data. Bioinformatics *20*, 3705-3706.

Whitton, J.L., Cornell, C.T., and Feuer, R. (2005). Host and virus determinants of picornavirus pathogenesis and tropism. Nat Rev Microbiol *3*, 765-776.

Wickner, W. (2002). Yeast vacuoles and membrane fusion pathways. EMBO J *21*, 1241-1247.

Wickner, W. (2010). Membrane Fusion: Five Lipids, Four SNAREs, Three Chaperones, Two Nucleotides, and a Rab, All Dancing in a Ring on Yeast Vacuoles. Annu Rev Cell Dev Biol.

Winge, D.R., Nielson, K.B., Gray, W.R., and Hamer, D.H. (1985). Yeast metallothionein. Sequence and metal-binding properties. J Biol Chem *260*, 14464-14470.

Winzeler, E.A., Shoemaker, D.D., Astromoff, A., Liang, H., Anderson, K., Andre, B., Bangham, R., Benito, R., Boeke, J.D., Bussey, H., Chu, A.M., Connelly, C., Davis, K., Dietrich, F., Dow, S.W., El Bakkoury, M., Foury, F., Friend, S.H., Gentalen, E., Giaever, G., Hegemann, J.H., Jones, T., Laub, M., Liao, H., Liebundguth, N., Lockhart, D.J., Lucau-Danila, A., Lussier, M., M'Rabet, N., Menard, P., Mittmann, M., Pai, C., Rebischung, C., Revuelta, J.L., Riles, L., Roberts, C.J., Ross-MacDonald, P., Scherens, B., Snyder, M., Sookhai-Mahadeo, S., Storms, R.K., Veronneau, S., Voet, M., Volckaert, G., Ward, T.R., Wysocki, R., Yen, G.S., Yu, K., Zimmermann, K., Philippsen, P., Johnston, M., and Davis, R.W. (1999). Functional characterization of the *S. cerevisiae* genome by gene deletion and parallel analysis. Science *285*, 901-906.

Wu, W.S., Li, W.H., and Chen, B.S. (2008). Reconstructing a Network of Stress-Response Regulators via Dynamic System Modeling of Gene Regulation. Gene Regul Syst Bio *2*, 53-62.

Xie, Y., and Varshavsky, A. (2001). RPN4 is a ligand, substrate, and transcriptional regulator of the 26S proteasome: a negative feedback circuit. Proc Natl Acad Sci U S A *98*, 3056-3061.

Yamaguchi-Iwai, Y., Dancis, A., and Klausner, R.D. (1995). *AFT1*: a mediator of iron regulated transcriptional control in *Saccharomyces cerevisiae*. EMBO J *14*, 1231-1239.
Yamaguchi-Iwai, Y., Stearman, R., Dancis, A., and Klausner, R.D. (1996). Iron-regulated DNA binding by the AFT1 protein controls the iron regulon in yeast. EMBO J *15*, 3377-3384.
Yamaguchi-Iwai, Y., Ueta, R., Fukunaka, A., and Sasaki, R. (2002). Subcellular localization of Aft1 transcription factor responds to iron status in *Saccharomyces cerevisiae*. J Biol Chem *277*, 18914-18918.
Yun, C.W., Ferea, T., Rashford, J., Ardon, O., Brown, P.O., Botstein, D., Kaplan, J., and Philpott, C.C. (2000). Desferrioxamine-mediated iron uptake in *Saccharomyces cerevisiae*. Evidence for two pathways of iron uptake. J Biol Chem *275*, 10709-10715.
Zhao, H., and Eide, D. (1996a). The yeast *ZRT1* gene encodes the zinc transporter protein of a high-affinity uptake system induced by zinc limitation. Proc Natl Acad Sci U S A *93*, 2454-2458.
Zhao, H., and Eide, D. (1996b). The *ZRT2* gene encodes the low affinity zinc transporter in *Saccharomyces cerevisiae*. J Biol Chem *271*, 23203-23210.
Zhao, H., and Eide, D.J. (1997). Zap1p, a metalloregulatory protein involved in zinc-responsive transcriptional regulation in *Saccharomyces cerevisiae*. Mol Cell Biol *17*, 5044-5052.

9. APPENDIX

Manuscript

"Functional Genomics of Drug-Induced Ion Homeostasis Identifies a Novel Regulatory Cross-Talk of Iron and Zinc Regulons in Yeast", Landstetter *et al*, OMICS, in print

Acknowledgements

Curriculum Vitae

APPENDIX

Functional Genomics of Drug-Induced Ion Homeostasis Identifies a Novel Regulatory Cross-Talk of Iron and Zinc Regulons in Yeast

Nathalie Landstetter, Walter Glaser, Christa Gregori, Joachim Seipelt and Karl Kuchler

Nathalie Landstetter, nathalie.landstetter@meduniwien.ac.at, Tel: +43-1-4277-61818, Fax: +43-1-4277-9618

Walter Glaser, walter.glaser@univie.ac.at, Tel: +43-1-4277-61812, Fax: +43-1-4277-9618

Christa Gregori, christa.gregori@meduniwien.ac.at, Tel: +43-1-4277-61818, Fax: +43-1-4277-9618

Joachim Seipelt, Joachim.seipelt@meduniwien.ac.at, Tel: +43-1-4277-61610, Fax: +43-1-4277-9616

To whom correspondence may be addressed:

Karl Kuchler

karl.kuchler@meduniwien.ac.at

Tel: +43-1-4277-61807, Fax: +43-1-4277-9618

Keywords: Antiviral drugs, yeast, zinc excess, metal ion homeostasis, cross-talk

Adresses:

Nathalie Landstetter, Christa Gregori, Walter Glaser, Karl Kuchler

Medical University Vienna, Max F. Perutz Laboratories, Campus Vienna Biocenter; A-1030 Vienna, Dr. Bohr-Gasse 9/2, Austria

Joachim Seipelt

Medical University Vienna, Max F. Perutz Laboratories, Campus Vienna Biocenter; A-1030 Vienna, Dr. Bohr-Gasse 9/3, Austria

ABSTRACT

Pyrrolidine dithiocarbamate (PDTC), a known inhibitor of NFκB-activation, has anti-oxidative as well as antiviral activities. PDTC is effective against several virus families, indicating that its antiviral mechanism targets host rather than viral functions. To investigate its mode of action, we used baker's yeast as a simple eukaryotic model system and two types of genome-wide analysis. First, expression profiling using whole-genome DNA microarrays identifies more than 200 genes differentially regulated upon PDTC exposure. Interestingly, the Aft1-dependent iron regulon is a main target of PDTC, indicating a lack of iron availability. Moreover, the PDTC-caused zinc influx triggers a strong regulatory effect on zinc transporters due to the cytoplasmic zinc excess. Second, phenotypic screening the EUROSCARF collection for PDTC hypersensitivity identifies numerous mutants implicated in vacuolar maintenance, acidification as well as in transport, mitochondrial organization and translation. Notably, the screening data indicate significant overlaps of PDTC-sensitive genes and those mediating zinc-tolerance. Hence, we show that PDTC induces cytoplasmic zinc excess, eliciting vacuolar detoxification, which in turn disturbs iron homeostasis and activates the iron-dependent regulator Aft1. Our work reveals a complex cross-talk in yeast ion homeostasis and the underlying regulatory networks.

INTRODUCTION

Pyrrolidine dithiocarbamate (PDTC), a low-molecular weight thiol compound, is a multifunctional drug exerting various effects in biological systems. For instance, it is an inhibitor of the nuclear factor kappa B (NFκB) activation (Schreck *et al.*, 1992) and it can exert both pro-apoptotic and anti-apoptotic effects depending on the cellular host system (Morais *et al.*, 2006, Erl *et al.*, 2000). Furthermore, PDTC shows inhibitory effects on protein degradation (Hayakawa *et al.*, 2003, Kim *et al.*, 2004), and elicits an oxidative stress response by inducing transcription of the manganese superoxide dismutase and the heme oxygenase HO-1 (Borrello & Demple, 1997, Hartsfield *et al.*, 1998). Interestingly, PDTC displays antiviral activity against picornaviruses including human rhinovirus, poliovirus and coxsackievirus (Gaudernak *et al.*, 2002, Lanke *et al.*, 2007), as well as on influenza viruses, the latter being orthomyxoviruses with a very different life cycle (Uchide *et al.*, 2002). Interestingly, PDTC prevents polyprotein processing and reduces virus titers mainly by shuttling zinc ions into host cells (Krenn *et al.*, 2005). Since different virus families are inhibited, and no resistant strains have been observed to date, it has been speculated that the antiviral mechanism of PDTC might target host cell rather than viral functions. To gain insight into the cellular mechanisms and control programs affected by PDTC, we decided to use the yeast *Saccharomyces cerevisiae* as a simple eukaryotic model system, since PDTC shows antifungal activity in yeast. Yeast is a model organism for chemogenomic approaches that has proven itself invaluable for the unraveling of many fundamental biological processes including drug target gene identification (Giaever, 2003, Parsons *et al.*, 2004). Due to the high evolutionary conservation of many cellular processes (Foury, 1997), phenotypic screening techniques in yeast have become advantageous for drug development and pharmacokinetic studies (Bharucha & Kumar, 2007). Phenotypic screening of the haploid yeast deletion collection revealed important insights in cellular processes and pathways affected by certain stress conditions or drug treatments (Tucker & Fields, 2004, Parsons *et al*., 2004). Likewise, microarray profiling using whole-genome DNA microarrays can yield conclusive insights into the mode of action of a drug and the genes modulated by comparing untreated to drug exposed cells (Hughes *et al.*, 2000). For example, microarray profiling for a set of different stresses and environmental conditions identified an extensive transcriptional network underlying cellular stress responses (Gasch *et al.*, 2000) but also enables the discovery of direct as well as off-targets of bioactive compounds (Ericson *et al.*, 2008, Parsons *et al.*, 2006).

The field of chemical genetics and chemogenomics aims at drug target identification by inhibiting gene functions in an entire organism using small-molecule exogenous

xenobiotics. Lack of a gene in combination with a sublethal dose of a drug can have a synthetic lethal effect such as reduced fitness, thus enabling to identify the pathway or the drug target that mediates the toxic effect imposed by the drug (Stockwell, 2000). In this study we aimed to apply this chemical genetic approach to decipher the mode of action of PDTC, and perhaps to identify a target gene for PDTC inhibition. Thus, we performed microarray-based profiling of the yeast PDTC response, as well as a genome-wide functional screening of the EUROSCARF yeast gene deletion collection. Strikingly, our data unravel major changes in cellular ion homeostasis, including the cross-talk of iron and zinc regulatory networks.

MATERIAL & METHODS

Yeast strains and growth conditions

All yeast strains used in this study are listed in the supplementary file S1. Rich medium (yeast extract-peptone-dextrose [YPD]) was prepared as described in (Kaiser, 1994). Unless otherwise indicated, all yeast strains were routinely grown at 30°C. Growth inhibition assays were performed with logarithmically grown cells, which were adjusted to an optical density at 600 nm (OD_{600}) of 0.2. Equal volumes of 1:10 serial dilutions were spotted onto agar plates containing different drug concentrations. *S. pombe* was grown on solid YES medium as described elsewhere (Moreno *et al.*, 1991). For viability assays, cells were grown in liquid medium supplemented with PDTC and/or metal ions for 24h. Afterwards, cells were plated onto YPD plates and colony-forming units were determined after 48h incubation. Stressed cells were normalized to untreated wild type cells. PDTC was purchased from Alexis Biochemicals, Lausen, Switzerland.

Functional screening for sensitivity phenotypes in the presence of PDTC

For large scale phenotypic profiling, the about 4800 haploid viable single gene deletion strains of the EUROSCARF deletion collection (http://web.uni-frankfurt.de/fb15/mikro/euroscarf/index.html) were grown on YPD plates in a 96-well format. For transferring strains to PDTC-containing plates and control YPD plates, we used the RoToR HAD robot (Singer Ltd., Roadwater, UK). Growth was inspected after 2, 4 and 6 days incubation at 30°C. After incubation, plates were scanned with an HPScanjet G3010, using the Adobe Photoshop CS3 software. All strains displaying PDTC-sensitivity in the first screening were manually re-spotted for confirmation. Equal volumes of serial dilutions of exponentially growing cells ranging from an OD_{600} of 0.2 to $2x10^{-4}$ were spotted onto PDTC-plates and control plates.

Preparation of total yeast RNA and microarray analysis

Yeast cells were grown in YPD to an OD_{600} of about 0.4. The medium was supplemented with 75µM PDTC; untreated control cells and PDTC-treated cells were harvested as 50ml samples after 1, 3 and 5 hours, washed with ice-cold water and frozen immediately at -80°C. Total RNA was prepared by the hot phenol method (Sambrook, 2001). About 20 µg of total RNA from each sample were used for cDNA synthesis using 200 units of Superscript II reverse transcriptase (Invitrogen) with either Cy3-dCTP or Cy5-dCTP. Labeled cDNAs were pooled, and RNA was hydrolyzed for 20min in 50mM NaOH at 65 °C, followed by neutralization with acetic acid and probe clean-up with the CyScribe GFX purification kit (Amersham).

Hybridization to whole genome cDNA microarrays (Yeast 6.4K Arrays, Microarray Centre, University Health Network, Toronto (www.microarrays.ca) was done in DigEasyHyb (Roche Applied Science) solution at 37 °C overnight with 70µg/ml of salmon sperm DNA as a carrier. Microarrays were washed three times in 1x SSC, 0.1% SDS at 50 °C, followed by a 1-min wash in 1x SSC at room temperature. Glass slides were spun dry for 5 min at 500 rpm in a tabletop centrifuge, and scanned in an Axon 4000B scanner (Molecular Devices). All microarray experiments were carried out with three independent RNA preparations and at least one technical replicate using dye-swaps.

Computational analysis of microarray data and screening results

Gridding and spot identification on microarrays were performed using the Gene Pix Pro4.1 software (Axon). For preprocessing, the background was subtracted and subsequently normalized, using the print-tip loess method of the limma Bioconductor/R package (Wettenhall & Smyth, 2004). To identify differentially expressed genes, a linear model and empirical Bayesian-moderated F-statistics were used with cut-off values of 0.001 for the adjusted p-value and a 2-fold expression change, as well as A-values ≥ 7 (Smyth, 2004).

Genes identified either on the microarrays or in the functional screening were grouped by gene ontology enrichment according to the predicted biological process using the GO Termfinder program provided by the *Saccharomyces* Gene Database (www.yeastgenome.org). Clustering of differentially expressed genes was performed using the MEV software using the linkage method and Euclidean distance (Saeed *et al.*, 2006, Saeed *et al.*, 2003). The clustering files are found in supplementary file S3. All microarray experiments were carried out under full MIAME compliancy and data have been submitted to the *Array Express* database.

Northern blot analysis

For Northern blots, 15µg of total RNA were fractionated in a 1.4% agarose gel and transferred to nylon membranes (Amersham Biosciences). Methylene blue staining was used as control for equal RNA loading. Northern blots were pre-hybridized for 3h at 65°C. PCR-amplified probes were radiolabeled by incorporation of [α-32P]dCTP using a MegaPrime labeling kit (Amersham Biosciences). Radiolabeled probes were purified on NICK columns (Amersham Biosciences) before adding to the prehybridization solution. Membranes were washed at 65°C three times each in 2xSSC, 1% SDS, in 1x SSC 1% SDS and exposed to X-ray films at -80 °C.

β-galactosidase assays and immunoblotting

Cells containing a genomically integrated *FET3*-lacZ reporter construct OCY355 (Kumanovics *et al.*, 2008) were grown in YPD medium to the mid-exponential growth phase. Cells were treated with 100µM PDTC or left untreated. β-galactosidase assays were performed in triplicate with cell extracts as described in (Kaiser, 1994).

For immunoblotting, total cell-free protein extracts were prepared by the trichloroacetic acid method exactly as described previously (Mamnun *et al.*, 2004). Cells were grown to the mid-logarithmic growth phase, left untreated or stressed with 100µM PDTC for 2h. Cell lysates equivalent to 0.5 OD_{600} units were resolved by 7.5% SDS-PAGE and transferred to nitrocellulose membranes. Polyclonal α-Swi6 antibodies (kindly provided by Kim Nasmyth) were used to verify equal loading.

Fluorescent detection of zinc influx into yeast cells

About 2x 10^8 cells of a *pdr5*Δ *pdr12*Δ double deletion strain (kindly provided by Ralf Egner) were loaded with 30µM mag-fura-2 (Molecular Probes, Invitrogen) for 30 minutes in 1xTBS; cells were washed three times and finally resuspended in 10ml TBS. Experiments were performed in 3ml silica cuvettes containing 2ml aliquots of a cells suspension with constant agitation. Intracellular zinc accumulation was monitored with real-time kinetics over a 500 second-period using a spectrofluorimeter LS-55 (Perkin-Elmer) by continually alternating the excitation wavelengths of 340 and 380nm in 20ms intervals and recording the emission at 509nm. 10µM $ZnSO_4$, 10µM $CaCl_2$ or 10µM $CuSO_4$, and 100µM PDTC and 50µM EDTA were added to the cell suspension at indicated time points.

RESULTS

PDTC shows antifungal activity in various yeast species

The effect of PDTC on growth of *Saccharomyces cerevisiae*, *Candida albicans*, *Candida glabrata* and *Schizosaccharomyces pombe* was analyzed by growth inhibition assays on agar plates. Serial dilutions of the yeast cells were spotted onto PDTC supplemented plates. Cell growth was inhibited in both non-pathogenic yeasts as well as in *Candida* spp, although not to the same extent (Fig. 1A). Namely, *S. cerevisiae*, *C. albicans* and *S. pombe* were sensitive at 30µM PDTC, whereas *C. glabrata* was more resistant growing up to a concentration of 75µM PDTC. However, it is known that *C. glabrata* shows increased inherent tolerance to antifungals such as azoles when compared to *S. cerevisiae* and *C. albicans* (Pfaller & Diekema, 2004).

Moreover, we performed growth curves with *Saccharomyces cerevisiae* wild type cells to investigate PDTC tolerance in liquid culture. Cells were grown in rich medium supplemented with increasing concentrations of PDTC and OD_{600} was monitored over time. The growth curves showed a dose-dependent growth inhibition (Fig.1B). At low concentrations (25µM), PDTC treated cells responded with an elongated lag-phase and a delayed period to reach the stationary phase. At higher concentrations (150µM), PDTC caused fungistatic growth inhibition. This broad antifungal activity of PDTC suggested using yeast as a model system by exploiting well-established large-scale screening techniques for PDTC drug target identification.

The PDTC transcriptome comprises of more than 200 genes

To identify regulatory effects and the kinetics of PDTC action on the yeast transcriptome, we performed whole-genome DNA microarray experiments. Therefore, wild type yeast cells were grown to the mid-logarithmic growth phase in rich medium, and treated with PDTC for 1, 3 or 5 hours (Fig. 1B). Transcript data of three independent biological and one technical replicate at every time point were generated, and PDTC-treated versus untreated cells were compared. Microarray results were statistically evaluated considering changes more than two-fold as significant. All major changes were confirmed at RNA level by Northern analysis.

PDTC-induced changes in transcriptome profiles consisted of more than 200 differentially expressed genes (Table 1), indicating a major transcriptional shift in yeast. Gene ontology (GO) enrichment of the microarray data using the *Saccharomyces* Gene Database GO Termfinder revealed that the main functional categories included the iron regulon, aerobic respiration and general metabolic changes. To identify the regulatory associations of the differentially expressed genes, we clustered the genes with

YEASTRACT (Teixeira *et al.*, 2006) (see supplementary Table S2). Thereby, differentially expressed genes identified through microarrays were grouped according to their transcription factors or potential regulators. Supporting the findings of the GO enrichment, the main transcription factors required for general and oxidative stress response genes, as well as proteasome and multidrug resistance genes were found. These included the transcriptional regulators Yap1, Msn2/4, Rpn4 and Sfp1 correlating with the activation of general stress response genes as well as with repression of ribosomal genes under various stress conditions (Wu *et al.*, 2008, Gasch *et al.*, 2000). Interestingly, the clustering specifically identified the iron-responsive transcription factor Aft1 as one of the major responders.

PDTC activates the Aft1-dependent iron regulon in yeast

Among the highest induced genes, we identified several genes of the high-affinity iron uptake system (*FET3*, *ARN4*), as well as cell wall mannoproteins required for siderophore-bound iron retention (*FIT1*, *FIT2*, *FIT3*). This set of genes is referred to as the yeast iron regulon, which is under the control of the transcription factors Aft1/Aft2. The iron regulon is rapidly activated under iron-limiting conditions (Yamaguchi-Iwai *et al.*, 1995, Yun *et al.*, 2000). Upon iron depletion, Aft1 traffics into the nucleus to orchestrate an immense cellular cascade response, inducing first the iron uptake machinery and mobilization of intracellular iron from storage compartments, followed by adaptations of metabolic iron usage (Yamaguchi-Iwai *et al.*, 2002). This includes a switch to less iron-consuming pathways, shutting down non-essential pathways while preserving essential ones (Kaplan & Kaplan, 2009). The pathways regulated in response to iron changes include the biotin, glutamate and purine biosynthetic pathways, as well as the TCA cycle. Furthermore, genes involved in heme biosynthesis and in the respiratory chain are down-regulated (Hausmann *et al*, 2008). Indeed, PDTC triggered both the primary and secondary wave response genes involved in iron-dependent cellular remodeling (Table 1).

To confirm the induction of the iron regulon in response to PDTC, and to investigate whether this activation is Aft1-dependent and iron-specific, we performed Northern analysis and growth inhibition assays comparing the wild type with the *aft1*Δ strain. Activation of the iron regulon (*FIT3*, *FIT2*) in response to PDTC was fully Aft1-dependent, whereas *GRE2*, encoding a metalloreductase involved in the high osmolarity glycerol pathway, served as control for Aft1-independent induction (Fig.2A). Furthermore, PDTC strongly induced the promoter of *FET3* encoding the ferroxidase of the high-affinity iron transport system as shown by a *FET3-lacZ* reporter assay (Fig.2B).

Aft1 is required for growth under iron-limited conditions (Yamaguchi-Iwai *et al.*, 1995). Consistently, the *aft1*Δ strain was hypersensitive to PDTC when compared to its

corresponding wild type, suggesting that Aft1 is required for PDTC tolerance (Fig. 2C). Iron-supplementation specifically rescued this sensitivity phenotype (Fig.2C), thus showing that PDTC must mimic or cause a lack of iron availability. Other ions such as Mg^{2+}, Ca^{2+}, Zn^{2+} and Mn^{2+} failed to rescue the PDTC-dependent growth inhibition, and Cd^{2+} supplementation even further increased PDTC-sensitivity. Notably, copper supplementation rescued growth of the *aft1*Δ strain in the presence of PDTC, but impaired PDTC-tolerance of the wild type strain. All in all, these data show that activation of the iron regulon by PDTC is Aft1-dependent and is required for PDTC-tolerance.

PDTC treatment causes intracellular zinc overload

On the one hand, PDTC caused activation of the iron uptake machinery. On the other hand, it was striking to note that PDTC strongly altered expression of plasma membrane and vacuolar zinc transporters (Fig.3A). In detail, expression of the plasma membrane low-affinity zinc transporter Zrt2 and the vacuolar zinc exporter Zrt3 was strongly decreased upon PDTC treatment, whereas the transporter importing zinc into the vacuole, Cot1, was highly induced. Transcript levels of the high-affinity zinc transporter Zrt1 stayed unchanged; however Zrt1 is regulated post-translationally via ubiquitination and endocytosis (Gitan & Eide, 2000). Although, yeast lacks a cellular zinc exporter, free zinc concentrations are kept low because excess zinc is highly toxic for cells. Spare zinc is bound to proteins or stored in vesicular compartments such as the vacuole as major site of storage and detoxification (Eide, 2009).

Consistent with our notion of PDTC-induced cellular zinc excess, transcript levels of the major zinc-conserving proteins like alcohol dehydrogenases (ADHs) and superoxide dismutase 1 (Sod1) were increased on our microarrays. We confirmed induction of the cytoplasmic superoxide dismutase *SOD1* gene by Northern blotting (Fig.3B). In the *aft1*Δ strain, *SOD1* gene induction was even more pronounced than in the wild type. Consistently, Sod1 deficiency led to increased PDTC and zinc-sensitivity, whereas deletion of the manganese superoxide dismutase Sod2 had less severe effects. (Fig.3B, C). Interestingly, iron supplementation failed to rescue the PDTC-induced growth defect of the *sod1*Δ strain. However, this failure might be due to a previously reported increase in iron demand of the *sod1*Δ mutant *per se* and its involvement in zinc detoxification (Tarhan *et al.*, 2007, De Freitas *et al.*, 2000). In this case, PDTC would worsen the lack of iron availability, thereby increasing the sensitivity of the *sod1*Δ strain.

To directly monitor PDTC-induced zinc accumulation inside yeast cells in real time, we used the fluorescent dye mag-fura-2. As the dye is normally effluxed from cells, all experiments were carried out in a strain lacking the ABC transporters Pdr5 and Pdr12. The excitation wavelength of mag-fura-2 is shifted from 380 to 340 nm when binding

bivalent cations (Raju *et al.*, 1989, Simons, 1993). After loading yeast cells with mag-fura-2, cells were extensively washed and $ZnSO_4$, $CuSO_4$, $CaCl_2$ or $MgCl_2$, PDTC and EDTA were added at indicated time points. While adding $ZnSO_4$ had only minor effects on the fluorescent ratio, the supplementation of PDTC caused a rapidly increasing signal as a readout for intracellular zinc accumulation. As expected, adding EDTA reduced the signal immediately. Other metal ions including Mg^{2+}, Cu^{2+} and Ca^{2+} had no effect on the fluorescent signal. Thus, PDTC caused an immediate influx of Zn^{2+} ions into the yeast cells and elevated intracellular zinc levels (Fig.4). Taken together, the observed regulation of the zinc homeostasis in response to PDTC indicates excess cytoplasmic zinc, leading to subsequent zinc detoxification by sequestration into the vacuole and by induction of zinc-binding proteins (Fig.3A).

PDTC enhances a cross-talk between iron and zinc homeostasis

Since both zinc homeostasis and the iron regulon were strongly affected by PDTC, we aimed to investigate a potential underlying regulatory cross-talk between these two pathways. Supporting this notion, it was previously reported that zinc overload activates the iron regulon (Pagani *et al.*, 2007). In addition, *aft1*Δ cells are sensitive to high concentrations of extracellular zinc, which indicates that Aft1 is required to counteract the growth defect caused by excess zinc (Pagani *et al.*, 2007). Hence, we performed viability assays with wild type and *aft1*Δ strains in the presence of PDTC, Zn^{2+} and Fe^{3+}, respectively (Fig.3D). Colony forming units were determined after 24h stress treatment with 200µM PDTC in liquid medium and set relative to the untreated wild type. As expected, iron supplementation rescued the cytotoxic effect of PDTC in wild type and *aft1*Δ cells. In contrast, this effect was enhanced by excess zinc. Growth deficiency of *aft1*Δ cells on high excess zinc was rescued by iron supplementation. Strikingly, the combined effect of PDTC, iron and zinc was almost fully rescued in the *aft1*Δ background but not in the wild type strain (Fig.3D). These data suggest that in wild type cells, Aft1 also controls a yet unidentified cellular function counteracting zinc detoxification, at least in the presence of PDTC.

Functional screening identifies essential processes mediating PDTC tolerance

To identify genes that confer tolerance to PDTC, we functionally screened the EUROSCARF deletion collection for altered growth in the presence of PDTC. Therefore, strains of the collection were replicated on YPD and PDTC-containing plates and grown at 30°C for 6 days monitoring growth every day. The previously identified PDTC hypersensitivity of the *aft1*Δ strain was used as a control in the screening procedure. Among more than 4800 haploid single deletion strains, we identified some 140 mutants as

PDTC-hypersensitive (see Supplementary File S2). Mutants showing increased PDTC sensitivity were manually re-spotted in serial dilutions on several PDTC concentrations to re-confirm the phenotype. To categorize the PDTC-sensitive strains, we grouped them based on gene ontology enrichment using the *Saccharomyces* Gene Database GO Termfinder (Fig.5A). The main functional categories comprised of vacuolar acidification and vacuolar transport, protein modifications, mitochondrial organization and translation. Interestingly, many mutants related to membrane and vesicular transport or trafficking systems were PDTC-sensitive (e.g. endosomal sorting complex required for transport (ESCRT); Golgi-associated retrograde protein complex (GARP), HOPS complex).
Furthermore, mutants disrupting vacuolar trafficking including vacuolar protein sorting genes such as *VPS3*, *VPS4*, *VPS8*, *VPS18*, *VPS33*, *VPS41*, *VPS45*, as well as function and assembly of the V-ATPase such as *VMA8*, *VMA22*, *VMA2*, *TFP1*, *VMA21*, *VMA6*, *PPA1* were PDTC-sensitive, suggesting that vacuolar biogenesis and maintenance is pivotal for cells responding to PDTC.

The vacuole is the main storage and detoxification compartment in yeast. Thus, components involved in vacuolar biogenesis and trafficking are essential under various stress conditions. Remarkably, we found a significant overlap of PDTC-sensitive mutants (Fig.5B) and deletion strains sensitive to excess zinc, cadmium, oxidative stress and alkaline pH (Pagani *et al.*, 2007, Outten *et al.*, 2005, Serrano *et al.*, 2004, Jin *et al.*, 2008). For example, a functional V-ATPase is crucial for establishing a proton gradient across the membrane to ensure vacuolar import of ions, especially for zinc sequestration (MacDiarmid *et al.*, 2002). Thus, PDTC tolerance requires several cellular mechanisms and processes to avoid a collapse of cellular ion homeostasis.

DISCUSSION

In this study, we exploit yeast and a chemical-genetic approach combining transcriptional profiling and phenotypic screening techniques to identify possible cellular targets of the antiviral drug pyrrolidine dithiocarbamate (PDTC). The transcriptional profiling indicates that PDTC massively disturbs metal ion homeostasis, including a strong induction of the iron regulon, as well as regulation of zinc transport. The screening of the yeast gene deletion collection for mutants with increased PDTC susceptibility identifies numerous genes essential for the PDTC response, including those required for vacuolar functions and transport complexes.

The transcriptional changes upon PDTC treatment involve more than 200 genes, including general stress response genes. Strikingly, we detect a specific activation of the Aft1 transcription factor driving the iron regulon. Beside iron deprivation, the iron regulon is activated by various stress conditions, ranging from changes in ion concentrations such as excess zinc (Pagani *et al.*, 2007) or cobalt (Stadler & Schweyen, 2002) to physiological changes induced by lactic or acetic acid (Kawahata *et al.*, 2006), as well as glucose depletion occurring during the diauxic shift (Haurie *et al.*, 2003). Moreover, drugs such as the fungicide mancozeb (Santos *et al.*, 2009), chloroquine toxicity (Emerson *et al.*, 2002), hydroxyurea (Dubacq *et al.*, 2006) or the anticancer drug cisplatin (Kimura *et al.*, 2007) mimic iron depletion and thus trigger activation of the iron regulon.

Like PDTC, the fungicide mancozeb is a dithiocarbamate that complexes manganese and zinc and also activates the Aft1 transcription factor (Santos *et al.*, 2009). Proteomic analysis suggests that mancozeb induces oxidative stress response genes, genes involved in translation and protein degradation (Santos *et al.*, 2009). An important property of dithiocarbamates is their metal chelating activity, thereby forming lipophilic dithiocarbamate-metal complexes and facilitating metal entry into cells (Krenn *et al.*, 2005). Mag-fura-2 experiments show an immediate PDTC-caused influx of Zn^{2+} ions into yeast cells. Thus, by changing the delicate ion balance inside cells, excess ions alter enzyme activities and metabolic functions. Thus, PDTC and dithiocarbamates in general might mask significant amounts of intracellular iron or disturb the intracellular zinc / copper homeostasis to drive induction of the iron regulon.

Maintenance of a proper metal ion homeostasis is of pivotal importance for yeast viability and metabolic functions. Cross-talk between responses to different ions has been proposed due to overlapping regulatory networks. For instance, iron and copper are tightly connected, since copper is the essential co-factor in the high-affinity iron permease complex Ftr1/Fet3 (Gross *et al.*, 2000). Consequently, inhibition of copper uptake results in reduced iron uptake. Fet3 is a multicopper ferroxidase whose deletion renders cells

highly sensitive to transition metal stress, alkaline pH and causes impaired growth on ethanol and galactose/raffinose (Rutherford & Bird, 2004). Moreover, relationships between cobalt-iron (Stadler & Schweyen, 2002) and zinc-iron (Pagani *et al.*, 2007, Santos *et al.*, 2003) responses are known. Notably, the vacuolar transporter Cot1 normally involved in zinc transport into the vacuole and cobalt accumulation, is induced under iron-limited conditions (Li & Kaplan, 1998). High excess of zinc disrupts iron homeostasis by altering the intracellular iron content and iron-dependent respiratory enzyme activities such as cytochrome c oxidase, and aconitase, connecting zinc, iron and iron/sulfur cluster (ISC) metabolism (Pagani *et al.*, 2007, Santos *et al.*, 2003). Studies of the yeast *ionome*, as well as the interplay of alkaline pH stress and ion metabolism confirm a tight and dynamic co-regulation at genomic (Eide *et al.*, 2005, Serrano *et al.*, 2004, Serrano *et al.*, 2002) and perhaps at proteomic and regulatory levels.

We here show the impact of various metal ions in combination with PDTC on ion homeostasis (Fig.2C). For example, the *aft1*Δ strain is sensitive to nickel, calcium, manganese, cobalt, zinc as well as alkaline pH (Stadler & Schweyen, 2002, Serrano *et al.*, 2004). These growth phenotypes can be compensated by the supplementation of high iron to the growth media, thereby increasing cellular iron concentrations. In the case of glucose exhaustion, addition of iron fails to rescue the growth defect indicating two independent signals inducing the iron regulon *(Haurie et al.*, 2003). In cells lacking the *AFT1* gene, the copper-binding metallothionein Cup1 is highly induced upon PDTC treatment, which might explain the increased copper-tolerance compared to the wild type (data not shown). Consistent with the fact that PDTC acts as a zinc ionophore mediating zinc influx into HeLa cells (Krenn *et al.*, 2005) as well as yeast cells (Fig. 4), it triggers changes in transcript levels of certain zinc transporters due to the intracellular ionic imbalance.

By functionally screening the yeast gene deletion collection for PDTC-sensitive strains, we identify genes involved in vacuolar functions and transport complexes (Fig.5A) that are also essential under excess zinc conditions (Fig.5B) (Jin *et al.*, 2008, Pagani *et al.*, 2007). For example, a functional V-ATPase is required for establishing a proton gradient across the vacuolar membrane and for zinc storage. Indeed, mutants lacking a functional V-ATPase are both zinc- and PDTC-hypersensitive. Furthermore, the chemical-genomic profile of yeast cells demonstrates that mutants involved in endosome transport, transcription, vacuolar degradation and function of the V-ATPase are sensitive to multiple stress conditions (Hillenmeyer *et al.*, 2008).

Taken together, and based on our data, we propose the *'ionic imbalance'* model for the cellular response to PDTC exposure and the PDTC mechanism of action (Fig.6). Zinc excess as caused by PDTC (Fig.3A) triggers dynamic expression changes of zinc

transporter genes and activation of the iron regulon, whose main transcriptional activator Aft1 is required to counteract ion toxicity as well as alkaline pH stress (Serrano *et al.*, 2004, Stadler & Schweyen, 2002, Pagani *et al.*, 2007), thus orchestrating the adaptive regulation of ion homeostasis pathways. This rapid response regulation prevents further zinc uptake, followed by subsequent activation of the Aft1 regulon. Viability assays investigating the supplementary effect of zinc and iron on PDTC treated cells point towards cross-regulatory networks, linking zinc and iron homeostasis (Fig.3D). Iron supplementation rescues the PDTC-induced growth defects in both wild type and *aft1*Δ cells. By contrast and as expected, additional zinc influx in combination with PDTC is highly toxic (Fig.3D). By investigating cumulative or additive effects of zinc plus iron in combination with PDTC treatment, the *aft1*Δ mutant survives whereas the wild type is hypersensitive. This suggests that Aft1 in wild type cells also controls a yet unidentified cellular function, which counteracts zinc detoxification at least in the presence of PDTC. Thus, we believe that PDTC-promotes zinc storage through zinc-binding proteins such as Sod1 (Fig.3B), as well as vacuolar detoxification, thereby disturbing intracellular metal ion balance causing cross-activation of the iron regulon (Fig.5).

In higher eukaryotes, PDTC is a known inhibitor of NF-κB activation (Schreck *et al.*, 1992), and the eukaryotic translation initiation factor eIF4G in rhinovirus-infected HeLa cells (Gaudernak *et al.*, 2002). Moreover, PDTC prevents protein degradation by inhibiting a E3 ubiquitin ligase (Hayakawa *et al.*, 2003) or the proteasome (Kim *et al.*, 2004) in a zinc-dependent manner. Hence, it will be interesting for future studies to test whether PDTC can affect related yeast transcription factors such as Rim101, a functional homologue of NF-κB implicated in pH regulation, especially since several deletion strains defective in alkaline pH regulation are also PDTC-sensitive (Fig.4; Table 2, Supplemental Data).

Taken together, this work demonstrates the importance of yeast as a model system for performing chemical genetics approaches at the genome-wide scale and its high potential for drug target identification. By combining transcriptional profiling datasets and genome-wide phenotypic screening, it is possible to identify complex and highly dynamic regulatory networks to disclose various biological processes involved in the response to a single drug.

CONCLUSION

In this study, we successfully exploit genome-wide screening tools and microarray profiling techniques in the eukaryotic model organism S. *cerevisiae* to identify genes, processes and signaling pathways involved in the response to the antiviral drug PDTC. The transcriptional changes upon PDTC-treatment involve more than 200 genes, including general stress response genes and other specific adaptations such as an intense cross-talk in metal ion homeostasis. The general stress response genes are involved in growth-related processes, RNA metabolism and repression of ribosomal protein genes. Interestingly, the specific response comprises of many genes involved in metal ion homeostasis, particularly genes of the iron regulon requiring Aft1-dependent activation and cellular remodeling as necessary during iron limitation. Furthermore, transcriptional regulation of cellular zinc transporters and fluorescent visualization of intracellular zinc accumulation hint a PDTC-induced zinc influx and vacuolar zinc sequestration.

By systematically screening of the yeast gene deletion collection, we identify about 140 genes that are essential for PDTC-tolerance. The main functional categories comprise vacuolar acidification and vacuolar transport, protein modifications, mitochondrial organization and translation. Many of these genes have previously been identified as non-transporter multidrug resistance genes, especially under excess zinc and alkaline pH stress conditions. By combining microarray datasets with phenotypic screening results, we suggest PDTC-induced increase in the intracellular zinc-content leading to vacuolar zinc storage accompanied by iron-limitation and full activation of the iron regulon.

ACKNOWLEDGEMENTS

This work was supported by WWTF grant “Molecular Mechanisms of Antivirals” (Vienna Science and Technology Fund) to JS and KK, and in part by the FP7-Integrated Project *UNICELLSYS* to KK. We thank Ralf Egner for providing the yeast strain lacking the Pdr5 and Pdr12 ABC transporters.

Author Disclosure Statement

No competing financial interests exist.

REFERENCES

Bharucha, N. & A. Kumar, (2007) Yeast genomics and drug target identification. Comb Chem High Throughput Screen **10**: 618-634.

Borrello, S. & B. Demple, (1997) NF kappa B-independent transcriptional induction of the human manganous superoxide dismutase gene. Arch Biochem Biophys **348**: 289-294.

De Freitas, J. M., A. Liba, R. Meneghini, J. S. Valentine & E. B. Gralla, (2000) Yeast lacking Cu-Zn superoxide dismutase show altered iron homeostasis. Role of oxidative stress in iron metabolism. J Biol Chem **275**: 11645-11649.

Dubacq, C., A. Chevalier, R. Courbeyrette, C. Petat, X. Gidrol & C. Mann, (2006) Role of the iron mobilization and oxidative stress regulons in the genomic response of yeast to hydroxyurea. Mol Genet Genomics **275**: 114-124.

Eide, D. J., (2009) Homeostatic and adaptive responses to zinc deficiency in *Saccharomyces cerevisiae*. J Biol Chem **284**: 18565-18569.

Eide, D. J., S. Clark, T. M. Nair, M. Gehl, M. Gribskov, M. L. Guerinot, *et al*. (2005) Characterization of the yeast ionome: a genome-wide analysis of nutrient mineral and trace element homeostasis in *Saccharomyces cerevisiae*. Genome Biol **6**: R77.

Emerson, L. R., M. E. Nau, R. K. Martin, D. E. Kyle, M. Vahey & D. F. Wirth, (2002) Relationship between chloroquine toxicity and iron acquisition in *Saccharomyces cerevisiae*. Antimicrob Agents Chemother **46**: 787-796.

Ericson, E., M. Gebbia, L. E. Heisler, J. Wildenhain, M. Tyers, G. Giaever, *et al*. (2008) Off-target effects of psychoactive drugs revealed by genome-wide assays in yeast. PLoS Genet **4**: e1000151.

Erl, W., C. Weber & G. K. Hansson, (2000) Pyrrolidine dithiocarbamate-induced apoptosis depends on cell type, density, and the presence of Cu(2+) and Zn(2+). Am J Physiol Cell Physiol **278**: C1116-1125.

Foury, F., (1997) Human genetic diseases: a cross-talk between man and yeast. Gene **195**: 1-10.

Gasch, A. P., P. T. Spellman, C. M. Kao, O. Carmel-Harel, M. B. Eisen, G. Storz, *et al.* (2000) Genomic expression programs in the response of yeast cells to environmental changes. Mol Biol Cell **11**: 4241-4257.

Gaudernak, E., J. Seipelt, A. Triendl, A. Grassauer & E. Kuechler, (2002) Antiviral effects of pyrrolidine dithiocarbamate on human rhinoviruses. J Virol **76**: 6004-6015.

Giaever, G., (2003) A chemical genomics approach to understanding drug action. Trends Pharmacol Sci **24**: 444-446.

Gitan, R. S. & D. J. Eide, (2000) Zinc-regulated ubiquitin conjugation signals endocytosis of the yeast Zrt1 zinc transporter. Biochem J 346 Pt **2**: 329-336.

Gross, C., M. Kelleher, V. R. Iyer, P. O. Brown & D. R. Winge, (2000) Identification of the copper regulon in *Saccharomyces cerevisiae* by DNA microarrays. J Biol Chem **275**: 32310-32316.

Hartsfield, C. L., J. Alam & A. M. Choi, (1998) Transcriptional regulation of the heme oxygenase 1 gene by pyrrolidine dithiocarbamate. FASEB J **12**: 1675-1682.

Haurie, V., H. Boucherie & F. Sagliocco, (2003) The Snf1 protein kinase controls the induction of genes of the iron uptake pathway at the diauxic shift in *Saccharomyces cerevisiae*. J Biol Chem **278**: 45391-45396.

Hayakawa, M., H. Miyashita, I. Sakamoto, M. Kitagawa, H. Tanaka, H. Yasuda, *et al.* (2003) Evidence that reactive oxygen species do not mediate NF-kappaB activation. EMBO J **22**: 3356-3366.

Hillenmeyer, M. E., E. Fung, J. Wildenhain, S. E. Pierce, S. Hoon, W. Lee, M. Proctor, R. P. St Onge, M. Tyers, D. Koller, R. B. Altman, R. W. Davis, C. Nislow & G. Giaever, (2008) The chemical genomic portrait of yeast: uncovering a phenotype for all genes. Science **320**: 362-365.

Hughes, T. R., M. J. Marton, A. R. Jones, C. J. Roberts, R. Stoughton, C. D. Armour, H. A., *et al*. (2000) Functional discovery via a compendium of expression profiles. Cell **102**: 109-126.

Jin, Y. H., P. E. Dunlap, S. J. McBride, H. Al-Refai, P. R. Bushel & J. H. Freedman, (2008) Global transcriptome and deletome profiles of yeast exposed to transition metals. PLoS Genet **4**: e1000053.

Kaiser, C., S. Michaelis & A. P. Mitchell, (1994) Methods in yeast genetics. A laboratory course manual. Cold Spring Harbor Laboratory Press, Cold Spring Harbor, NY.

Kaplan, C. D. & J. Kaplan, (2009) Iron acquisition and transcriptional regulation. Chem Rev **109**: 4536-4552.

Kawahata, M., K. Masaki, T. Fujii & H. Iefuji, (2006) Yeast genes involved in response to lactic acid and acetic acid: acidic conditions caused by the organic acids in *Saccharomyces cerevisiae* cultures induce expression of intracellular metal metabolism genes regulated by Aft1p. FEMS Yeast Res **6**: 924-936.

Kim, I., C. H. Kim, J. H. Kim, J. Lee, J. J. Choi, Z. A. Chen, M. G. Lee, *et al* (2004) Pyrrolidine dithiocarbamate and zinc inhibit proteasome-dependent proteolysis. Exp Cell Res **298**: 229-238.

Kimura, A., K. Ohashi & A. Naganuma, (2007) Cisplatin upregulates *Saccharomyces cerevisiae* genes involved in iron homeostasis through activation of the iron insufficiency-responsive transcription factor Aft1. J Cell Physiol **210**: 378-384.

Krenn, B. M., B. Holzer, E. Gaudernak, A. Triendl, F. J. van Kuppeveld & J. Seipelt, (2005) Inhibition of polyprotein processing and RNA replication of human rhinovirus by pyrrolidine dithiocarbamate involves metal ions. J Virol **79**: 13892-13899.

Kumanovics, A., O. S. Chen, L. Li, D. Bagley, E. M. Adkins, H. Lin, *et al*. (2008) Identification of *FRA1* and *FRA2* as genes involved in regulating the yeast iron regulon in response to decreased mitochondrial iron-sulfur cluster synthesis. J Biol Chem **283**: 10276-10286.

Lanke, K., B. M. Krenn, W. J. Melchers, J. Seipelt & F. J. van Kuppeveld, (2007) PDTC inhibits picornavirus polyprotein processing and RNA replication by transporting zinc ions into cells. J Gen Virol **88**: 1206-1217.

Li, L. & J. Kaplan, (1998) Defects in the yeast high affinity iron transport system result in increased metal sensitivity because of the increased expression of transporters with a broad transition metal specificity. J Biol Chem **273**: 22181-22187.

MacDiarmid, C. W., M. A. Milanick & D. J. Eide, (2002) Biochemical properties of vacuolar zinc transport systems of *Saccharomyces cerevisiae*. J Biol Chem **277**: 39187-39194.

Mamnun, Y. M., C. Schüller & K. Kuchler, (2004) Expression regulation of the yeast *PDR5* ATP-binding cassette (ABC) transporter suggests a role in cellular detoxification during the exponential growth phase. FEBS Lett **559**: 111-117.

Morais, C., B. Pat, G. Gobe, D. W. Johnson & H. Healy, (2006) Pyrrolidine dithiocarbamate exerts anti-proliferative and pro-apoptotic effects in renal cell carcinoma cell lines. Nephrol Dial Transplant **21**: 3377-3388.

Moreno, S., A. Klar & P. Nurse, (1991) Molecular genetic analysis of fission yeast *Schizosaccharomyces pombe*. Methods Enzymol **194**: 795-823.

Outten, C. E., R. L. Falk & V. C. Culotta, (2005) Cellular factors required for protection from hyperoxia toxicity in *Saccharomyces cerevisiae*. Biochem J **388**: 93-101.

Pagani, M. A., A. Casamayor, R. Serrano, S. Atrian & J. Arino, (2007) Disruption of iron homeostasis in *Saccharomyces cerevisiae* by high zinc levels: a genome-wide study. Mol Microbiol **65**: 521-537.

Parsons, A. B., R. L. Brost, H. Ding, Z. Li, C. Zhang, B. Sheikh, *et al*. (2004) Integration of chemical-genetic and genetic interaction data links bioactive compounds to cellular target pathways. Nat Biotechnol **22**: 62-69.

Parsons, A. B., A. Lopez, I. E. Givoni, D. E. Williams, C. A. Gray, J. Porter, G. Chua, R. Sopko, *et al*. (2006) Exploring the mode-of-action of bioactive compounds by chemical-genetic profiling in yeast. Cell **126**: 611-625.

Pfaller, M. A. & D. J. Diekema, (2004) Rare and emerging opportunistic fungal pathogens: concern for resistance beyond *Candida albicans* and *Aspergillus fumigatus*. J Clin Microbiol **42**: 4419-4431.

Raju, B., E. Murphy, L. A. Levy, R. D. Hall & R. E. London, (1989) A fluorescent indicator for measuring cytosolic free magnesium. Am J Physiol **256**: C540-548.

Rutherford, J. C. & A. J. Bird, (2004) Metal-responsive transcription factors that regulate iron, zinc, and copper homeostasis in eukaryotic cells. Eukaryot Cell **3**: 1-13.

Saeed, A. I., N. K. Bhagabati, J. C. Braisted, W. Liang, V. Sharov, E. A. Howe, *et al*. (2006) TM4 microarray software suite. Methods Enzymol **411**: 134-193.

Saeed, A. I., V. Sharov, J. White, J. Li, W. Liang, N. Bhagabati, *et al*. (2003) TM4: a free, open-source system for microarray data management and analysis. Biotechniques **34**: 374-378.

Sambrook, J., E. Fritsch & T. Maniatis, (2001) Molecular cloning: A laboratory manual. 3rd edition. Cold Spring Harbor, Press, New York.

Santos, P. M., T. Simoes & I. Sa-Correia, (2009) Insights into yeast adaptive response to the agricultural fungicide mancozeb: a toxicoproteomics approach. Proteomics **9**: 657-670.

Santos, R., A. Dancis, D. Eide, J. M. Camadro & E. Lesuisse, (2003) Zinc suppresses the iron-accumulation phenotype of *Saccharomyces cerevisiae* lacking the yeast frataxin homologue (Yfh1). Biochem J **375**: 247-254.

Schreck, R., B. Meier, D. N. Mannel, W. Droge & P. A. Baeuerle, (1992) Dithiocarbamates as potent inhibitors of nuclear factor kappa B activation in intact cells. J Exp Med **175**: 1181-1194.

Serrano, R., D. Bernal, E. Simon & J. Arino, (2004) Copper and iron are the limiting factors for growth of the yeast *Saccharomyces cerevisiae* in an alkaline environment. J Biol Chem **279**: 19698-19704.

Serrano, R., A. Ruiz, D. Bernal, J. R. Chambers & J. Arino, (2002) The transcriptional response to alkaline pH in *Saccharomyces cerevisiae*: evidence for calcium-mediated signalling. Mol Microbiol **46**: 1319-1333.

Simons, T. J., (1993) Measurement of free Zn2+ ion concentration with the fluorescent probe mag-fura-2 (furaptra). J Biochem Biophys Methods **27**: 25-37.

Smyth, G. K., (2004) Linear models and empirical bayes methods for assessing differential expression in microarray experiments. Stat Appl Genet Mol Biol **3**: Article3.

Stadler, J. A. & R. J. Schweyen, (2002) The yeast iron regulon is induced upon cobalt stress and crucial for cobalt tolerance. J Biol Chem **277**: 39649-39654.

Stockwell, B. R., (2000) Chemical genetics: ligand-based discovery of gene function. Nat Rev Genet **1**: 116-125.

Tarhan, C., M. Pekmez, S. Karaer, N. Arda & A. T. Sarikaya, (2007) The effect of superoxide dismutase deficiency on zinc toxicity in *Schizosaccharomyces pombe*. J Basic Microbiol **47**: 506-512.

Teixeira, M. C., P. Monteiro, P. Jain, S. Tenreiro, A. R. Fernandes, N. P. Mira, M. Alenquer, A. T. Freitas, A. L. Oliveira & I. Sa-Correia, (2006) The YEASTRACT database: a tool for the analysis of transcription regulatory associations in *Saccharomyces cerevisiae*. Nucleic Acids Res **34**: D446-451.

Tucker, C. L. & S. Fields, (2004) Quantitative genome-wide analysis of yeast deletion strain sensitivities to oxidative and chemical stress. Comp Funct Genomics **5**: 216-224.

Uchide, N., K. Ohyama, T. Bessho, B. Yuan & T. Yamakawa, (2002) Effect of antioxidants on apoptosis induced by influenza virus infection: inhibition of viral gene replication and transcription with pyrrolidine dithiocarbamate. Antiviral Res **56**: 207-217.

Wettenhall, J. M. & G. K. Smyth, (2004) limmaGUI: a graphical user interface for linear modeling of microarray data. Bioinformatics **20**: 3705-3706.

Wu, W. S., W. H. Li & B. S. Chen, (2008) Reconstructing a network of stress-response regulators via dynamic system modeling of gene regulation. Gene Regul Syst Bio **2**: 53-62.

Yamaguchi-Iwai, Y., A. Dancis & R. D. Klausner, (1995) *AFT1*: a mediator of iron regulated transcriptional control in *Saccharomyces cerevisiae*. EMBO J **14**: 1231-1239.

Yamaguchi-Iwai, Y., R. Ueta, A. Fukunaka & R. Sasaki, (2002) Subcellular localization of Aft1 transcription factor responds to iron status in *Saccharomyces cerevisiae*. J Biol Chem **277**: 18914-18918.

Yun, C. W., T. Ferea, J. Rashford, O. Ardon, P. O. Brown, D. Botstein, *et al*. (2000) Desferrioxamine-mediated iron uptake in *Saccharomyces cerevisiae*. Evidence for two pathways of iron uptake. J Biol Chem **275**: 10709-10715.

Figure Legends

Figure 1: PDTC inhibits growth of several yeast species

A. The effect of PDTC on growth of various yeast species was examined by spot assays on solid medium. Logarithmically growing wild type strains were spotted in serial dilutions ranging from OD_{600} of 0.2 to $2x10^{-4}$ onto YPD and PDTC containing plates and grown at 30°C for 2 days. *S. pombe* (OD_{600} of 0.2) was spotted on YES medium containing a gradient from 0 to 50µM PDTC.
B. Growth curves of the *S. cerevisiae* wild type strain BY4741 with increasing concentrations of PDTC. Cells were grown in rich medium supplemented with PDTC for 8 hours at 30°C. Growth was monitored by measuring OD_{600} every hour. Data are displayed as mean ± 1 SD of three independent growth experiments. Arrows indicate the time points at which samples were harvested for microarray analysis of unstressed cells and cells treated with 75µM PDTC.

Figure 2: PDTC activates the Aft1-dependent iron regulon

A. Induction of the iron regulon is Aft1-dependent. Northern blot analysis comparing PDTC-induced gene expression of the iron-responsive genes *FIT2*, *FIT3* and the Aft1-independent gene *GRE2* in wild type and *aft1*Δ cells. Cells were treated for 1, 3 and 5h with PDTC. Untreated and PDTC treated cells were harvested, total RNA was isolated for Northern blot analysis.

B. PDTC activates the *FET3*-promoter. Cells containing an integrated *lacZ-FET3* reporter construct were grown to the mid-log phase (OD600 ~ 0.6) in YPD and treated with 100µM PDTC for 3 hours. Cells were harvested and assayed for β-galactosidase activity. Data of a representative experiment are shown and the error bars represent ± 1 SD of three replicates.

C. PDTC-induced growth deficiency is rescued by iron supplementation. Wild type and *aft1*Δ cells were spotted in serial dilutions on rich media containing PDTC and/or different ions. Growth was monitored after 2 days incubation at 30°C.

Figure 3: PDTC causes intracellular zinc overload

A. Northern blot comparing the PDTC-induced changes of transcript levels of various zinc transporters whose cellular location is indicated in the scheme on the left. These alterations in gene expression indicate intracellular zinc accumulation and

subsequent vacuolar zinc sequestration. Cells were grown in rich medium to an OD_{600} of ~0.5, 75µM PDTC was supplemented and cells were harvested at the indicated time points and prepared for Northern analysis.

B. PDTC induces the transcript levels of the copper/zinc superoxide dismutase *SOD1* gene. Cells were treated with PDTC, harvested at the indicated time points and total RNA was prepared for Northern analysis.
C. Deletion of the *SOD1* gene renders cells zinc and PDTC-hypersensitive. Wild type and deletion mutants were spotted in serial dilutions (OD_{600} of 0.2 to $2x10^{-4}$) on YPD plates supplemented with 20µM PDTC, 4mM $ZnSO_4$ and 2 mM $FeCl_3$, respectively. Growth was monitored after a 2 day incubation at 30°C.
D. Cell viability assays to investigate the nature of a probable cross-talk between iron and zinc homeostasis. Wild type and *aft1*Δ were grown in liquid rich medium for 24h in the presence of PDTC, $ZnSO_4$ and $FeCl_3$, respectively. Afterwards, cells were plated on YPD and colony forming units (CFU) were determined after a 2 day incubation at 30°C. Data are presented as percent CFU relative to the untreated wild type. Error bars represent ± 1 SD of three independent growth experiments; stars indicate significance of data valued by a Students t-test.

Figure 4: PDTC induces immediate influx of zinc ions into yeast cells

Cells were loaded with the mag-fura-2 dye and fluorescence was monitored in real-time after adding metal ions such as $ZnSO_4$, $CaCl_2$, $CuSO_4$, $MgCl_2$, PDTC and EDTA at the indicated time points. The excitation wavelength of mag-fura-2 is shifted by binding bivalent metal ions. Thus, change of the fluorescent ratio of F340/380nm following addition of zinc and PDTC, but not by calcium, magnesium or copper, show accumulation of intracellular labile zinc.

Figure 5: Functional screening identifies processes mediating PDTC tolerance

A. Functional categories of genes required for PDTC tolerance in yeast. The about 4800 deletion strains were screened on YPD and PDTC-containing plates using a Singer RoToR HAD Robot. Growth was monitored after 2 days. Sensitive strains were verified by manual re-spotting and clustered into functional categories using the Gene Ontology termfinder. The number of genes per category and the percentages of each category to the dataset are indicated. All PDTC-sensitive genes are listed in supplementary data S2.

B. Venn diagrams showing the overlap of PDTC-sensitive genes and genes required during zinc and cadmium toxicity, as well as under alkaline pH conditions. Screening data for comparison were taken from published datasets (Jin *et al.*, 2008, Serrano *et al.*, 2004, Pagani *et al.*, 2007).

Figure 6: The ionic imbalance model

We show that PDTC mediates intracellular zinc accumulation, leading to zinc detoxification by vacuolar sequestration, thereby causing a decrease in iron availability. Hence, the iron-dependent transcription factor Aft1 activates the iron regulon and stimulates cellular remodeling as under iron scarcity. Consequently, PDTC might link intracellular disturbance of iron and zinc homeostasis to other cellular processes, including vacuolar and vesicular transport or even pH regulation.

Table 1: Functional categories of differentially expressed genes after PDTC stress

Wild type yeast cells were grown to the logarithmic growth phase in rich medium, treated with PDTC for 1, 3 or 5 hours. RNA was extracted and labeled samples were used to probe yeast DNA microarrays. We carried out three independent comparisons of PDTC-treated versus untreated cells considering changes more than two-fold as significant. The PDTC transcriptome comprises of a general and a specific stress response, all together involving more than 200 genes that were categorized by gene ontology enrichment. Overlapping processes were manually collapsed. All genes affected by PDTC treatment are listed in Supplementary Data S2, including data of all time points, fold-expression and p-values.

Table 1. Functional categories of genes regulated upon PDTC stress

Categories	Gene names	N° of genes
Iron regulon Aft1/Aft2 target genes	*FTH1, SIT1, FTR1, ARN1, ARN2, CTR2, FRE1, CCS1, FET3, ENB1, FIT1, FIT2, FIT3, YLR126C, ISU2, ISU1, FTR1*	17
Carboxylic acid metabolic process	*CYS3, GCV3, SHM1, CHA1, SFA1, GLT1, GCV1, ARO3, HOM3, MET6, LPD1, ARO9, POT1, ELO1, FBA1, FAS1, ILV5, ILV2, GCV2, LEU4, LYS9, LEU9, HIS3, GDH1, CAR1, GLN1, SHM2, URA1, GTT1, URA4*	30
Purine biosynthetic process	*ADE1, ADE8, ADE5,7, ADE13, ADE17, ADE3, ADE12*	7
Stress response to drug / toxin	*AAD3, RPN4, UBC5, YCF1, SNF1, AAD6, AAD16,* YML131W, *DDR48, HOR7, LAP3, GRE2, TIR2, OYE3, HSP31, SFP1, OYE2*	17
Response to oxidative stress	YDL124W, *CTA1, TRR1, YPR1, GRX2, TRX2, STB5, SOD1, CCP1, TRX1, AHP1, ZWF1, ATX1, GLR1, PEP4*	15
Respiration and citric acid cycle	*COX6, COX5A, COX9, COX13, IDH1, ACO1, RIB3, POR1, QCR7*	9
Transport	*STP22, TRS23, INH1, VHT1, TOM6, HNM1, MUP1, TPO1, DIC1, SFH5, HXT10, HXT4, HXT5, HXT8, GAL2, HXT11, HXT12*	18
Heme and ergosterol biosynthesis	*ERG3, ERG1, ERG27, ERG11, HEM13, YHB1, YCP4*	7
Telomere maintenance	YGL039W, *NMD2, CST6, HCR1, LST7, SWD1, PNC1*	7
Transcription / translation	*MRP8, EFB1, GCD2, RLI1, GAT1, ERB1, UTP23, SSZ1, RLP7, TUF1*	10
DNA replication / repair	*RNR2, RNR4, DON1, WTM1, YPL033C, NNF1, RFA2, SIM1*	8
Oxidoreductase activity	*ADH7,* YDR541C, *DLD3, YGL157W, ADH6,* YNL134C	6
Other	*PHO5, PHO11, PHO86, IRC7, IZH1, FRM2, MFA1, EMI2, AGA2, KOG1, BAR1, BNR1, MSG5, LAP4, AIM46, RIB4, SLA1, EHD3, FLO9, NDE1, SNC2, PAC11, TEC1, PEX5, UGP1, RMD6, AIM18, PMI40, SCW4, CWP1, SRP40, EMI1, VHS1, YRO2, PRE8, MRH1, APT2, TIP1, LRG1, CNS1, WWM1, RPN6, DPH5, FRQ1, FMP43*	45
Unknown	YAL065C, YMR173W-A, YCR102C, YJL217W, YER156C, YGR146C, YDR476C, YOR285W, YKL088W, YDR154C, YKL030W, YPL067C, YKL066W, YLL044W, YDR271C, YBR053C, YJL068C, YFR024C, YHR213W, YAR073W, YKL171W, YEL033W, YDR119W, YLR460C, YNL208W, YCR074C	26

Figure 1

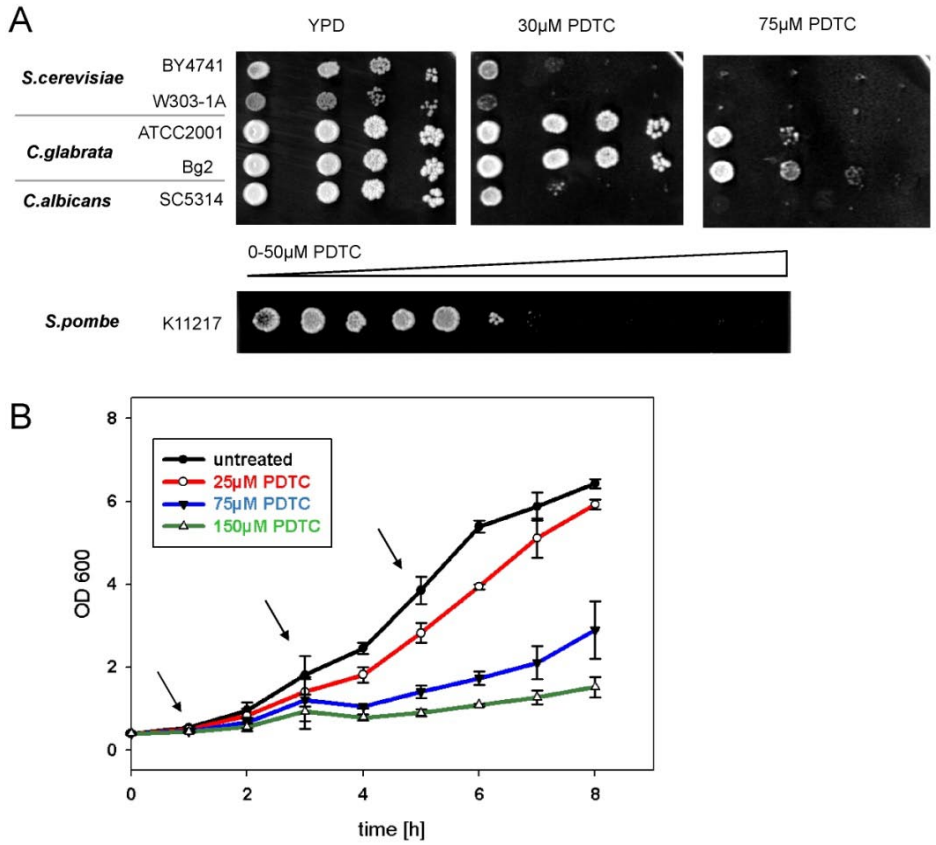

Figure 2

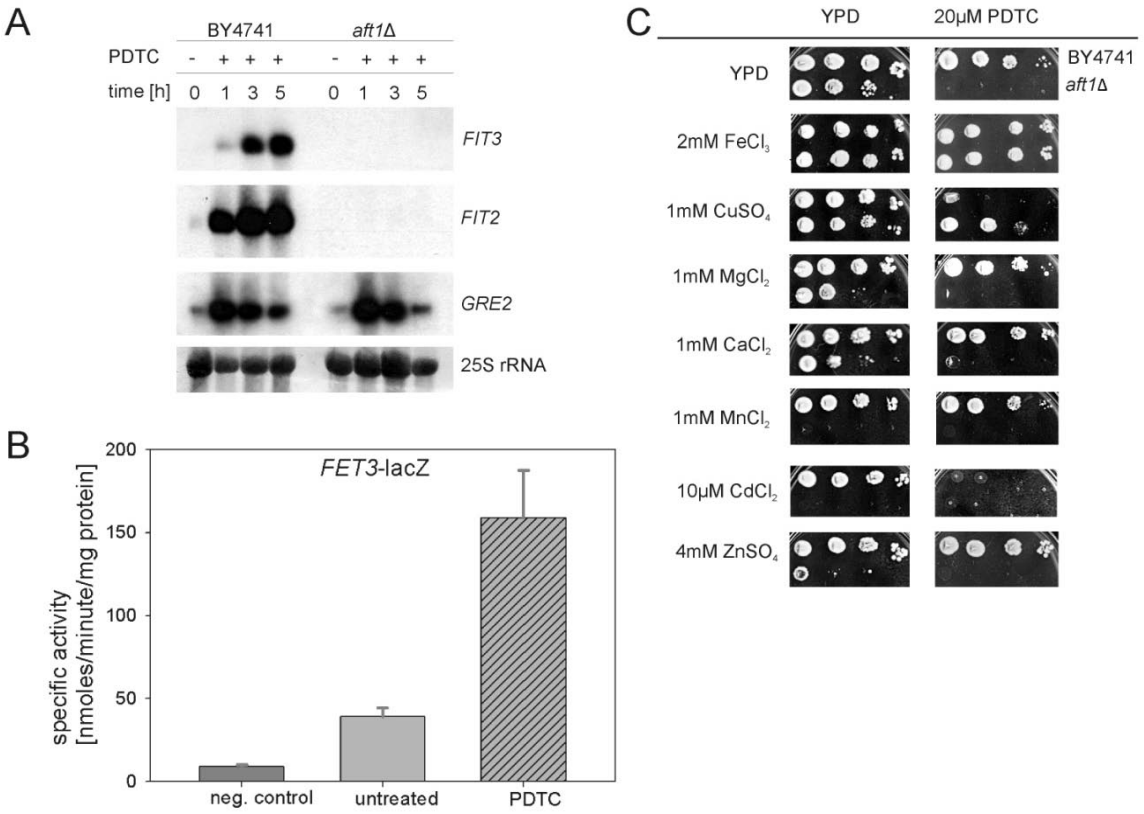

Figure 3

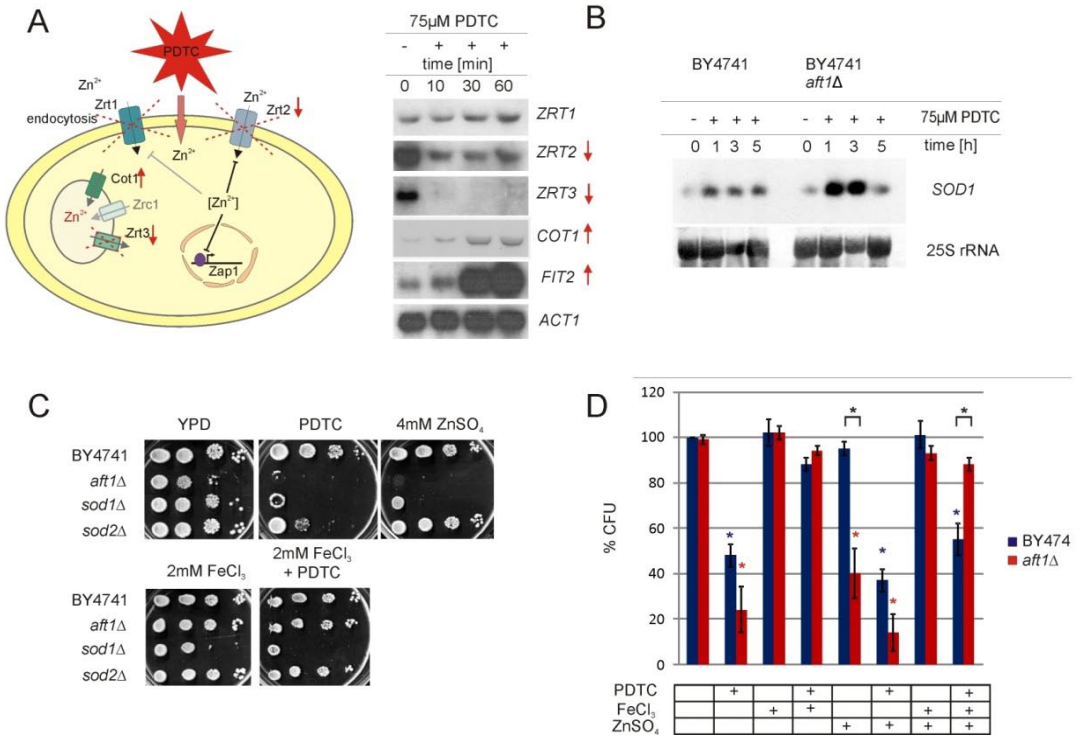

Figure 4

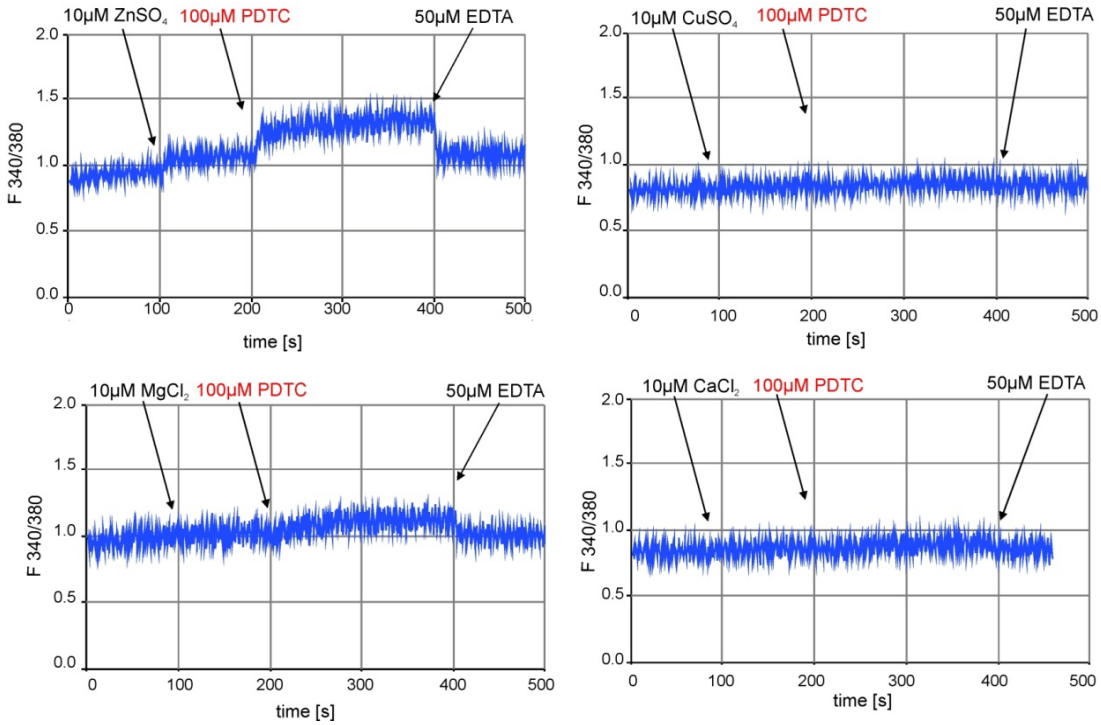

Figure 5

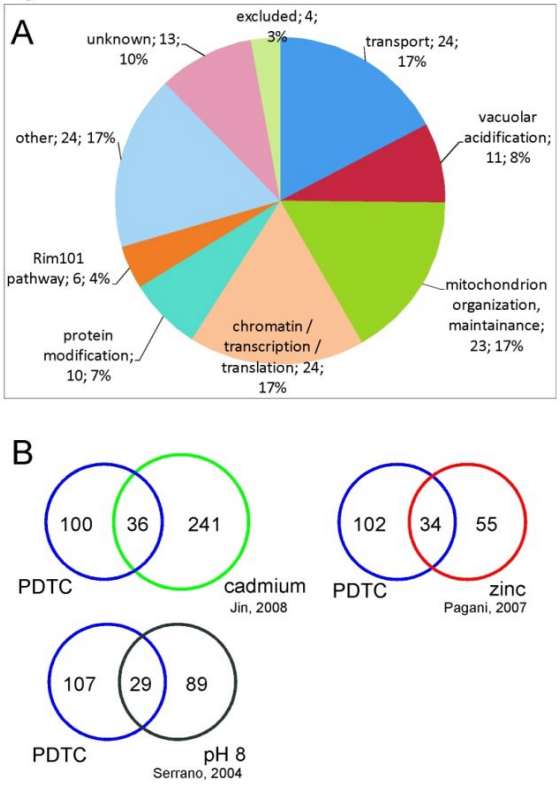

Figure 6

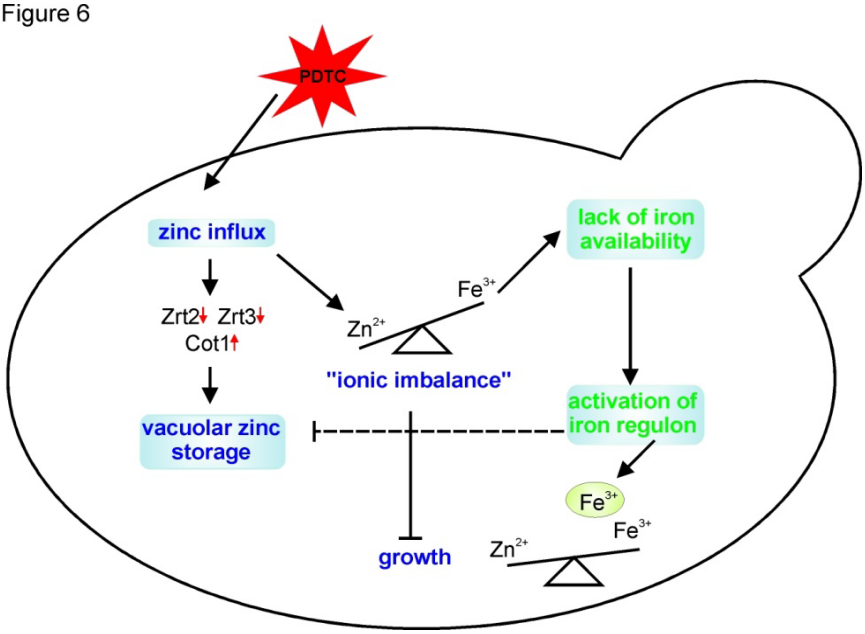

Supplementary Table 1 - Yeast strains used in this study

Name	Genotype	Reference
BY4741	*MAT***a** *his3Δ1*; *leu2Δ0*; *met15Δ0*; *ura3Δ0*	(Brachmann *et al.*, 1998)
BY4742	*MAT*α ; *his3Δ1*; *leu2Δ0*; *lys2Δ0*; *ura3Δ0*	(Brachmann et al., 1998)
EUROSCARF yeast deletion collection		http://web.uni-frankfurt.de/fb15/mikro/euroscarf/index.html
DY1457	*MAT*α, *ura3-52, leu2-3, trp2-1, his3-11, can1-100(oc), ade6*	(Chen *et al.*, 2004)
OCY355	*MAT*α, *ura3-52, leu2-3, trp2-1, his3-11, can1-100(oc), ade2, ho::FET3LacZ*	(Kumanovics *et al.*, 2008)
ATCC2001	*C. glabrata* wild type strain available at www.atcc.org	
SC5314	*C. albicans* wild type strain	
K11217	*S. pombe* wild type strain	Kindly provided by K. Nasmyth
YRE107	YPH499 *MAT***a**, *leu2Δ1, ura3Δ52, his3Δ200, ade2Δ10 lys2Δ801a pdr5Δ::TRP1 pdr12Δ::URA3*	Kindly provided by R. Egner

Supplementary File S2

Microarray Data – Differentially expressed genes at 1, 3 and 5h PDTC exposure (cut-off values of 0.001 for the adjusted p-value and a 2-fold expression change)

Sc ORF	Gene	1h-fold	3h-fold	5h-fold	min p-val	Biological Process	Function	Subcellular Localization
YOR004W	***UTP23***	-1,23	1,25	2,07	7,51133E-06	35S primary transcript processing*	molecular function unknown	mitochondrion*
YIL159W	***BNR1***	-1,27	-1,45	-2,09	4,65257E-10	actin filament organization*	cytoskeletal protein binding	contractile ring (sensu Saccharomyces)
YGL191W	***COX13***	-1,09	-1,45	-2,06	7,11238E-07	aerobic respiration	enzyme regulator activity*	respiratory chain complex IV (sensu Eukaryota)
YDR529C	***QCR7***	-2,14	-3,10	-3,79	3,00235E-09	aerobic respiration*	ubiquinol-cytochrome-c reductase activity	respiratory chain complex III (sensu Eukaryota)
YDR487C	***RIB3***	2,24	1,52	1,50	3,02885E-06	aerobic respiration*	3,4-dihydroxy-2-butanone-4-phosphate synthase activity	cytosol*
YNL055C	***POR1***	2,24	1,64	-1,63	9,83167E-11	aerobic respiration*	voltage-gated ion-selective channel activity	mitochondrial outer membrane*
YGL032C	***AGA2***	2,43	-1,99	-3,16	2,37633E-06	agglutination during conjugation with cellular fusion	cell adhesion molecule binding	cell wall (sensu Fungi)
YCR105W	***ADH7***	3,49	2,24	1,41	6,46982E-05	alcohol metabolism	alcohol dehydrogenase (NADP+) activity	soluble fraction
YFL057C	***AAD16***	8,88	2,60	2,02	1,02598E-11	aldehyde metabolism	aryl-alcohol dehydrogenase activity	cellular component unknown
YFL056C	***AAD6***	5,85	2,00	1,63	2,25567E-08	aldehyde metabolism	aryl-alcohol dehydrogenase activity	cellular component unknown
YCR107W	***AAD3***	5,56	2,19	2,05	3,63895E-08	aldehyde metabolism	aryl-alcohol dehydrogenase activity	cellular component unknown
YMR318C	***ADH6***	5,69	2,32	1,76	4,3974E-08	aldehyde metabolism*	alcohol dehydrogenase (NADP+) activity	soluble fraction
YDR368W	***YPR1***	4,53	1,86	-1,91	4,37888E-14	arabinose catabolism*	oxidoreductase activity*	cytoplasm*
YPL111W	***CAR1***	2,35	1,66	-1,03	8,35886E-08	arginine catabolism to ornithine	zinc ion binding*	Cytosol
YDR035W	***ARO3***	-1,63	-2,05	-1,95	1,02254E-06	aromatic amino acid family biosynthesis	3-deoxy-7-phosphoheptulonate synthase activity	cytoplasm*
YHR137W	***ARO9***	-1,40	-1,96	-2,05	5,50495E-07	aromatic amino acid family metabolism	aromatic-amino-acid transaminase activity	cytoplasm*
YDL181W	***INH1***	-1,05	-1,59	-3,29	4,16164E-11	ATP synthesis coupled proton transport	enzyme inhibitor activity	proton-transporting ATP synthase complex (sensu Eukaryota)
YDR533C	***HSP31***	58,65	9,02	4,55	1,65637E-15	biological process unknown	unfolded protein binding*	soluble fraction
YNL134C		52,69	7,76	6,18	3,00983E-11	biological process unknown	alcohol dehydrogenase (NADP+) activity	cytoplasm*

YLR460C		31,39	10,03	5,12	3,10104E-13	biological process unknown	molecular function unknown	cellular component unknown
YAL065C		8,67	21,18	16,51	1,50726E-10	biological process unknown	molecular function unknown	cellular component unknown
YML131W		11,65	3,46	2,18	3,38101E-11	biological process unknown	molecular function unknown	Cytoplasm
YPL171C	***OYE3***	9,52	4,00	3,01	9,83167E-11	biological process unknown	NADPH dehydrogenase activity	cellular component unknown
YGL157W		7,83	3,41	3,11	9,63025E-15	biological process unknown	oxidoreductase activity*	cytoplasm*
YNL208W		5,21	2,29	-1,23	3,38101E-11	biological process unknown	molecular function unknown	Mitochondrion
YJL217W		-5,13	-1,70	-2,67	3,50744E-10	biological process unknown	molecular function unknown	Cytoplasm
YER156C		-5,00	-4,52	-3,30	2,08038E-08	biological process unknown	molecular function unknown	cytoplasm*
YGR146C		2,39	3,18	4,81	4,62474E-09	biological process unknown	molecular function unknown	cellular component unknown
YDR541C		4,76	2,01	1,57	9,83167E-11	biological process unknown	dihydrokaempferol 4-reductase activity	cellular component unknown
YDR476C		3,96	4,32	4,65	1,96296E-10	biological process unknown	molecular function unknown	endoplasmic reticulum
YHR199C	***AIM46***	4,58	3,81	3,57	1,10258E-09	biological process unknown	molecular function unknown	Mitochondrion
YOR285W		4,32	2,47	-1,94	1,48091E-12	biological process unknown	molecular function unknown	mitochondrion*
YJL200C	***ACO2***	-4,28	-2,33	-2,11	9,46215E-11	biological process unknown	aconitate hydratase activity	Mitochondrion
YHR179W	***OYE2***	4,23	2,98	1,81	3,9155E-07	biological process unknown	NADPH dehydrogenase activity	cytoplasm*
YCR004C	***YCP4***	3,05	1,31	-1,16	2,25323E-10	biological process unknown	electron carrier activity	cytoplasm*
YEL072W	***RMD6***	1,88	1,78	2,82	8,33849E-10	biological process unknown	molecular function unknown	cellular component unknown
YHR198C	***AIM18***	2,74	2,37	1,78	1,12538E-06	biological process unknown	molecular function unknown	Mitochondrion
YGR243W	***FMP43***	2,48	1,79	1,38	1,51395E-10	biological process unknown	molecular function unknown	Mitochondrion
YBR054W	***YRO2***	-1,84	-2,16	-2,37	4,95717E-08	biological process unknown	molecular function unknown	mitochondrion*
YPL067C		-1,35	-1,92	-2,24	3,57568E-06	biological process unknown	molecular function unknown	Cytoplasm
YDR033W	***MRH1***	-1,54	-1,77	-2,18	6,14167E-07	biological process unknown	molecular function unknown	mitochondrion*
YBR053C		-1,25	-1,45	-2,15	1,97731E-08	biological process unknown	molecular function unknown	cellular component unknown
YDR441C	***APT2***	1,31	1,15	2,13	0,000376073	biological process unknown	molecular function unknown*	Cytoplasm
YHR213W		-1,28	-1,55	-2,09	0,000178934	biological process unknown	molecular function unknown	cellular component unknown
YDR119W		1,35	-1,20	-2,03	7,61006E-07	biological process unknown	molecular function unknown	vacuolar membrane (sensu Fungi)
YFL010C	***WWM1***	2,02	1,28	1,02	1,32837E-09	biological process unknown	molecular function unknown	cytoplasm*
YIL170W	***HXT12***	-1,04	1,18	-2,05	0,00023407	biological process unknown*	molecular function unknown*	cellular component unknown

YGR065C	***VHT1***	2,92	2,02	2,96	6,71791E-06	biotin transport	biotin transporter activity	plasma membrane
YMR108W	***ILV2***	-2,11	-2,22	-1,60	0,000302065	branched chain family amino acid biosynthesis	acetolactate synthase activity*	mitochondrion*
YKL096W	***CWP1***	2,21	-1,65	-2,66	1,90103E-08	cell wall organization and biogenesis	structural constituent of cell wall	cell wall (sensu Fungi)
YBR067C	***TIP1***	1,48	2,12	1,95	0,000216321	cell wall organization and biogenesis	structural constituent of cell wall*	cell wall (sensu Fungi)
YBL007C	***SLA1***	3,98	5,29	4,89	1,31656E-06	cell wall organization and biogenesis*	protein binding, bridging*	actin cortical patch
YGL077C	***HNM1***	-2,15	-1,84	-2,03	4,44125E-08	choline transport	choline transporter activity	plasma membrane
YGL037C	***PNC1***	2,54	-1,03	-1,75	3,42139E-08	chromatin silencing at telomere*	nicotinamidase activity	cytoplasm*
YJR112W	***NNF1***	2,09	-1,05	1,45	0,00037014	chromosome segregation	molecular function unknown	kinetochore*
YMR145C	***NDE1***	-1,34	-1,90	-2,17	0,000122532	chronological cell aging*	NADH dehydrogenase activity	Mitochondrion
YGR279C	***SCW4***	1,73	2,67	2,36	5,30319E-10	conjugation with cellular fusion	glucosidase activity	cell wall (sensu Fungi)
YFR055W	***IRC7***	-3,83	-1,69	-1,80	2,96119E-09	copper ion homeostasis*	cystathionine beta-lyase activity	cellular component unknown
YMR120C	***ADE17***	-1,99	-3,36	-8,11	2,39643E-10	'de novo' IMP biosynthesis*	IMP cyclohydrolase activity*	Cytosol
YLR359W	***ADE13***	-1,71	-2,00	-3,26	1,22968E-08	'de novo' IMP biosynthesis*	adenylosuccinate lyase activity	cellular component unknown
YGL234W	***ADE5,7***	-1,78	-1,87	-2,39	0,000137037	'de novo' IMP biosynthesis*	phosphoribosylamine-glycine ligase activity*	Cytoplasm
YAR015W	***ADE1***	-1,41	-1,57	-2,39	3,93387E-09	'de novo' IMP biosynthesis*	phosphoribosylaminoimidazolesuccinocarboxamide synthase activity	cytoplasm*
YDR408C	***ADE8***	-1,51	-1,74	-2,39	1,04042E-08	'de novo' IMP biosynthesis*	phosphoribosylglycinamide formyltransferase activity	cytoplasm*
YKL216W	***URA1***	-4,22	-2,20	-2,37	1,99817E-11	'de novo' pyrimidine base biosynthesis	dihydroorotate dehydrogenase activity	cytoplasm*
YLR420W	***URA4***	-2,06	-1,48	-1,83	3,12986E-08	'de novo' pyrimidine base biosynthesis*	dihydroorotase activity	cytoplasm*
YLR348C	***DIC1***	-1,51	-2,18	-1,65	1,6088E-06	dicarboxylic acid transport	dicarboxylic acid transporter activity	mitochondrial envelope
YNL312W	***RFA2***	2,03	1,11	1,10	3,9155E-07	DNA recombination*	DNA binding	chromosome, telomeric region*
YMR173W	***DDR48***	14,25	3,38	1,28	6,08658E-15	DNA repair	ATPase activity*	Cytoplasm
YGR180C	***RNR4***	-3,09	-3,51	-2,60	1,13232E-07	DNA replication	ribonucleoside-diphosphate reductase activity	cytoplasm*
YJL026W	***RNR2***	-2,11	-2,68	-2,73	2,61035E-07	DNA replication	ribonucleoside-diphosphate reductase activity	cytoplasm*
YLR056W	***ERG3***	1,32	3,85	3,10	3,29195E-09	endocytosis*	C-5 sterol desaturase activity	endoplasmic reticulum
YDR036C	***EHD3***	-2,70	-3,37	-1,66	0,000585689	endocytosis*	3-hydroxyisobutyryl-CoA hydrolase activity	Mitochondrion
YBR207W	***FTH1***	2,12	2,54	2,39	4,10896E-08	endocytosis*	iron ion transporter activity	vacuolar membrane (sensu Fungi)

YDR059C	***UBC5***	2,20	1,43	1,19	1,17047E-08	endocytosis*	ubiquitin conjugating enzyme activity	proteasome complex (sensu Eukaryota)
YDR246W	***TRS23***	-1,30	-1,11	-3,62	1,76906E-07	ER to Golgi vesicle-mediated transport	molecular function unknown	TRAPP complex
YGR209C	***TRX2***	5,46	2,15	-1,09	4,04376E-16	ER to Golgi vesicle-mediated transport*	thiol-disulfide exchange intermediate activity	cytosol*
YLR043C	***TRX1***	1,91	1,51	-2,12	3,54014E-05	ER to Golgi vesicle-mediated transport*	thiol-disulfide exchange intermediate activity	cytosol*
YHR007C	***ERG11***	-4,43	-2,37	-2,01	3,06725E-12	ergosterol biosynthesis	sterol 14-demethylase activity	endoplasmic reticulum
YGR175C	***ERG1***	-3,59	-2,04	-2,10	2,05393E-10	ergosterol biosynthesis	squalene monooxygenase activity*	endoplasmic reticulum*
YLR100W	***ERG27***	1,85	2,51	2,04	2,67519E-06	ergosterol biosynthesis	3-keto sterol reductase activity	endoplasmic reticulum*
YIL160C	***POT1***	2,86	2,95	2,64	0,000300542	fatty acid beta-oxidation	acetyl-CoA C-acyltransferase activity	peroxisomal matrix
YKL182W	***FAS1***	-2,04	-1,23	-1,47	3,40608E-05	fatty acid biosynthesis	[acyl-carrier protein] S-malonyltransferase activity*	mitochondrion*
YJL196C	***ELO1***	-1,31	-1,97	-2,38	5,79968E-08	fatty acid elongation, unsaturated fatty acid	fatty acid elongase activity	Membrane
YOL158C	***ENB1***	5,59	3,36	5,13	7,53054E-06	ferric-enterobactin transport	ferric-enterobactin transporter activity	integral to membrane*
YAL063C	***FLO9***	3,33	3,18	1,59	1,74816E-06	flocculation (sensu Saccharomyces)	mannose binding	cell wall (sensu Fungi)
YDL168W	***SFA1***	3,31	1,94	1,80	1,01867E-05	formaldehyde catabolism	alcohol dehydrogenase activity*	cytoplasm*
YJL068C		2,15	1,07	-1,81	1,48802E-07	formaldehyde catabolism	S-formylglutathione hydrolase activity	Cytosol
YLR081W	***GAL2***	-1,33	1,01	-2,75	0,000197301	galactose metabolism*	glucose transporter activity*	plasma membrane
YDL171C	***GLT1***	-3,45	-2,76	-2,12	1,09675E-09	glutamate biosynthesis	glutamate synthase (NADH) activity	mitochondrion*
YOR375C	***GDH1***	1,22	-1,82	-2,74	0,000169205	glutamate biosynthesis	glutamate dehydrogenase (NADP+) activity	cytoplasm*
YIR038C	***GTT1***	2,77	1,29	-1,48	1,67415E-09	glutathione metabolism	glutathione transferase activity	mitochondrion*
YFL018C	***LPD1***	1,01	-1,60	-2,62	3,28322E-08	glycine catabolism*	glycine dehydrogenase (decarboxylating) activity*	mitochondrial nucleoid*
YKL060C	***FBA1***	-1,39	-1,33	-2,23	3,00235E-09	glycolysis*	fructose-bisphosphate aldolase activity	Cytoplasm
YDR044W	***HEM13***	-7,24	-4,30	-3,54	2,6884E-08	heme biosynthesis	coproporphyrinogen oxidase activity	mitochondrial inner membrane
YHR092C	***HXT4***	-1,50	-1,13	-2,74	0,000238609	hexose transport	glucose transporter activity*	plasma membrane
YOL156W	***HXT11***	-1,76	-1,50	-2,40	0,00051152	hexose transport	glucose transporter activity*	plasma membrane
YFL011W	***HXT10***	-1,88	-1,03	-2,29	0,000198859	hexose transport	glucose transporter activity*	mitochondrion*
YJL214W	***HXT8***	-1,24	1,02	-2,22	0,000433264	hexose transport	glucose transporter activity*	plasma membrane
YHR096C	***HXT5***	-1,54	-1,03	-2,12	0,000745868	hexose transport	glucose transporter activity*	plasma membrane

YER145C	***FTR1***	5,14	6,28	6,37	7,40753E-07	high affinity iron ion transport	iron ion transporter activity	plasma membrane
YMR058W	***FET3***	4,03	3,32	3,41	3,24405E-06	high affinity iron ion transport*	ferroxidase activity	plasma membrane
YOR202W	***HIS3***	-1,30	-1,87	-2,73	3,29477E-07	histidine biosynthesis	imidazoleglycerol-phosphate dehydratase activity	Intracellular
YMR038C	***CCS1***	4,08	2,76	2,76	2,21309E-10	intracellular copper ion transport	superoxide dismutase copper chaperone activity	cytosol*
YHR175W	***CTR2***	2,30	2,41	2,44	5,4829E-09	intracellular copper ion transport*	copper uptake transporter activity*	vacuolar membrane (sensu Fungi)
YHL047C	***ARN2***	7,34	9,83	7,71	2,30174E-07	iron ion homeostasis*	siderophore-iron transporter activity	plasma membrane*
YOR226C	***ISU2***	3,07	2,88	3,67	1,98724E-10	iron ion homeostasis*	molecular function unknown	mitochondrial matrix
YPL135W	***ISU1***	1,47	2,26	2,12	1,61566E-06	iron ion homeostasis*	protein binding	mitochondrion*
YEL065W	***SIT1***	1,51	1,97	2,13	3,20822E-05	iron ion homeostasis*	siderophore-iron (ferrioxamine) uptake transporter activity	endosome*
YLR126C		2,05	2,00	1,31	3,86266E-07	iron ion homeostasis*	molecular function unknown	Cytoplasm
YLR214W	***FRE1***	1,41	2,71	1,83	8,13349E-05	iron ion transport*	ferric-chelate reductase activity	plasma membrane
YEL071W	***DLD3***	1,35	1,61	2,76	5,72791E-09	lactate metabolism	D-lactate dehydrogenase (cytochrome) activity	cytoplasm*
YOR108W	***LEU9***	-2,36	-2,85	-2,18	6,14953E-06	leucine biosynthesis	2-isopropylmalate synthase activity	Mitochondrion
YNL104C	***LEU4***	-2,12	-2,38	-1,89	5,05694E-06	leucine biosynthesis	2-isopropylmalate synthase activity	cytoplasm*
YDR492W	***IZH1***	-2,17	-1,10	-1,05	1,04583E-08	lipid metabolism*	metal ion binding	endoplasmic reticulum*
YNR050C	***LYS9***	-1,30	-1,31	-2,15	4,86684E-05	lysine biosynthesis via aminoadipic acid	saccharopine dehydrogenase (NADP+, L-glutamate-forming) activity	Cytoplasm
YDR273W	***DON1***	-3,48	-4,27	-7,39	1,00307E-07	meiosis*	molecular function unknown	spindle*
YPL033C		-1,18	-1,02	-2,30	3,10073E-07	meiosis*	molecular function unknown	cellular component unknown
YDL124W		13,88	5,70	3,25	1,5632E-12	Metabolism	alpha-keto amide reductase activity*	cytoplasm*
YER091C	***MET6***	-1,52	-2,17	-1,76	4,87252E-07	methionine biosynthesis	5-methyltetrahydropteroyltriglutamate-homocysteine S-methyltransferase activity	Cytoplasm
YER052C	***HOM3***	2,04	1,62	1,63	6,85735E-08	methionine metabolism*	aspartate kinase activity	Cytoplasm
YIL123W	***SIM1***	2,98	2,83	2,61	6,77738E-07	microtubule cytoskeleton organization and biogenesis	molecular function unknown	cell wall (sensu Fungi)
YHR051W	***COX6***	-2,95	-4,28	-6,44	6,78731E-09	mitochondrial electron transport, cytochrome c to oxygen	cytochrome-c oxidase activity	respiratory chain complex IV (sensu Eukaryota)
YNL052W	***COX5A***	-1,55	-2,52	-4,14	2,3686E-09	mitochondrial electron transport, cytochrome c to oxygen	cytochrome-c oxidase activity	respiratory chain complex IV (sensu Eukaryota)
YDL067C	***COX9***	-1,61	-1,76	-2,46	3,89744E-07	mitochondrial electron transport, cytochrome c to oxygen	cytochrome-c oxidase activity	respiratory chain complex IV (sensu Eukaryota)
YLR304C	***ACO1***	-5,91	-3,09	-2,21	7,13678E-11	mitochondrial genome maintenance*	aconitate hydratase activity	cytosol*

YLR355C	***ILV5***	-2,50	-2,91	-1,71	6,64534E-11	mitochondrial genome maintenance*	ketol-acid reductoisomerase activity	mitochondrion*
YPR035W	***GLN1***	2,76	1,64	-1,40	2,22861E-09	nitrogen compound metabolism*	glutamate-ammonia ligase activity	Cytoplasm
YDR488C	***PAC11***	2,00	2,88	2,46	5,3931E-05	nuclear migration, microtubule-mediated*	microtubule motor activity*	cytoplasmic microtubule*
YKR092C	***SRP40***	2,02	2,57	2,39	8,26061E-07	nucleocytoplasmic transport	unfolded protein binding	Nucleolus
YLR058C	***SHM2***	-2,13	-2,75	-5,60	1,98682E-09	one-carbon compound metabolism	glycine hydroxymethyltransferase activity	Cytoplasm
YBR263W	***SHM1***	-1,23	-1,50	-2,02	6,36091E-07	one-carbon compound metabolism	glycine hydroxymethyltransferase activity	Mitochondrion
YMR189W	***GCV2***	-1,05	-1,94	-4,75	6,81319E-09	one-carbon compound metabolism*	glycine dehydrogenase (decarboxylating) activity	mitochondrion*
YDR019C	***GCV1***	-1,02	-2,05	-4,23	4,89185E-11	one-carbon compound metabolism*	glycine dehydrogenase (decarboxylating) activity	mitochondrion*
YDR256C	***CTA1***	-1,07	1,33	2,44	2,80899E-08	oxygen and reactive oxygen species metabolism	catalase activity	mitochondrion*
YNL241C	***ZWF1***	2,01	1,54	1,77	0,000213503	pentose-phosphate shunt, oxidative branch*	glucose-6-phosphate 1-dehydrogenase activity	Cytoplasm
YLR172C	***DPH5***	1,09	1,42	2,01	7,8644E-06	peptidyl-diphthamide biosynthesis from peptidyl-histidine	diphthine synthase activity	Cytoplasm
YDR244W	***PEX5***	1,88	2,83	2,45	3,71098E-10	peroxisome organization and biogenesis*	peroxisome targeting sequence binding*	cytosol*
YDR461W	***MFA1***	2,35	1,26	-1,15	1,85914E-06	pheromone-dependent signal transduction during conjugation with cellular fusion	mating pheromone activity	soluble fraction*
YAR071W	***PHO11***	2,23	1,98	1,34	1,36173E-07	phosphate metabolism	acid phosphatase activity	extracellular region
YBR093C	***PHO5***	2,93	1,87	1,68	6,90419E-09	phosphate metabolism*	acid phosphatase activity*	cell wall (sensu Fungi)*
YJL145W	***SFH5***	1,38	1,40	2,11	4,28712E-07	phospholipid transport	phosphatidylinositol transporter activity	cytosol*
YLL028W	***TPO1***	2,42	1,71	1,89	0,000486673	polyamine transport	spermine transporter activity*	plasma membrane*
YNL053W	***MSG5***	-1,33	-1,80	-2,00	8,48573E-06	protein amino acid dephosphorylation*	prenylated protein tyrosine phosphatase activity	Cytoplasm
YKL035W	***UGP1***	-1,19	-2,77	-2,82	0,000355231	protein amino acid glycosylation*	UTP:glucose-1-phosphate uridylyltransferase activity	Cytoplasm
YER003C	***PMI40***	-1,65	-2,70	-2,04	3,602E-10	protein amino acid glycosylation*	mannose-6-phosphate isomerase activity	cytoplasm*
YDR477W	***SNF1***	4,29	8,29	11,15	9,97601E-13	protein amino acid phosphorylation*	AMP-activated protein kinase activity	cytoplasm*
YDR247W	***VHS1***	-1,24	-1,08	-2,49	2,27783E-05	protein amino acid phosphorylation*	protein kinase activity*	Cytoplasm
YHR064C	***SSZ1***	-1,05	1,03	-2,07	7,57592E-06	protein biosynthesis*	unfolded protein binding	Cytoplasm
YIL015W	***BAR1***	-1,03	-2,16	-2,51	5,49872E-08	protein catabolism	aspartic-type endopeptidase activity	periplasmic space (sensu Fungi)
YBR155W	***CNS1***	1,01	1,34	2,09	5,79968E-08	protein folding	unfolded protein binding	Cytoplasm

YJL117W	***PHO86***	1,70	1,86	2,10	2,30085E-07	protein folding*	molecular function unknown	endoplasmic reticulum
YOR045W	***TOM6***	-1,09	-1,21	-2,26	2,15172E-05	protein import into mitochondrial matrix	protein transporter activity	mitochondrial outer membrane translocase complex
YKL171W		1,11	2,06	1,40	2,94535E-05	Proteolysis	protein kinase activity	Cytoplasm
YBR083W	***TEC1***	1,11	2,84	1,47	0,000835527	pseudohyphal growth*	RNA polymerase II transcription factor activity	Nucleus
YGR204W	***ADE3***	1,04	-1,53	-2,23	0,000409594	purine base biosynthesis*	formate-tetrahydrofolate ligase activity*	cytoplasm*
YHR186C	***KOG1***	2,52	1,51	1,39	8,46451E-09	regulation of cell growth*	molecular function unknown	mitochondrion*
YDR353W	***TRR1***	1,90	2,21	1,15	4,06151E-05	regulation of cell redox homeostasis	thioredoxin-disulfide reductase activity	Cytoplasm
YLR109W	***AHP1***	6,15	2,24	1,10	6,87333E-16	regulation of cell redox homeostasis*	thioredoxin peroxidase activity	Cytoplasm
YOR230W	***WTM1***	-3,59	-4,86	-4,08	6,87687E-09	regulation of meiosis	transcription corepressor activity	Nucleus
YDR373W	***FRQ1***	2,01	1,54	1,28	6,02415E-08	regulation of signal transduction	enzyme activator activity*	Membrane
YNL239W	***LAP3***	2,00	1,43	1,09	1,98502E-07	response to antibiotic	transcription regulator activity*	cytoplasm*
YCR102C		20,64	8,68	4,22	1,69046E-12	response to copper ion	molecular function unknown	cellular component unknown
YDR135C	***YCF1***	3,29	2,18	2,02	1,08645E-08	response to metal ion*	bilirubin transporter activity*	vacuolar membrane
YKR066C	***CCP1***	-2,28	-1,93	-1,93	4,80904E-05	response to oxidative stress	cytochrome-c peroxidase activity	mitochondrion*
YPL091W	***GLR1***	2,03	1,60	1,29	3,37519E-06	response to oxidative stress	glutathione-disulfide reductase activity	cytoplasm*
YDR513W	***GRX2***	3,30	1,30	-1,23	6,70908E-08	response to oxidative stress*	thiol-disulfide exchange intermediate activity*	mitochondrion*
YNL259C	***ATX1***	2,80	3,24	1,99	4,85992E-10	response to oxidative stress*	copper chaperone activity	Cytosol
YKL088W		2,34	3,36	2,64	1,15207E-08	response to salt stress*	purine nucleotide binding*	Cytoplasm
YOL151W	***GRE2***	46,46	10,06	4,92	5,33853E-13	response to stress	oxidoreductase activity*	cytoplasm*
YMR251W-A	***HOR7***	1,22	-2,40	-5,14	2,3686E-09	response to stress	molecular function unknown	endoplasmic reticulum*
YOR010C	***TIR2***	1,77	4,62	3,93	1,15207E-08	response to stress	molecular function unknown	cell wall (sensu Fungi)
YGR234W	***YHB1***	4,34	4,55	4,33	4,24914E-09	response to stress	nitric oxide reductase activity	cytoplasm*
YOL143C	***RIB4***	-2,63	-2,19	-3,98	2,29314E-11	riboflavin biosynthesis	6,7-dimethyl-8-ribityllumazine synthase activity	cytoplasm*
YNL002C	***RLP7***	-1,18	1,51	2,05	3,1909E-08	ribosomal large subunit biogenesis*	rRNA binding	Nucleolus
YMR049C	***ERB1***	-1,12	1,24	2,50	3,65947E-07	rRNA processing	molecular function unknown	nucleus*
YDR534C	***FIT1***	30,84	64,14	78,89	4,14174E-11	siderophore transport	molecular function unknown	cell wall (sensu Fungi)
YOR382W	***FIT2***	46,09	45,13	30,29	9,87273E-12	siderophore transport	molecular function unknown	cell wall (sensu Fungi)

YOR383C	***FIT3***	18,58	27,42	23,98	1,1794E-08	siderophore transport	molecular function unknown	cell wall (sensu Fungi)
YHL040C	***ARN1***	19,59	12,84	12,26	1,16314E-08	siderophore-iron transport	siderophore-iron transporter activity	endosome*
YDL240W	***LRG1***	-2,12	-1,57	1,12	7,17063E-05	small GTPase mediated signal transduction*	Rho GTPase activator activity	cytoplasm*
YDR512C	***EMI1***	2,51	1,20	-1,14	1,98502E-07	sporulation (sensu Fungi)	molecular function unknown	cellular component unknown
YDR516C	***EMI2***	2,40	1,18	-2,16	5,82485E-05	sporulation (sensu Fungi)	molecular function unknown	Cytoplasm
YPL154C	***PEP4***	2,29	1,41	-1,04	5,70433E-06	sporulation*	endopeptidase activity*	mitochondrion*
YAL012W	***CYS3***	2,17	1,59	2,03	0,00019831	sulfur amino acid metabolism*	cystathionine gamma-lyase activity	Cytoplasm
YGR055W	***MUP1***	2,46	1,73	1,73	0,000590636	sulfur amino acid transport	L-methionine porter activity	integral to plasma membrane
YGL039W		8,88	5,58	4,62	5,33853E-13	telomere maintenance	oxidoreductase activity*	Cytoplasm
YHR077C	***NMD2***	3,54	4,19	3,15	1,11356E-09	telomere maintenance*	protein binding	cytoplasm*
YCL008C	***STP22***	3,95	1,81	-1,06	5,03273E-15	telomere maintenance*	protein binding	endosome*
YIL036W	***CST6***	2,14	3,65	3,67	5,85428E-08	telomere maintenance*	specific RNA polymerase II transcription factor activity	Nucleus
YLR192C	***HCR1***	1,66	1,87	3,31	4,16164E-11	telomere maintenance*	translation initiation factor activity*	eukaryotic translation initiation factor 3 complex
YGR057C	***LST7***	2,89	2,59	3,31	1,05549E-06	telomere maintenance*	protein transporter activity	vesicle coat
YAR003W	***SWD1***	1,63	2,60	3,03	2,72762E-08	telomere maintenance*	histone lysine N-methyltransferase activity (H3-K4 specific)	COMPASS complex
YAL044C	***GCV3***	-1,11	-1,58	-2,63	1,77651E-10	telomere maintenance*	glycine dehydrogenase (decarboxylating) activity	mitochondrion*
YDL020C	***RPN4***	2,44	1,95	2,34	2,93678E-10	telomere maintenance*	transcriptional activator activity	proteasome regulatory particle (sensu Eukaryota)*
YNL220W	***ADE12***	-1,72	-2,19	-2,14	0,000569341	telomere maintenance*	adenylosuccinate synthase activity	Cytoplasm
YOR327C	***SNC2***	2,01	1,52	1,52	2,04121E-05	telomere maintenance*	v-SNARE activity	transport vesicle
YCL064C	***CHA1***	1,09	1,54	5,49	4,16164E-11	threonine catabolism*	L-serine ammonia-lyase activity*	mitochondrion*
YLR403W	***SFP1***	3,35	6,10	8,02	2,66552E-08	transcription from RNA polymerase III promoter*	transcription factor activity	cytoplasm*
YFL021W	***GAT1***	-1,56	-2,53	-1,17	0,000323374	transcription initiation from RNA polymerase II promoter*	specific RNA polymerase II transcription factor activity*	nucleus*
YHR178W	***STB5***	6,03	3,72	2,72	5,21475E-11	transcription*	transcription factor activity	Nucleus
YKL142W	***MRP8***	3,16	2,23	2,16	1,07556E-09	Translation	structural constituent of ribosome	mitochondrial ribosome
YAL003W	***EFB1***	1,26	2,02	3,09	1,88987E-06	translational elongation	translation elongation factor activity	ribosome*
YOR187W	***TUF1***	1,09	-1,36	-2,02	3,00413E-05	translational elongation	GTPase activity*	mitochondrial matrix

YGR083C	***GCD2***	1,33	2,23	3,05	9,17858E-06	translational initiation	translation initiation factor activity*	ribosome*
YDR091C	***RLI1***	-2,68	-2,09	-1,62	1,88162E-08	translational initiation*	ATPase activity*	cytoplasm*
YNL037C	***IDH1***	1,06	1,72	2,10	3,42894E-05	tricarboxylic acid cycle*	isocitrate dehydrogenase (NAD+) activity	mitochondrial matrix*
YML092C	***PRE8***	2,31	1,29	1,36	1,32333E-07	ubiquitin-dependent protein catabolism	endopeptidase activity	proteasome core complex, alpha-subunit complex (sensu Eukaryota)
YDL097C	***RPN6***	1,53	1,38	2,01	9,54166E-10	ubiquitin-dependent protein catabolism	structural molecule activity	proteasome regulatory particle, lid subcomplex (sensu Eukaryota)
YKL103C	***LAP4***	4,75	3,19	1,89	1,50992E-09	vacuolar protein catabolism	aminopeptidase I activity	vacuole (sensu Fungi)
YJR104C	***SOD1***	4,09	1,78	1,67	9,60563E-13	zinc ion homeostasis*	copper, zinc superoxide dismutase activity	cytosol*
YMR173W-A		20,86	3,40	1,51	1,07204E-16			
YCLX08C	***FRM2***	14,24	5,45	3,47	2,10682E-08			
YCR074C		2,53	4,21	3,41	6,87687E-09			
YDR154C		2,69	1,18	1,03	4,52369E-08			
YKL030W		-2,67	-1,95	-1,78	2,49685E-09			
YKL066W		2,21	1,23	-1,53	1,00734E-08			
YLL044W		-2,19	-1,67	-1,57	2,14521E-06			
YDR271C		1,64	2,18	1,68	3,88956E-06			
YFR024C		2,12	2,08	1,47	4,42415E-05			
YAR073W		-1,25	-1,27	-2,07	0,000108108			

List of PDTC-sensitive genes

	PDTC-sensitive genes		
	Sc ORF	***Gene***	**Biological Process**
	Transport		
1	YAL002W	***VPS8***	late endosome to vacuole transport
2	YJR102C	***VPS25***	telomere maintenance
3	YMR231W	***PEP5***	vacuole fusion, non-autophagic
4	YNL246W	***VPS75***	telomere maintenance
5	YOR036W	***PEP12***	Golgi to vacuole transport
6	YOR106W	***VAM3***	vesicle fusion
7	YKL041W	***VPS24***	late endosome to vacuole transport
8	YLR148W	***PEP3***	telomere maintenance
9	YBR097W	***VPS15***	telomere maintenance
10	YDL077C	***VAM6***	telomere maintenance
11	YDL226C	***GCS1***	ER to Golgi vesicle-mediated transport
12	YDR080W	***VPS41***	vacuole fusion, non-autophagic
13	YDR129C	***SAC6***	Endocytosis
14	YDR264C	***AKR1***	Endocytosis
15	YDR323C	***PEP7***	vesicle fusion
16	YDR484W	***VPS52***	Golgi to vacuole transport
17	YDR485C	***VPS72***	protein targeting to vacuole
18	YDR495C	***VPS3***	telomere maintenance
19	YGL095C	***VPS45***	protein complex assembly
20	YGL124C	***MON1***	protein targeting to vacuole

21	YGL212W	***VAM7***	telomere maintenance
22	YMR319C	***FET4***	intracellular copper ion transport
23	YLR396C	***VPS33***	vacuole fusion, non-autophagic

vacuolar acidification

1	YEL051W	***VMA8***	vacuolar acidification
2	YHR060W	***VMA22***	protein complex assembly
3	YBR127C	***VMA2***	vacuolar acidification
4	YDL185W	***TFP1***	vacuolar acidification
5	YGR020C	***VMA7***	vacuolar acidification
6	YGR105W	***VMA21***	protein complex assembly
7	YHR026W	***PPA1***	vacuolar acidification
8	YLR447C	***VMA6***	vacuolar acidification
9	YPR036W	***VMA13***	vacuolar acidification
10	YBR171W	***SEC66***	filamentous growth
11	YKL119C	***VPH2***	protein complex assembly

mitochondrium related

1	YMR286W	***MRPL33***	Translation
2	YPR100W	***MRPL51***	Translation
3	YBR122C	***MRPL36***	Translation
4	YCR003W	***MRPL32***	Translation
5	YDR237W	***MRPL7***	Translation
6	YGR076C	***MRPL25***	Translation
7	YKR085C	***MRPL20***	Translation
8	YGR171C	***MSM1***	methionyl-tRNA aminoacylation
9	YML001W	***YPT7***	telomere maintenance
10	YDR069C	***DOA4***	telomere maintenance

11	YDR175C	***RSM24***	Translation
12	YHR168W	***MTG2***	protein biosynthesis
13	YKL155C	***RSM22***	Translation
14	YLR369W	***SSQ1***	DNA-dependent DNA replication
15	YBR179C	***FZO1***	mitochondrion organization and biogenesis
16	YER154W	***OXA1***	protein import into mitochondrial inner membrane
17	YMR072W	***ABF2***	mitochondrial genome maintenance
18	YPR024W	***YME1***	mitochondrion organization and biogenesis
19	YMR098C	***ATP25***	mitochondrial proton-transporting ATP synthase complex assembly
20	YJL180C	***ATP12***	protein complex assembly
21	YDR405W	***MRP20***	Translation
22	YKL194C	***MST1***	threonyl-tRNA aminoacylation
23	YMR097C	***MTG1***	protein biosynthesis

chromatin / telomere / transcription / translation

1	YAR002W	***NUP60***	telomere maintenance
2	YJL140W	***RPB4***	telomere maintenance
3	YJL176C	***SWI3***	chromatin remodeling
4	YLR025W	***SNF7***	telomere maintenance
5	YNL229C	***URE2***	telomere maintenance
6	YNL236W	***SIN4***	transcription from RNA polymerase II promoter
7	YPL129W	***TAF14***	chromatin remodeling
8	YPL161C	***BEM4***	telomere maintenance
9	YBL058W	***SHP1***	telomere maintenance
10	YBL093C	***ROX3***	transcription from RNA polymerase II promoter
11	YBR231C	***SWC5***	chromatin remodeling
12	YCL008C	***STP22***	telomere maintenance
13	YDL006W	***PTC1***	telomere maintenance

14	YDL160C	***DHH1***	deadenylylation-dependent decapping
15	YDR138W	***HPR1***	telomere maintenance
16	YDR364C	***CDC40***	nuclear mRNA splicing, via spliceosome
17	YGR006W	***PRP18***	nuclear mRNA splicing, via spliceosome
18	YGR252W	***GCN5***	histone acetylation
19	YLR357W	***RSC2***	telomere maintenance
20	YLR399C	***BDF1***	DNA repair
21	YMR091C	***NPL6***	telomere maintenance
22	YNL107W	***YAF9***	chromatin remodeling
23	YPR163C	***TIF3***	translational initiation
24	YGL071W	***AFT1***	high-affinity iron transport
25	YGL220W	***FRA2***	negative regulation of transcription from RNA polymerase II promoter in response to iron

Other

1	YAL009W	***SPO7***	sporulation (sensu Fungi)
2	YML028W	***TSA1***	response to oxidative stress
3	YMR032W	***HOF1***	Cytokinesis
4	YMR205C	***PFK2***	Glycolysis
5	YMR293C		aerobic respiration
6	YOR205C	***FMP38***	biological process unknown
7	YBL022C	***PIM1***	Proteolysis
8	YDR098C	***GRX3***	response to oxidative stress
9	YDR126W	***SWF1***	spore wall assembly (sensu Fungi)
10	YDR207C	***UME6***	sporulation (sensu Fungi)
11	YDR245W	***MNN10***	actin filament organization
12	YAL016W	***TPD3***	protein biosynthesis
13	YAL047C	***SPC72***	mitotic sister chromatid segregation
14	YER155C	***BEM2***	cell wall organization and biogenesis

15	YFL014W	***HSP12***	response to oxidative stress
16	YJR104C	***SOD1***	zinc ion homeostasis
17	YJR122W	***CAF17***	biological process unknown
18	YLR260W	***LCB5***	response to heat
19	YLR370C	***ARC18***	actin filament organization
20	YPR160W	***GPH1***	glycogen catabolism
21	YPL148C	***PPT2***	protein-cofactor linkage
22	YLR056W	***ERG3***	Endocytosis
23	YLR079W	***SIC1***	G1/S transition of mitotic cell cycle
24	YCR009C	***RVS161***	Endocytosis

protein modification

1	YNL080C	***EOS1***	Protein involved in N-glycosylation; response to oxidative stress
2	YML112W	***CTK3***	protein amino acid phosphorylation
3	YGR262C	***BUD32***	protein amino acid phosphorylation
4	YGR092W	***DBF2***	protein amino acid phosphorylation
5	YDR507C	***GIN4***	protein amino acid phosphorylation
6	YDR523C	***SPS1***	protein amino acid phosphorylation
7	YGL017W	***ATE1***	protein modification
8	YDL232W	***OST4***	protein amino acid N-linked glycosylation
9	YJL095W	***BCK1***	protein amino acid phosphorylation
10	YDL090C	***RAM1***	protein amino acid farnesylation

Rim101 pathway

1	YHL027W	***RIM101***	neg. regulation of transcription; response to pH; meiosis
2	YMR154C	***RIM13***	protein processing
3	YMR063W	***RIM9***	ascospore formation
4	YKL002W	***DID4***	late endosome to vacuole transport

5	YPR173C	***VPS4***	intralumenal vesicle formation
6	YGL045W	***RIM8***	protein processing; meiosis

	unknown		
1	YML013C-A		Dubious open reading frame
2	YPR109W		Predicted membrane protein; dipoid deletion strain has high budding index
3	YMR073C		response to drug
4	YOL087C		Putative protein of unknown function
5	YDR532C	***KRE28***	Protein of unknown function; forms a complex with Spc105p
6	YDR433W		Dubious open reading frame unlikely to encode a functional protein
7	YCL007C	***CWH36***	Dubious ORF unlikely to encode a protein;
8	YDL183C		biological process unknown
9	YBL012C		Dubious open reading frame
10	YNL171C		Dubious open reading frame
11	YNL198C		Dubious open reading frame
12	YNL296W		Dubious open reading frame
13	YDL167C	***NRP1***	biological process unknown

	Excluded		
1	YLR338W	***OPI9***	Dubious open reading frame
2	YLR358C		Dubious open reading frame
3	YPR099C		Dubious open reading frame
4	YKL118W		Dubious open reading frame

N° Genes / Category	Functional Categories	Gene Names
24	Transport	VPS8, VPS25, PEP5, VPS75, PEP12, VAM3, VPS24, PEP3, VPS15, VAM6, GCS1, VPS41, SAC6, AKR1, PEP7, VPS52, VPS72, VPS3, VPS45, MON1, VAM7, FET4, VPS33, STP22
11	vacuolar acidification	VMA8, VMA22, VMA2, TFP1, VMA7, VMA21, PPA1, VMA6, VMA13, SEC66, VPH2
23	mitochondria organization / maintainance	MRPL33, MRPL51, MRPL36, MRPL32, MRPL7, MRPL25, MRPL20, MSM1, YPT7, DOA4, RSM24, MTG2, RSM22, SSQ1, FZO1, OXA1, ABF2, YME1, ATP25, ATP12, MRP20, MST1, MTG1
24	chromatin / telomere / transcription / translation	NUP60, RPB4, SWI3, SNF7, URE2, SIN4, TAF14, BEM4, SHP1, ROX3, SWC5, PTC1, DHH1, HPR1, CDC40, PRP18, GCN5, RSC2, BDF1, NPL6, YAF9, TIF3, AFT1, FRA2
10	protein modification	EOS1, CTK3, BUD32, DBF2, GIN4, SPS1, ATE1, OST4, BCK1, RAM1
6	Rim101 pathway	RIM101, RIM13, RIM9, DID4, VPS4, RIM8
24	Other	SPO7, TSA1, HOF1, PFK2, YMR293C, FMP38, PIM1, GRX3, SWF1, UME6, MNN10, TPD3, SPC72, BEM2, HSP12, SOD1, CAF17, LCB5, ARC18, GPH1, PPT2, ERG3, SIC1, RVS161
13	Unknown	YML013C-A, YPR109W, YMR073C, YOL087C, KRE28, YDR433W, CWH36, YDL183C, YBL012C, YNL171C, YNL198C, YNL296W, NRP1,
4	Excluded	OPI9, YLR358C, YPR099C, YKL118W

YEASTRACT - Differentially expressed genes were grouped according to their transcription factors or potential regulators

Transcription Factor	%	Sc Gene Name
Yap1	60.3	*EFB1, CYS3, ADE1, PHO11, IMD1, SLA1,* YBR053C, *YRO2, TIP1*, *PHO5*, *CNS1*, *FTH1*, *SHM1*, YCL026C-A, *YCP4*, YCR102c, *ADH7*, *AAD3*, *RPN4*, *RPN6*, *YDL124w, SFA1*, *GLT1*, *GCV1*, *MRH1*, *ARO3*, *EHD3*, *VBA4*, *YCF1*, YDR154c, *CTA1*, *DON1*, *TRR1*, *YPR1*, *FRQ1*, *ADE8*, *RIB3*, *GRX2*, *EMI2*, *HSP31*, *FIT1*, *DLD3*, *RMD6*, *PMI40*, *MET6*, YER156c, *GAT1*, *AAD6*, *AAD16*, *IRC7*, *PNC1*, *HNM1*, *MUP1*, *VHT1*, YGR146c*, ERG1*, *RNR4*, *ADE3*, *TRX2*, *YHB1*, *ARN1*, *ERG11*, *COX6*, *HXT4*, *HXT5*, *ARO9*, *CTR2*, *STB5*, *OYE2*, *KOG1*, *FMP22*, *FMP34*, *SIM1*, *HXT12*, *GTT1*, *RNR2*, *SOD1*, YKL030w, *FBA1*, YKL066w, *CWP1*, *LAP4*, *MRP8*, *FAS1*, *URA1*, *CCP1*, *SRP40*, *TPO1*, *TRX1*, *ERG3*, *SHM2*, *AHP1*, *DPH5*, *FRE1, ACO1, ILV5, SFP1, URA4, YLR460c, PRE8, YML131w, CCS1, ERB1, FET3, ADE17, DDR48, YMR173w-a, GCV2, HOR7, ADH6, LEU4, YNL134c, YNL208w, ADE12, LAP3, ZWF1, RFA2, RIB4, GRE2, HXT11, LEU9, ISU2, WTM1, YOR285w, GDH1, FIT3, YPL067c, GLR1, CAR1, PEP4, OYE3, GLN1*
Sfp1	47.0	*EFB1*, *GCV3*, *FLO9*, *IMD1*, *SLA1*, YBR053c*, CNS1*, *STP22*, YCL026c-a*,* YCR102c*, RPN4*, *RPN6*, *LRG1*, *GCV1*, *MRH1*, *HEM13*, *RLI1*, *VBA4*, *YCF1*, YDR154c*, TRS23*, *TRR1*, *YPR1*, *FRQ1*, *MFA1*, *PAC11*, *IZH1*, *HSP31*, *FIT1*, *SIT1*, *DLD3*, *PMI40*, *HOM3*, *FTR1*, YER156c*, HXT10*, *AAD16*, *AGA2*, YGL039w*,* YGL157w*, VHT1*, YGR146c, *ERG1*, *ADE3*, *YHB1*, *ARN1*, *ERG11*, *SSZ1*, *HXT4*, *CTR2*, *STB5*, *OYE2*, YHR213w*, BAR1*, *POT1*, *HXT12*, *RNR2*, YJL068c, *ELO1*, *NNF1*, *CWP1*, *FAS1*, *URA1*, *SRP40*, *ERG3*, *SHM2*, *GAL2*, *ERG27*, *AHP1*, *HCR1*, *ACO1*, *ILV5*, *SFP1*, YLR460c, YML131w*, ERB1*, *FET3*, *ILV2*, *ADE17*, YMR173w-*a*, *GCV2*, *HOR7*, *ADH6*, *RLP7*, *MSG5*, *LEU4*, YNL134c, *LAP3*, *ZWF1, RFA2, LYS9, RIB4, GRE2, ENB1, UTP23, LEU9, HIS3, ISU2, FIT2, YPL067c, CAR1, OYE3, GLN1*
Msn2	34.2	*EFB1*, *PHO11*, *SLA1*, YBR053c*, PHO5*, *RPN4*, YDL124w*, MRH1*, YDR154c*, CTA1*, *TRR1*, *APT2*, *EMI1*, *GRX2*, *EMI2*, *HSP31*, *MET6*, *FTR1*, *GAT1*, *AAD16*, *PNC1*, *HNM1*, YGL157w*, ADE5,7*, *MUP1*, *LST7*, *VHT1*, *ERG1*, *TRX2*, *YHB1*, *HXT4*, *HXT5*, *ARO9*, *CTR2*, *SIM1*, *POT1*, *GTT1*, *ACO2*, *REE1*, *SOD1*, *UGP1*, *FBA1*, *CWP1*, *LAP4*, *MRP8*, *CCP1*, *ERG3*, *AHP1*, YLR126c*, FRE1*, *ILV5*, YML131w*, ERB1*, *FET3*, *DDR48*, YMR173w-a*, HOR7*, *RLP7*, *IDH1*, *COX5a*, YNL134c*, LAP3*, *ATX1*, *RIB4*, *GRE2*, *UTP23*, *LEU9*, *HIS3*, *ISU2*, *WTM1*, YOR285w*, GDH1*, *FIT2*, *PEP4*, *OYE3*
Ste12	34.2	*EFB1*, *FLO9*, *ADE1*, *PHO11*, YBR053c*, YRO2*, *TIP1*, *TEC1*, YCL026c-a, *CHA1*, YCR102c*, SFA1*, *GLT1*, *LRG1*, *EHD3*, *HEM13*, *RLI1*, *APT2*, *MFA1*, *HSP31*, *RMD6*, *MET6*, *FTR1*, *LPD1*, *GAT1*, *IRC7*, *AGA2*, *PNC1*, YGL039w*,* YGR146c*, RNR4*, *YHB1*, *FMP43*, *SCW4*, *ARN1*, *ERG11*, *HXT4*, *HXT5*, *ARO9*, *OYE2*, *BAR1*, *CST6*, *SIM1*, *BNR1*, *POT1*, *HXT12*, *GTT1*, *SFH5*, *ELO1*, *ACO2*, *HXT8*, *CWP1*, *LAP4*, *TPO1*, *TRX1*, *GAL2*, *AHP1*, *ACO1*, *DIC1*, *URA4*, YLR460c*, CCS1*, *ERB1*, *ILV2*, *NDE1*, *DDR48*, *HOR7*, *MSG5*, *POR1*, YNL208w*, LYS9*, *TIR2*, *SNC2*, *GDH1*, *ISU1*
Sok2	30.1	*EFB1*, *FLO9*, YBR053c*, YRO2*, *TIP1*, *TEC1*, *CHA1*, *AAD3*, YDL124w*, SFA1*, *HEM13*, *APT2*, *IZH1*, *EMI2*, *HSP31*, *SIT1*, *DLD3*, *FTR1*, *AAD16*, *IRC7*, *AGA2*, *PNC1*, YGL157w*,* YGR146c*, RNR4*, *YHB1*, *SCW4*, *ERG11*, *HXT4*, *HXT5*, *OYE2*, *SIM1*, *HXT12*, *GTT1*, *RNR2*, *HXT8*, *CWP1*, *LAP4*, *FAS1*, *SRP40*, *TPO1*, *ERG3*, *SHM2*, *ACO1, ILV5*, YLR460c*,* YML131w*, NDE1*, *DDR48*, *HOR7*, *LEU4*, *ZWF1*, *LYS9*, *GRE2*, *HXT11*, *ENB1*, *TIR2*, *TUF1*, *WTM1*, *SNC2*, *GDH1*, *FIT3*, YPL067c*, ISU1*, *PEP4*, *OYE3*
Met4	28.8	*CYS3*, *GCV3*, *FLO9*, *IMD1*, YBR053c*, YRO2*, *SHM1*, *YCP4*, *AAD3*, *RPN4*, *INH1*, *GCV1*, *HEM13*, *UBC5*, *YCF1*, YDR154c*,* YDR476c*, RIB3*, *GRX2*, *QCR7*, *HSP31*, *SIT1*, *DLD3*, *MET6*, *HXT10*, *GAT1*, *AAD6*, *AAD16*, YFR024c-a*, PNC1*, *ADE5,7*, *MUP1*, *LST7*, *VHT1*, *ADE3*, *ARO9*, *BNR1, RNR2*, *PHO86*, *ACO2*, *REE1*, *SOD1*, *UGP1*, *MRP8*, *URA1*, *CCP1*, *TRX1*, *SHM2*, *SFP1*, *PRE8*, YML131w*, ERB1*, *NDE1*, *GCV2*, *MSG5*, YNL208w*, ADE12*, *LAP3*, *LYS9*, *HXT11*, *WTM1*, *FIT2*, *OYE3*
Rpn4	28.8	*GCV3*, *IMD1*, YBR053c*, YRO2*, *TIP1*, *PHO5*, *STP22*, YCL026c-a*, CHA1*, *YCP4*, YCR102c, *RPN4*, *RPN6*, *GCV1*, *MRH1*, *TRR1*, *FRQ1*, *FIT1*, *MTC7*, *DLD3*, *PMI40*, *HOM3*, *MET6*, *AAD6*, *AAD16*, *PNC1*, YGL039w*, TRX2*, *YHB1*, *FMP43*, *SCW4*, *ARN1*, *ARN2*, *HXT4*, *HXT5*, *ARO9*, *GTT1*, *UGP1*, *CWP1*, *LAP4*, *FAS1*, *URA1*, *ERG3*, *FRE1*, *DIC1*, YLR460c*, PRE8*, YML131w*, FET3*, *ILV2*, *ADE17*, *NDE1*, *GCV2*, *HOR7*, *IDH1*, *POR1*, *ENB1*, *TIR2*, YOR285w*, FIT2*, *FIT3*, *PEP4*, *GLN1*
Pdr1	27.9	*EFB1*, YAL065c*, PHO11*, YBR053c*, YRO2*, *TEC1*, *PHO5*, YCL026c-a*, ADH7*, *RPN4*, YDL124w*, TRR1*, *YPR1*, *IZH1*, *EMI2*, *HSP31*, *FIT1*, *SIT1*, *DLD3*, *HOM3*, *FTR1*, *AAD16*, *PNC1*, YGL039w*,* YGL157w*,* YGR146c*, FMP43*, *SCW4*, *HXT4*, *OYE2*, *HXT12*, *GTT1*, YKL030w*, UGP1*, *CWP1*, *FAS1*, *URA1*, *TPO1*, *ERG27*, *AHP1*, *ACO1*, *DIC1*, *ILV5*, YML131w*, FET3*, *NDE1*, *HOR7*, *ADH6*, YNL134c*, ZWF1*, *ATX1*, *LYS9*, *GRE2*, *HXT11*, *ENB1*, *HIS3*, *SNC2*, *FIT2*, *ISU1*, *PEP4*, *GLN1*

Aft1	25.6	*FLO9*, *YRO2*, *FTH1*, *YCP4*, *ADH7*, *AAD3*, *RPN4*, YDL124w, YDR154c, YDR271c, *HSP31*, *FIT1*, YDR541c, *SIT1*, *FTR1*, YER156c, *PNC1*, *COX13*, *VHT1*, YGR146c, *YHB1*, *FMP43*, *ARN1*, *ARN2*, *HXT4*, *HXT5*, *FMP22*, *GTT1*, *ELO1*, *SOD1*, *UGP1*, *LAP4*, *TPO1*, *ERG3*, *GAL2*, *AHP1*, *HCR1*, *FRE1*, YML131w, *FET3*, *NDE1*, *DDR48*, *GCV2*, *HOR7*, *IDH1*, *ZWF1*, *ATX1*, *HXT11*, *ENB1*, *TUF1*, *ISU2*, *FIT2*, *FIT3*, *ISU1*, *PEP4*, *OYE3*
Gcn4	24.7	*CYS3*, *GCV3*, *ADE1*, *PHO11*, *YRO2*, *PHO5*, YCL026c-a, *CHA1*, *COX9*, *GLT1*, *GCV1*, *ARO3*, *PEX5*, *ADE8, RIB3*, *EMI1*, *GRX2*, *HOM3*, *LPD1*, *GAT1*, *IRC7*, *PNC1*, *ADE5,7*, *VHT1*, *ADE3*, *YHB1*, *HXT5*, *ARO9*, *FMP34*, *ACO2*, *SOD1*, *NNF1*, *FBA1*, *CWP1*, *LAP4*, *ILV5*, *ADE13*, *ILV2*, *ADE17*, *DDR48*, *GCV2*, *IDH1*, *LEU4*, *ADE12*, *LAP3*, *ZWF1*, *LYS9*, *LEU9*, *HIS3*, *WTM1*, *GDH1*, *CAR1*, *ISU1*, *GLN1*
Pdr3	24.2	*EFB1*, YAL065c, *PHO11*, *SLA1*, *YRO2*, *PHO5*, YCL026c-a, YCR102c, *RPN4*, YDL124w, *MRH1*, *TRR1*, *IZH1*, *EMI2*, *HSP31*, *DLD3*, *HOM3*, *FTR1*, *AAD6*, *AAD16*, *PNC1*, YGL039w, YGL157w, *TRX2*, *YHB1*, *FMP43*, *SSZ1*, *HXT4*, *UGP1*, *LAP4*, *URA1*, *SRP40*, *TPO1*, *ERG27*, *DPH5*, *ACO1*, YLR460c, *ERB1*, *HOR7*, YNL134c, *GRE2*, *HXT11*, *ENB1*, *UTP23*, *TIR2*, *HIS3*, *ISU2*, *SNC2*, *FIT2*, *CAR1*, *ISU1*, *PEP4*, *OYE3*
Cin5	20.5	*GCV3*, *FLO9*, *ADE1*, YBR053c, *YRO2*, YCR102c, *SFA1*, *GLT1*, *MRH1*, *APT2*, *HSP31*, *RNR4*, *TRX2*, *ARN1*, *COX6*, *STB5*, *OYE2*, *SIM1*, *HXT12*, *GTT1*, *LAP4*, *MRP8*, *FAS1*, *CCP1*, *SHM2*, *GAL2*, *AHP1*, YLR126c, *FRE1*, *ACO1*, *ADE13*, YLR460c, YML131w, *CCS1*, *ADE17*, *DDR48*, YMR173w-a, *GCV2*, *ZWF1*, *GRE2*, *HXT11*, *WTM1*, YOR285w, *FIT2*, *GLN1*

Supplementary Figure S3

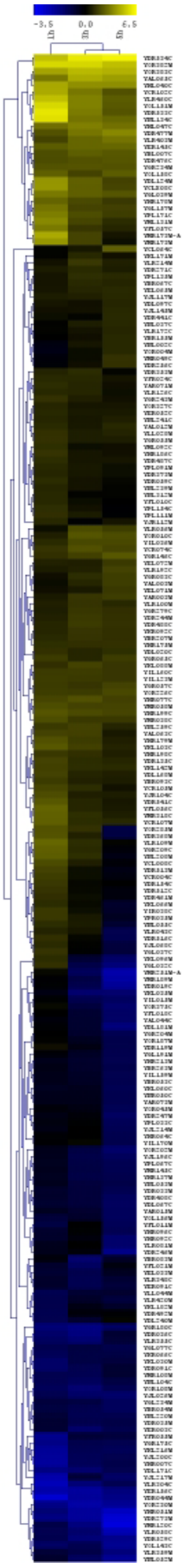

ACKNOWLEDGEMENTS

It is a pleasure to thank all those who made this thesis possible:

I want to thank Karl Kuchler and Joachim Seipelt for giving me the opportunity to do my Ph.D thesis under their supervision.

Special thanks go to my parents for their love, guidance, patience and for supporting me in any respect throughout my life.

Without my friends, their enthusiasm and encouragement, I would not have achieved the success of the last years. Stefan has been the world's-best listener, the support and companionship, my partner in crime whenever I needed him. Martina, Bernhard and Roland made my studies a fruitful lesson and a wonderful time. Kathi and Stefan were supportive "dramaqueens", telephone jokers and shopping guidance whenever the chaos increased.

Last but not least, I would like to thank all former and current lab members for the nice working atmosphere, their support, comments and discussions. I am especially grateful to Christa, Kristina, Flo, Ingrid, Tobi, Conny, Michi, Olivia and Martin for all the coffee breaks, fun in and outside the lab and the sleepless nights in due course of the "Trinkkameraden"-get-togethers.

Knowledge is in the end based on acknowledgement.

(Ludwig Wittgenstein)

APPENDIX – Acknowledgements

Curriculum Vitae

Name:	Nathalie Landstetter
Birthday:	1. May 1983, in Lilienfeld
Nationality:	Austria
Address:	Hüffelstrasse 2/1/9, A-3170 Hainfeld
Telephone, E-mail:	+43 664 75020846, Nathalie.landstetter@univie.ac.at

Education:

04. 2006 – 08.2010	**Ph.D thesis** at the Institute of Medical Biochemistry, Ao. Prof. Dr. Karl Kuchler: Antiviral Drug Target Identification Using Yeast as a Model System
10. 2001 – 01. 2006	**Master of Science** Microbiology and Genetics at the University of Vienna, obtained with outstanding records
06. 2001	**Final exams (Matura)** with outstanding record
1993 – 2001	Bundesgymnasium Lilienfeld
1989 – 1993	Volksschule Hainfeld

Research and professional experience:

Since April 2006	**Ph.D thesis** at the Institute of Medical Biochemistry, Ao. Prof. Dr. Karl Kuchler: Antiviral Drug Target Identification Using Yeast as a Model System
04. 2008 – 07. 2008	Webpage maintenance and actualization of www.lisavr.at, LISA VR
01. 2005 – 01.2006	**Diploma thesis** in the group of Ao. Prof. Dr. Dieter Blaas at the Department of Medical Biochemistry, Medical University of Vienna
07. 2004	**Research internship** at the University of Agriculture in Vienna, Dr. Boris Ferko
2003 – 2005	**Tutorial assistant** at the "Physikalisches Praktikum für Biologen", University of Vienna

APPENDIX – Curriculum Vitae

Personal skills and competences:

Languages:

German:	first language
English:	excellent skills, fluent in speech and writing
French:	basic skills

Driving licence: Class B

Social skills and competences:

08. 2002	Caritas Social Work Camp in Oradea, Rumania, Organizing Committee
08. 2001	Caritas Social Work Camp in Oradea, Rumania

Organisatorial skills and competences:

11. 2005 – 11. 2007	head of the Austrian student's platform Club Biotech, organization of courses, meetings, presentations and excursions
07. 2007	32nd FEBS Congress 2007: Molecular Machines, Organizing Committee: Selection, Scheduling Supervision of 80 congress helpers
03. 2007	FEBS Sysbio2007, in Gosau, Assistance of Organizing Committee
03. 2006	organizer of the 1st YEBN Internal Meeting in Vienna

Computer skills and competences:

Windows XP and Vista, MS Office, Sigma Plot, Corel Draw, Adobe Illustrator, Adobe Photoshop - excellent skills

MS Access – basic knowledge

Artistic skills:

Photography, painting, Standard and Latin American dancing – excellent skills

Workshops and congresses

Short Talk – 5th PhD Symposium of the Medical University of Vienna, June 17-19 2009, Vienna, Austria

Short Talk – 2nd VBC Student Symposium, November 18 2008, Vienna, Austria

Poster Presentation – Yeast 2008 Meeting, July 22-27 2008, Toronto, Canada

Poster Presentation – 4th PhD Symposium of the Medical University of Vienna, May 28-29 2008, Vienna, Austria

Poster Presentation – 32nd FEBS Congress, July 7-12 2007, Vienna, Austria

Poster Presentation – 3rd YSA PhD Symposium of the Medical University of Vienna, June 21-22 2007, Vienna, Austria

Poster Presentation – 2nd FEBS Advanced Lecture Course on Systems Biology From Molecules to Life, March 10-16, 2007, Gosau, Austria

Poster Presentation – Northern Lights EUROPIC, November 26 – December 1 2006, Finland

Short Talk – YSBN 1st Workshop Vienna, November 15-19, 2006, Vienna, Austria

Publications:

Landstetter, N., Glaser, W., Gregori, C., Seipelt, J., and Kuchler, K. (2010). Functional Genomics of Drug-Induced Ion Homeostasis Identifies a Novel Regulatory Cross-Talk of Iron and Zinc Regulons in Yeast. (OMICS, in print)

Nizet, S., Wruss, J., Landstetter, N., Snyers, L., and Blaas, D. (2005). A mutation in the first ligand-binding repeat of the human very-low-density lipoprotein receptor results in high-affinity binding of the single V1 module to human rhinovirus 2. J Virol *79*, 14730-14736.